THESIS FOR THE DEGREE OF DOCTOR OF PHILOSOPHY

Green Aromatics: Catalytic Valorisation of bio-derived 2,5-dimethylfuran over Zeolites and Zeotypes

Christopher Sauer

Department of Chemistry and Chemical Engineering
CHALMERS UNIVERSITY OF TECHNOLOGY
Gothenburg, Sweden 2022

Green Aromatics: Catalytic Valorisation of bio-derived 2,5-dimethylfuran over Zeolites and Zeotypes

Christopher Sauer

ISBN 978-91-7905-746-6

Doktorsavhandlingar vid Chalmers tekniska högskola

Ny serie Nr. 5212

ISSN 0346-718X

Department of Chemistry and Chemical Engineering
Chalmers University of Technology
SE-412 96 Göteborg
Telephone +46 31 772 1000

Cover:
Furans (pentagons) as bio-based precursors for BTX aromatics (hexagons) capturing the materials and energy of our forests. Illustrator: Wang Xueting

Typeset in LaTeX using the kaobook class

Printed by Chalmers Digitaltryck

Göteborg, Sweden 2022

Green Aromatics: Catalytic Valorisation of bio-derived 2,5-dimethylfuran over Zeolites and Zeotypes

Christopher Sauer
Department of Chemistry and Chemical Engineering
Chalmers University of Technology

Abstract

This thesis discusses the use of biomass as a potentially green feedstock for the chemical industry in the urgent shift away from fossil resources. I elaborate on reasons why we cannot afford to burn virgin biomass for energy production, among them a variety of ecosystem services that forests and other lands provide. In addition, the utilisation of biomass should be focused on products that sequester and lock away carbon for more extended periods, e.g. timber, materials and chemicals. In particular, biomass can be used as an alternative "carbon neutral" feedstock for the chemical industry, where we can preserve the already existing chemical complexity in the bio-based molecules. One example is the upgrading of furans to benzene, toluene and xylene (BTX) aromatics with the help of zeolite catalysis. These aromatics are important commodity chemicals, where the shift to a bio-based resource could make use of already existing knowledge, catalyst and production infrastructure. However, research is necessary to understand these new feedstock molecules and their interaction with the catalysts and to enable the design of applicable catalysts.

In order to study the interaction of the furans, in particular 2,5-dimethylfuran (2,5-dmf), I describe and discuss the development of an analytical methodology that utilises infrared spectroscopy and mass spectrometry for the on-line identification and quantification of product molecules during catalytic reactions.

This on-line analysis method is then applied to the catalytic conversion of 2,5-dmf to aromatics over a range of zeolite and zeotype catalysts. In-depth studies with ammonia as a probe molecule of the catalytic active acid sites, as well as temperature programmed experiments with ammonia and 2,5-dmf give insights into product distribution, selectivity changes and deactivation of the catalyst. For example, olefins and aromatics are initially preferred products, while with increasing time on stream, the isomerisation of 2,5-dmf becomes dominant. The incorporation of Ga into the zeotype framework, resulting in a Ga-Silicate, shows how targeted catalyst design can increase overall aromatics production. This catalyst is also suitable for selective isomerisation of 2,5-dmf to 2,4-dimethylfuran, which has a rare substitution pattern. Finally, it was found that the most valuable of BTX, *p*-xylene, can be produced more selectively when 2,5-dmf is pre-adsorbed onto zeolite ZSM-5 and then released during a temperature programmed product desorption.

Keywords: Biomass conversion, Catalysis, Zeolite, Zeotype, BTX Aromatics, On-line Analysis, infrared spectroscopy, 2,5-dimethylfuran

List of Publications

This thesis is based on the following appended papers, referred to by Roman numerals in the text:

I. On-Line Composition Analysis of Complex Hydrocarbon Streams by Time-Resolved Fourier Transform Infrared Spectroscopy and Ion-Molecule Reaction Mass Spectrometry

C. Sauer, A. Lorén, A. Schaefer and P.-A. Carlsson

Analytical Chemistry 93, # 39 **(2021)**, 13187–13195

II. Valorisation of 2,5-dimethylfuran over zeolite catalysts studied by on-line FTIR-MS gas phase analysis

C. Sauer, A. Lorén, A. Schaefer and P.-A. Carlsson

Catalysis Science & Technology 12, #3 **(2022)**, 750-761

III. Isomorphous Substitution of Gallium into MFI-Framework Zeolite Increases 2,5-Dimethylfuran to Aromatics Selectivity and Suppresses Catalyst Deactivation

C. Sauer, G. J. L. de Reijer, A. Schaefer and P.-A. Carlsson

Submitted to Topics in Catalysis, currently under revision **(2022)**

IV. Accessing the 2,4-disubstition in furans: selective catalytic isomerisation of 2,5-dimethylfuran to 2,4-dimethylfuran by Ga-silicalite

C. Sauer, G. J. L. de Reijer and P.-A. Carlsson

Submitted

V. Temperature programmed experiments reveal catalyst deactivation and high *p*-xylene selectivity from 2,5-dimethylfuran over ZSM-5 zeolites

C. Sauer, P. Mestre Tosas, A. Schaefer and P.-A. Carlsson

Manuscript

My Contributions to the Publications

Paper I

I proposed the idea and was responsible for planning and performing all experimental work, except of the GC–MS analysis. I developed the FTIR/MS analysis method and carried out the calibrations. I performed all data analysis. I interpreted the results together with my co-authors and I wrote the first draft of the manuscript.

Paper II

I proposed the idea and was responsible for planning and performing all experimental work and data analysis. I interpreted the results together with my co-authors, I wrote the first draft of the manuscript.

Paper III

I was responsible for the conceptualisation, I planned and carried out the synthesis and experimental work with Guido de Rejer, I interpreted the results together with my co-authors, I wrote the first draft of the manuscript.

Paper IV

I proposed the idea, carried out the experimental work and data analysis with the help of my co-author, I wrote the first draft of the manuscript.

Paper V

I was responsible for the conceptualisation, supervised and participated in carrying out the experimental work, analysed and interpreted the results together with my co-authors and I wrote the first draft of the manuscript.

Conference Contributions

Green aromatics for a biobased economy
Christopher Sauer, Marcus Vestergren, Anders Lorén and Per-Anders Carlsson
Poster presentation at the Materials for Tomorrow conference at Chalmers
8-9 November 2018, Gothenburg, Sweden

Green aromatics for a biobased economy
Christopher Sauer, Marcus Vestergren, Anders Lorén and Per-Anders Carlsson
Poster presentation at the 26th North American Catalysis Society Meeting (NAM26)
23-28 June 2019, Chicago, USA

On-line FTIR-MS gas phase analysis of 2,5-dimethylfuran valorization over zeolites
Christopher Sauer, Anders Lorén, Andreas Schaefer and Per-Anders Carlsson
Oral presentation at the 27th North American Catalysis Society Meeting (NAM27)
21-28 May 2022, New York, USA
Financial support in form of a travel grant from Nils Philblad fond is gratefully acknowledged

On-line FTIR-MS gas phase analysis of dimethylfuran conversion over zeolites for production of green aromatics
Christopher Sauer, Anders Lorén, Andreas Schaefer and Per-Anders Carlsson
Oral presentation at the 19th Nordic Symposium on Catalysis (NSC19)
6-8 June 2022, Espoo, Finland
Financial support in form of a travel grant from Sven och Gurli Hanssons donationsfond is gratefully acknowledged

Valorisation of 2,5-dimethylfuran over zeolite catalysts studied by on-line FTIR-MS gas phase analysis
Christopher Sauer, Anders Lorén, Andreas Schaefer and Per-Anders Carlsson
Oral presentation at the 9th Tokyo Conference on Catalysis Science and Technology (TOCAT9)
24-29 July 2022, Fukuoka, Japan
Financial support in form of a travel grant from Chalmersska forskningsfonden is gratefully acknowledged

Contents

List of Figures

List of Tables

Notation

BAS	Brønsted acid site
BEA	Framework structure of zeolite **be**ta polymorph **A**
BET	Brunauer Emmett Teller
BTX	Benzene, Toluene, Xylenes
CC	Carbon capture and storage
CFP	Catalytic fast pyrolysis
CP	Catalytic pyrolysis
DACD	Diels Alder cycloaddition dehydration
dmf	Dimethylfuran
DRIFTS	Diffuse reflectance infrared Fourier transform spectroscopy
EI	Electron ionization
FFCA	furan/furfural combined with catalytic pyrolysis of lignin
FTIR	Fourier transform infrared
GC	Gas chromatography
GHG	Green house gas
GMA	Gasification methanol to aromatics
GWP	Global warming potential
HC	Hydrocarbon
IMR	Ion molecule reaction
LAS	Lewis acid site
m/z	Mass to charge ratio
mcpo	methyl-2-cyclopenten-1-one
MFC	Mass flow controller

MFI	Framework type MFI from ZS**M**-5 (**fi**ve)
MS	Mass spectrometry
MTO/A	Methanol to olefins/aromatics
NACR	Naphtha catalytic reforming
PEF	Polyethene furanoate
PET	Polyethene terephthalate
SAR	SiO_2 to Al_2O_3 ratio
TGA	Thermo gravimetric analysis
TOS	Time on stream
TP	Temperature programmed
TPD	Temperature programmed desorption
TPO	Temperature programmed desorption
XRD	X-ray diffraction
ZSM-5	Zeolite Socony Mobil-5

Introduction 1

1.1 Global challenges

The world is facing global environmental challenges that require drastic and immediate action. Rapidly increasing levels of greenhouse gases in the atmosphere causes global warming, which results in climate change that is an imminent danger – threatening the extinction of many[1].

The decade-long and ever-growing use of fossil resources for fuels, energy and chemicals has created a situation that puts millions of people and thousands of species at risk. Our own species has long challenged the planetary boundaries, that offer "a safe [known] operating space for humanity", and important boundaries have now been transgressed.[4] Humanity must instead operate societies in a safe and just corridor for people and the planet.[5] As of today, the amount of carbon dioxide (CO_2) in the atmosphere has increased from around 280 ppm since pre-industrial times to more than 420 ppm at the moment of writing this thesis. This increase can be attributed to emitting over 1.5 trillion tonnes of CO_2 since 1750, from burning fossil fuels and land use change, e.g. deforestation.[6][1] As a result, the global mean temperature has risen by 1.2 °C. In the Paris Agreement of 2015, most countries have pledged to keep this temperature increase "well below 2 °C". But even with today's pledges and targets,[2] this goal seems out of reach.[6–8] The increasing temperatures themselves and the induced sea level rise and extreme weather phenomena, such as droughts[9] put hundreds of millions, if not billions of people at risk.[3] Not only humans, but thousands of other species are also threatened. Besides climate change, their populations and habitats are endangered by increased human land use, such as urban expansion[1, 10–13]. These factors reach so far that some experts discuss if the world is heading towards a 6th mass extinction.[14] But this can be prevented. By changing human behaviours, our currently highly polluting economies can be transformed into circular and sustainable economies. This necessarily includes a rapid phase-out of fossil resources and net zero commitments, so that global warming could be limited to below 2 °C.[15] Besides using renewable solar and wind for this transformation, biomass has emerged as a praised candidate with the potential to solve many of these problems. However, the use of biomass, especially for energy needs has to be approached with great care, because understanding scale and impacts on sustainability are highly complex with both positive but also negative implications.[16]

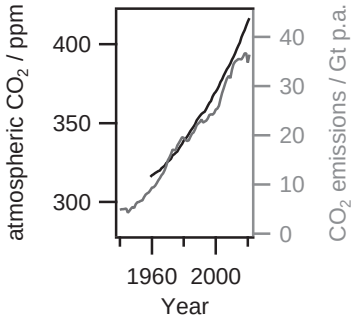

Figure 1.1: Carbon dioxide levels in the atmosphere (black)[2] and emissions per year (grey)[3] in the last decades.

1: For example in 2019, 36.70 and 3.83 billion tonnes of CO_2 were emitted from fossil fuels and land use change respectively.[6]

2: not even policies and laws. Not achievements either

3: Such risks are flooding, sea level rise, droughts or wet bulb temperatures above 32 °C.

1.2 Why we cannot afford to burn biomass

A growing demand for biomass to cover energy needs in form of wood chips, food waste for biogas, as well as biofuels has emerged. But biomass also faces increasing demand for materials needs such as timber for building materials, cellulose for bio-based materials, bio-based plastics and bio-based value-added chemicals. This shift of feedstock, from fossil to biomass-based is also known as biorefinery.[17] The International Energy Agency predicts a growing demand for biofuels of 28% within the next five years. Before addressing what one *can* do with bio-derived molecules, one first needs to discuss what one *should* do with biomass. In the following, I, therefore, go through different demands on biomass utilisation such as GHG mitigation, energy, food, conservation, and bioeconomy products.[18]

The first questions that come to mind, might ask if there is enough biomass in the world to fulfil the demands[19, 20] and how biomass sustainability should be defined[21]. A large part of biomass is obtained from forests in form of wood.[22] Utilising this source for energy and materials is not competing with food production in contrast to most biomass from agriculture. In fact, it might be necessary to restore agricultural land to forests, natural grazing lands and swamps, which are considered carbon sinks themselves, but even these efforts are at risk in a warming climate [23]. Besides storing carbon, forests and other natural lands provide many ecosystem services.[24] For instance, they provide a home to many species and are thus central biodiversity hubs. In fact, these ecosystems need to be better protected from human intervention to prevent further habitat loss and to meet our sustainability goals for biodiversity.[10, 25]

The second question relates to indigenous people, who have used these natural landscapes for centuries and whose way of living depends on intact ecosystems, which industrial forestry threatens. One such example is Sámi communities in northern Europe and their reindeer husbandry.[26, 27]

These combined considerations lead to calls for the conservation of at least 30% of our land (and seas) in a "global deal for nature".[28] This is also the aim of the European Commission in perspective of the upcoming 15th meeting of the Conference of the Parties to the Convention on Biological Diversity (CBD COP 15)[29].[4]

4: Immediate action is necessary if the loss of wildlife is to be reverted. Global wildlife populations have plummeted by 69% on average since 1970.

Moreover, it needs to be ensured, that the remaining land is used in a sustainable way. This is unfortunately not the case today. Biomass production is suspect to a lot of problems. Deforestation[30] and illegal logging in protected areas even within the EU, where ancient forests are sacrificed to make wood pellets for energy conversion[31]

are among these problems. Such forests, and the ecosystem they host, cannot just be regrown and are hence not renewable on a short timescale. Ineffective law enforcement and controls, as well as required ecological assessments rarely being carried out dilute sustainability efforts that are made on paper. But even when such assessments are made and companies gain sustainability certificates, for example from the Forest Stewardship Council (*FSC*), they cannot always guarantee that sustainability promises are kept.[32] Industrialised forest-agriculture for intensified production also leads to biodiversity loss and reduced ecosystem services, because large areas resemble tree plantages of same-aged monocultures rather than natural forests.[24] This is a result of clear-cutting vast areas with heavy machinery because it is economically more attractive. Such practices are common worldwide[33] and within Europe, Estonia,[34] Romania,[31] and Sweden[35] (see Figure 1.2). In the latter, progress has been made since the 1970 and 80s, but environmental goals are still far from reached.[5]

Most importantly, one needs to clearly understand if bioenergy is carbon neutral at all. Many interest groups, especially those in the forest and bioenergy sector advocate the use of bio-derived energy as carbon neutral because the emitted carbon stems from biomass that has previously absorbed CO_2 from the atmosphere. This assumption might hold in a macro perspective over centuries, but it is questionable, in a time scale that matters for urgent climate change mitigation within the next years and decades. Although the use of bioenergy could reduce overall CO_2 emissions in certain cases, if compared to fossil fuels, they are not carbon neutral.[37, 38] This is partly because it takes time until the emitted CO_2 is absorbed again and greenhouse gas potential is dependent on the sequestration cycle and its time scale. One metric is the global warming potential of biogenic CO_2 (GWP_{bio}). Some examples: "GWP_{bio} factors ranged from 0.13–0.32, indicating that biomass could be an attractive energy resource when compared with fossil fuels." However, "By considering the GWP_{bio} factors and the forest carbon change, the production of ethanol and bio-power appeared to have higher GHG emissions than petroleum-derived diesel at the highest GWP_{bio}."[39] The International Council on Clean Transportation finds in their carbon assessment that accounts for GWP_{bio} that "Category III, including bioenergy from whole trees via forest thinning, RIL, and short-rotation temperate forestry, offers no GHG savings over 30 years." and "Category I, which includes bioenergy from agricultural residues and energy crops, is expected to deliver at least 50% carbon savings with a maximum 10-year payback period. Category II consists of bioenergy from forest residues, offering some GHG savings depending on the choice of bioenergy production pathway, with payback periods up to 25 years. Provided that soil carbon loss is minimised, slash can deliver

5: For example, only 9% of Swedish forests are formally protected with another 5.6% of voluntary contributions.[36]

Figure 1.2: A recently clear-cut area in southern Sweden. In the background a field of mono-aged trees. Own courtesy.

greater than 50% GHG savings for ethanol pathways."[40] The International Panel on Climate Change estimates GHG emissions of biomass for energy use to be 230 g_{CO2eq}/kW/h, which is far above that of other renewables.[6][38]

6: For example: 11 g_{CO2eq}/kW/h for wind, 24 g_{CO2eq}/kW/h for hydro, 38 g_{CO2eq}/kW/h for geothermal and 45 g_{CO2eq}/kW/h for solar respectively.[38]

If biomass for energy use is not a good alternative, how can it be utilised to mitigate climate change instead? Besides the already mentioned increased dedication of land to habitat restoration, and natural carbon sequestration, the remaining use of biomass, must store the already absorbed carbon long term to be most effective. This means it must not be allowed back into the atmosphere. For example, forest biomass can be used increasingly to produce timber and logs as building materials. Whole timber cities could store huge amounts of CO_2.[41] Residues from timber production should however not be burned. They could be utilised, besides agriculture residues from food production for other materials, such as paper, bio-based plastics and chemicals. However, even for those materials, circularity must be ensured, so that at the end of their life cycle these products are preferably reused, up- or recycled[42] and not incinerated for energy recovery (see also Figure 2.3).

In summary, there are various demands on biomass that limit its use. These demands include ecosystem services for increased conservation, local communities and climate change mitigation.[37] The latter makes the most effective use of biomass if it ensures long-term sequestration, which excludes or at least strictly limits the use of biomass for fuel and energy. Instead, the sustainably available biomass should be used for the production of timber, bio-based materials and chemicals. In other words, if one can make high-value chemicals instead of fuels, that is a good incentive not to burn biomass.

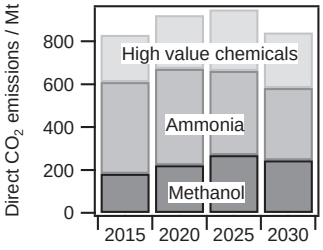

Figure 1.3: Direct CO_2 emissions for primary chemicals in the IEA net-zero scenario.[43]

1.3 This thesis in perspective of the global challenges: sustainable feedstocks for the chemical industry

With the hindsight of a net zero emission goal in 2050, the demand for primary chemical production is expected to increase significantly.[43] At the same time, also the chemical industry must reduce its emissions (compare Figure 1.3). In contrast to the energy sector which can be decarbonised, the chemical industry cannot be decarbonised.[7] This is because many chemicals are in itself carbon-based, such as plastics and solvents. The chemical industry thus needs renewable feedstocks that are carbon-based. For this, three main sources are available. Carbon dioxide, plastic waste and biomass.

7: that means removing all carbon energy carriers, such as coal, oil, gas and biomass and switching to electricity or hydrogen.

Ultimately, humanity needs to remove CO_2 from the atmosphere and sequester it for a long time. A good way to use CO_2 would be to transform it into highly valuable chemicals. However, carbon capture utilisation is not yet practically feasible at a large scale and its future growth is highly uncertain[44]. Even though there have been many ideas on how to utilise CO_2 for organic synthesis[45], these rely on carbon capture from concentrated CO_2 sources.[46]

today CO_2 emissions from fossil resources or biomass

Plastic waste is another main source of pollution and its increased use as source material for future up- and recycling is highly desirable.[42, 47] Thanks to increased pollution awareness [48] and strong research interest, this field has attained a lot of attention and is now quickly moving forward,[49–53] with large recycling plants planned for future operation[54]. In fact, plastic waste should be prioritised as the main source for making new plastics and chemicals encouraging a circular economy, before using alternative virgin feedstocks.

Biomass is the third available feedstock and its use for the chemical industry makes sense where demand cannot be fulfilled by existing waste, or where recycling is yet not possible. With respect to the overall growing demand for commodity chemicals, another virgin source might anyway be necessary. Here, biomass can play an important role to reduce the use of fossil resources quickly. It also offers the potential to reuse already existing production plants and avoid stranded assets.[55] Lastly, the chemical complexity already existing in biomass molecules can be preserved when making chemicals. This can be an advantage over using C_1 building blocks, where it is necessary to transform CO_2 to methanol and then methanol to olefins and aromatics[56] (MTO/MTA) or Fischer-Tropsch synthesis.[57] Simple molecules can be easier obtained from CO_2 and used as fuels instead, whereas complex biomass molecules should be made into complex chemicals and materials.

1.4 Motivation of the thesis: Utilising renewable bio-derived feedstocks for the production of commodity chemicals

The utilisation of biomass for the production of commodity chemicals has been identified as a way to replace fossil feedstock. However, biomass requires some pre-treatments before high-purity chemicals can be obtained. These treatments include the extraction of bio-derived molecules, transformations and refining. They can be physical, in form of drying, milling, chipping, pelleting etc., chemical, in form of hydrolysis, solvation etc. or biological, in

form of biochemical and enzymatic processes.[58, 59] These pre-treatments are not an easy undertaking and are the subject of many studies, which go beyond the scope of this thesis. In the following, I narrow the scope on how a certain type of bio-derived molecules called furans, can be utilised for the *catalytic* production of only certain types of commodity chemicals: the aromatic target molecules benzene, toluene and xylene (BTX). The molecules of interest are introduced in the next chapter. I then discuss how they can be efficiently obtained.

Chemicals of interest and how to produce them

2

BTX aromatics are important platform molecules and commodity chemicals. In the following, I discuss their importance in the chemical industry and how they can be produced from bio-derived furan molecules. I introduce furans and briefly describe how they are obtained from cellulosic biomass. I give a short perspective on the techno-economic analysis of BTX production. Then I explain what role catalysis plays in the efficient production of aromatics from furans. Finally, I define the research problem and the objective of this thesis.

2.1 The chemicals of interest

2.1.1 Target products: Aromatics

To make an effective impact on the chemical industry, it is important to ask which molecules should be targeted. Benzene, toluene and xylene aromatics have been chosen as target molecules for this thesis because they are one of the most important commodity chemicals. Together they make up more than one-quarter of primary petrochemical consumption, after ethene, propene and methanol.[60] Nowadays, BTX are almost exclusively produced from fossil fuels via petroleum refining and catalytic reforming.[61]More than 12 Mt per year are produced in Europe alone [62].The estimated market value in 2018 was $186 billion with growing future demand.[63, 64] Table 2.1 shows market volumes and commodity prices for BTX, of which *p*-xylene is often named the most valuable.

Their huge production output is because BTX are used as solvents and fuel additives as well as precursors and building blocks for fine chemicals and many polymers like polystyrene, nylon, polyurethane and polyethene terephthalate (PET).[69] Some of the most important products derived from BTX are shown in Figure 2.1.

Table 2.1: Prices and global market volume (MV) of BTX as of September 2022.[65–68]

	Price / $/t	MV / Mt
Benzene	828	60.2
Toluene	1067	30.7
Xylenes	1082	61.0

2.1.2 Model platform feedstock: Furans

Using biomass for research purposes can be challenging because of its complex nature. To understand the behaviour of individual molecules, one might initially rely on simplified systems. Furans and furfural, which are 5-membered cyclic carbohydrates, are great candidates for several reasons:

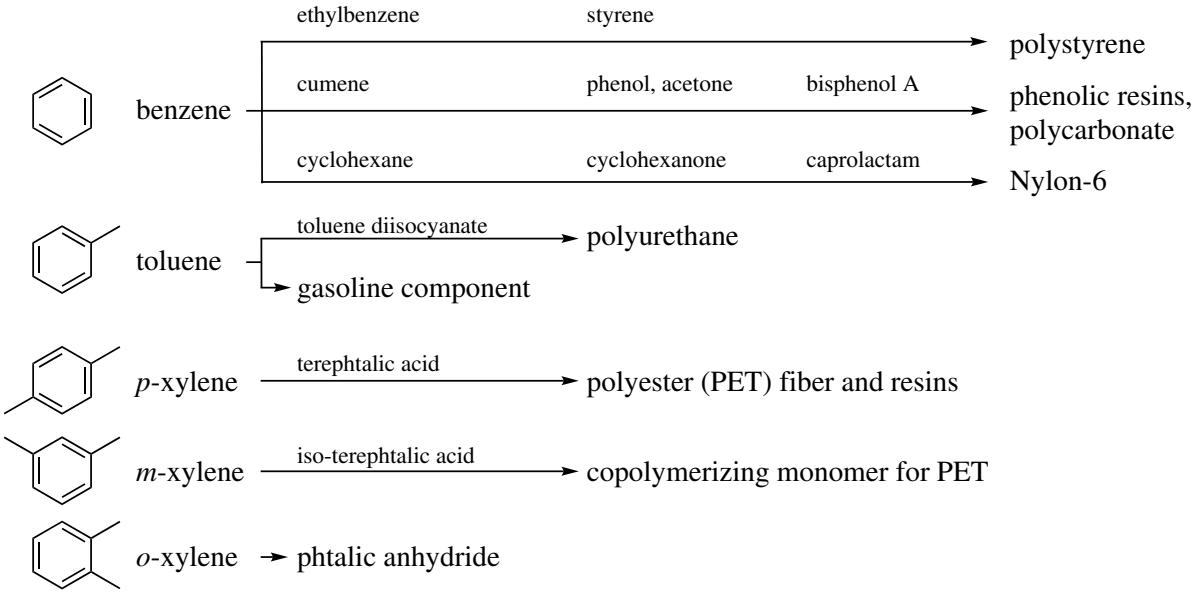

Figure 2.1: Illustration of benzene, toluene, *p*-, *m*- and *o*-xylene and some of their main derived products.

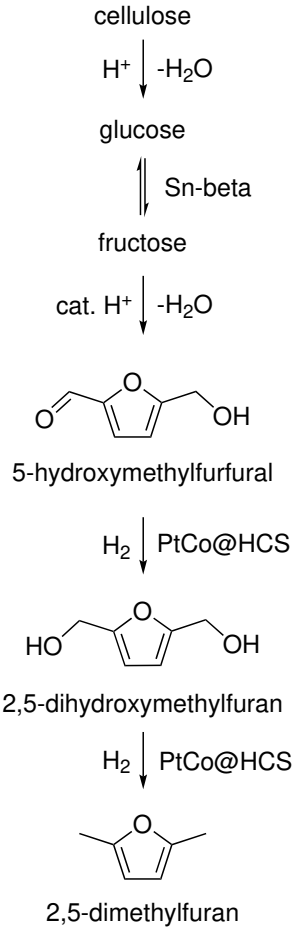

Figure 2.2: Established pathway to 2,5-dimethylfuran. [70–73]

First, they have been identified as important platform molecules, from which many other compounds can be obtained and incorporated into the existing production processes.[74, 75] They can be obtained from (ligno)cellulose biomass. They can further work as model compounds to represent a simplified biomass feedstock. Finally, they offer the potential to be converted to aromatics via Diels-Alder cycloaddition reactions highly selective way.[76] Another reason to study furans is the potential use of furan dicarboxylic acid, which is a very promising candidate to replace xylene-based polyethene terephthalate (PET) to make furan-based poly ethylene furanoate (PEF) instead.[77] This would potentially eliminate the necessity to make *p*-xylene for PET production in the first place. For now, PET is the state of the art and xylene demand is growing, but this might change quickly in favour of PEF in the search for even more sustainable pathways.[78] The inevitable chemical recycling of PEF requires also knowledge of the furan building blocks and their interactions with the catalyst.

Out of several furans, I have chosen 2,5-dimethylfuran as my model compound. For one reason, it is the least toxic to work with. For another, it has the potential to be converted to *p*-xylene selectively.[79] Figure 2.2 shows one route of how 2,5-dmf can be obtained from biomass. First, depolymerisation and hydrolysis of (hemi)cellulose release the monomeric building blocks, such as the monosaccharide glucose. The latter is isomerised to fructose via enzymatic or heterogeneous catalysis e.g. using Sn-beta.[71] Fructose is then converted to 5-hydroxymethylfurfural.[72] Finally,

hydrodeoxygenation of the latter with platinum-cobalt bimetallic carbon nanospheres yields 2,5-dimethylfuran with a 98% selectivity.[73]

2.1.3 The chemicals in perspective: Techno-economic analysis

To put aromatics production further into perspective, I briefly discuss some techno-economic analyses. I look at the greenhouse gas (GHG) emissions of aromatics production from fossil fuels, methanol and biomass and discuss the potential reduction in GHG emissions. The economic viability is discussed based on product prices and estimates and I point out what that means for the necessary progress to succeed.

In a recent study, GHG emissions for aromatics production via crude oil-based naphtha catalytic reforming (NACR) were found to be 43.4 and 43.9 tCO_2eq/t aromatics with and without carbon capture and storage (CCS).[80] Besides the gasification of methanol to aromatics (GMA), several other biomass routes were evaluated. Here, I only comment on two more: catalytic pyrolysis (CP) and Diels-Alder of furan/furfural combined with catalytic pyrolysis of lignin (FFCA). The GMA process produced 3.27 and $-6.08\,t_{CO_2eq}/t$ aromatics including CCS.[1] CP was found to have 0.82 and $-3.82\,t_{CO_2eq}/t$ aromatics (CCS). Finally, the evaluated FFCA process had emissions of 6.33 and $-1.07\,t_{CO_2eq}/t$ aromatics (CCS).[80] Compared to fossil resources, biomass feedstocks always show lower GHG emissions, especially when combined with CCS. In that case, GMA has the most potential with the highest storing capacity (negative emissions) as summarised in Table 2.2. However, as discussed before, where readily available and necessary, bio-based methanol could be readily used as a fuel, while other biomass should be converted into chemically more complex aromatics. Further, only CP showed negative emissions in the case study without CCS. All the studied biobased routes are for now hypothetical, except for the CP route, which has a pilot plant running.[81]

1: Negative emissions mean, they are *net* negative, in other words, they reduce CO_2 in the atmosphere.

Route	GHG e./ t_{CO_2eq}/t_{BTX}		total GHG e.
	no CCS	CCS	/ Gt_{CO_2eq} p.a.
NACR	43.4	43.9	0.67
GMA	3.27	−6.08	−0.09
FFCA	6.33	−1.07	−0.02
CP	−0.82	−3.82	−0.06
difference			
NACR–CP	44.22	47.72	0.72

Table 2.2: GHG emissions of BTX and saving potential if all 151.9 Mt BTX of 2022 were made from biomass via CP.[80]

With the above-reported numbers, it is possible to calculate a potential annual saving in GHG emissions, if all aromatics were made from biomass. Assuming that in 2022 a total of 151.9 Mt BTX aromatics were produced (compare Table 2.1) and these were made from a fossil feedstock (NACR), this results in a total of 0.66 Gt_{CO_2eq} of GHG emissions per year. With the use case of CP, one could have net negative emissions of 0.058 Gt_{CO_2eq}. If the total production of aromatics from fossils is replaced by CP of biomass and CCS is applied, that could save 0.71 Gt_{CO_2eq} per year. That is approximately 1.8% of the annual global 40 Gt_{CO_2eq} in GHG emissions or comparable to Germany's yearly emissions. To harvest the full potential of long-term carbon sequestration, sustainability efforts must also ensure that the intrinsic carbon in aromatics and their derived products is not released back into the atmosphere, for example by incineration and energy recovery, which is among the least favoured in the waste hierarchy (see Figure 2.3).[82, 83] Instead, a circular economy from the end products must be established.

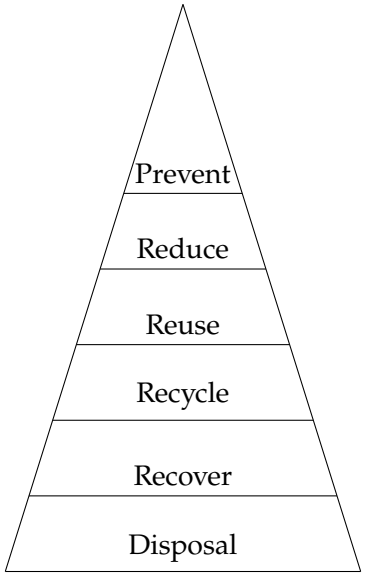

Figure 2.3: Waste hierarchy, from top to bottom: most favoured least favoured approach of treating waste.[82, 83]

As of now, none of the biomass to BTX routes was found to be cost-competitive.[80] For example, the production of BTX from fossils via NACR costs 1077 \$/t aromatics (not considering valuable by-products), whereas various biomass routes based on different biomass feedstocks, had widely varying production costs, from ca. \$1500 to more than \$5000, with most cases around \$2000.[57, 80] One way to increase cost competitiveness for biomass routes and thus stimulate more sustainable production is by enabling higher BTX selectivities and yields in the production processes. Catalysis plays an important role in increasing these parameters, and improving the catalysts is crucial for efficient conversion processes.

2.2 The route to efficient chemical production: Catalysis

Approximately 80-85% of all products in the chemical industry are made via catalytic processes.[84] In fact, the role of catalysis in the world has been tremendous. The invention of the Haber-Bosch process to produce ammonia from nitrogen and hydrogen to make fertilisers, for example, was the main contributor (praise or blame – pick your side)[2] to the rapid growth of the global population.[85] Catalysis is so important because it helps reduce energy consumption and the formation of undesired waste products by increasing selectivity and overall efficiency. In that way, catalysis is a powerful tool to contribute to rapid change. It has to be acknowledged that this tool has contributed to rapid climate change by enabling the

2: The efficient and thus cheap production of artificial fertiliser prevents us from starvation through increased farming yields. But because this fertiliser is not used effectively, humanity has exceeded the biogeochemical flow boundary of nitrogen, with devastating consequences on nature and ourselves.[4]

efficient large-scale use of fossil fuels. But catalysis can also be the tool that helps cut down pollution and mitigate climate change.[3]

In a catalysed reaction, the catalyst is a material that accelerates the chemical reaction. This happens by providing an alternative path compared to the uncatalysed chemical reaction. In the latter, the reactants have to collide with sufficient energy to overcome an energy barrier E_a as shown in the blue curve in Figure 2.4 The change in potential energy between reactants and products is the change in enthalpy (ΔH).

For heterogeneous catalysts, the catalysed reaction, on the other hand, starts with an adsorption step of the reactant(s) on the catalyst surface, on the so-called active site. Here, the products are formed, again by overcoming an activation barrier which is, however, significantly lower than that of the uncatalysed reaction. In a final endothermic step, the product(s) separates from the catalyst. In this whole process, the catalyst remains unaltered and is available for catalysing the next cycle. In contrast to the uncatalysed reaction, an alternative pathway is offered by introducing several elementary steps. This path is more complex but energetically favourable due to the reduced activation barrier. The overall change in free energy is however the same. This means, that the catalyst accelerates the reaction rate kinetically, but does not change the equilibrium of a reaction, *i.e.* the thermodynamics.[84]

Even the production of BTX aromatics from biomass is a catalysed process. When focusing on furans as starting materials, two approaches are pointed out:

The first is catalytic fast pyrolysis (CFP). Here, the biomass or furan feedstock is rapidly heated, vaporised and then directed to a catalyst bed, where it reacts at high temperatures. The products include the desired aromatics, but also olefins, carbon oxides, water and coke.[88, 89] Reaction pathways and chemical mechanisms are complex, because many different cracking, oligomerisation, aromatisation, isomerisation, decarbonylation and dehydration reactions are taking place.[90] This process can usually be operated continuously in the gas phase and at low pressures, which is advantageous for large-scale production. However, aromatic yields are rather low.

The second approach is based on a Diels-Alder reaction followed by a dehydration reaction. This is a thermally allowed [4+2]-cycloaddition between a diene, such as a furan, and a dienophile, such as an olefin, to form a bicyclic intermediate called oxa-norbornene. This intermediate is dehydrated to form the six-membered aromatic ring. It was found that the cycloaddition reaction can be catalysed by Lewis acid sites (LAS) but not by Brønsted acid sites (BAS).[91] The dehydration reaction can be

3: To become inherently sustainable, the catalysis community needs to consider taking a more holistic approach: by working closely together with life cycle analysis, toxicology, ecology and social science.[86]

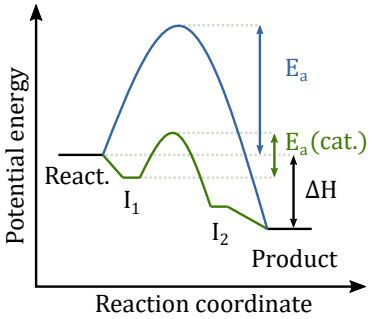

Figure 2.4: Schematic energy diagram for a catalysed and non-catalysed reaction, where E_a is the activation energy, ΔH is the enthalpy and I a reaction intermediate.[84, 87]

catalysed by LAS but even more by BAS. Yields of more than 90% of *p*-xylene have been achieved with different catalysts.[76, 79, 92] However, reaction conditions usually require a high-pressure batch reactor, and a solvent, such as *n*-heptane and take many hours to complete, which is unfavourable for large-scale production.

In both cases, zeolites have been promising candidates as catalysts.[4] It seems hence compelling to combine the advantages of the CFP continuous process, with the selective production and high yields of the cycloaddition and dehydration process. If and how this can be achieved is the topic of the following sections and chapters.

4: More about zeolites in section Section 4.1.

2.3 Defining the research problem

2.3.1 A new feedstock

In the previous chapter, biomass was introduced as a better feedstock in the chemical industry to shift to a renewable and potentially sustainable source. Furans were identified as model and platform molecules and are the focus of this thesis, and 2,5-dimethylfuran was chosen as the main reactant. Compared to fossil feedstocks, which have been used for many decades and are well known, the scientific understanding of biomass and bio-derived molecules is not as advanced. This is a challenge when it comes to analysing the feedstock and its reaction products, but also for designing catalysts that suit the specific needs of the new feedstock.

2.3.2 The need for better catalysts

As discussed above, catalysis can be the solution to efficiently use bioderived molecules for chemical production. In this specific case, 2,5-dimethylfuran should be catalytically converted to the target products: the aromatics BTX. To make BTX production from renewables viable and competitive, better catalysts are necessary. Zeolites and their derivatives are promising candidates, because of their tunable Lewis and Brønsted acidity, shape selectivity and stability. Under continuous production, selectivity and yields of BTX products are rather low and the catalyst experiences deactivation due to coking. It can be attributed to not well enough understanding of the underlying processes, chemical reactions and reactant-catalyst interactions, which shall be investigated in this thesis.

2.3.3 The need for analytical methodology

To understand the above-mentioned chemical reactions, analytical tools and methodologies are necessary. Often these are not well adapted for new bio-derived feedstocks. In this particular case of catalysis research, it would be desirable to track reactants and products of the reaction stream in high time resolutions. This will help to understand reactant-catalyst interaction, changes in product distribution and selectivity, and deactivation and ultimately help make conclusions on how to design better catalysts. The focus of this thesis is the use of Fourier Transform infrared spectroscopy (FTIR) and mass spectrometry (MS) for the on-line analysis of the hydrocarbon stream because they can readily be operated at high time resolutions and are established tools in related fields.

2.4 Objective of the thesis

According to the above described research problems, the objective and scope of the thesis can be clarified: This thesis aims to improve the understanding of how to produce BTX aromatics from bio-derived feedstocks catalytically by using on-line analysis. The tools for the on-line analysis focus on FTIR and MS. The feedstock is limited to the model compound 2,5-dimethylfuran and the catalysts are limited to zeolites and zeotypes of the MFI and BEA framework structure. The objective guides this thesis based on the following three hypotheses:

Hypothesis I: IR spectroscopy in combination with mass spectrometry is a suitable and practical technique to monitor a complex hydrocarbon stream.

Hypothesis II: The developed method can be applied to catalytic conversion reactions of 2,5-dimethylfuran for a number of known zeolite catalysts.

Hypothesis III: The method improves understanding of the reactions and catalysts that is necessary to ultimately design better catalysts.

Developing a Methodology: On-line gas composition analysis for complex hydrocarbon streams

3

This chapter guides the reader through the development of a method that shall allow the continuous on-line analysis of a complex hydrocarbon stream and aims to answer hypothesis I in Section 2.4. This complex product stream stems from the catalytic conversion of 2,5-dimethylfuran and the method presented in this work is limited to the conditions described herein. However, the principles that are presented are general and the analytical method can with certain adjustments be applied and extended to a wide range of scenarios. In the following, some concepts are described that are necessary for understanding the instrumentation, development process, and product analysis. Challenges, limitations, and advantages are discussed and comparisons to other analytical methods are made.

In perspective to my research papers, this chapter is mainly related to Paper I, and in parts to Paper III and V.

3.1 A short introduction to product analysis

One of the main challenges in catalysis science is the evaluation of catalyst performance. Often, the performance of a catalyst is then expressed in terms such as conversion, selectivity, yield, turnover number and turnover frequency.[93] In order to assess how a catalyst performs, it is necessary to analyse the reactant and reaction products, which means identification **and** quantification. Useful methods are also crucial to understand the involved chemical reactions and mechanistic pathways. This knowledge in combination with a deep comprehension of the catalyst structure is required to rationally develop catalyst functions.

In the following, some commonly applied techniques that are relevant to this thesis are introduced.

3.1.1 Gas Chromatography

In the specific case of converting furans to aromatics, product analysis is commonly based on sample collection, separation and subsequent analysis. In a continuous flow setup, light gaseous products can for example be captured in gas bags, whereas heavier molecules are collected in a cold trap. The collected sample is then transferred to an analytic instrument for separation, most

commonly a gas chromatograph coupled with a detector for specification and quantification. This procedure is often manual and requires on-site personal.[94–96]

The gas chromatography (GC) technique is used for the separation of compounds that can be vaporised. The principle is based on carrying sample molecules in a *mobile phase*[1] through a stationary phase. The latter can be a glass or metal tube with microscopic layers of liquid or polymer fastened on a solid support. Molecular interactions of the species in the mobile phase with the stationary phase such as dipole and *Van der Waals* forces lead to a separation of different species in the mobile space. How well the species are separated is determined by the strength of these forces, which depend on the physical and chemical properties of the species and the stationary phase. This means that one type of species is remaining longer in the stationary phase than another type of species, which is known as the retention time. The retention times can be used to analyse the specimen by comparing them to calibration standards.

1: Usually an inert or non-reactive gas such as He or N_2.

Another way to analyse the specimen is to couple GC with a detector for identification and quantification. The flame ionisation detector (FID) and the thermal conductivity detector (TCD) are among the most common ones and are sensitive to a wide range of compounds. GC can also be coupled to a mass spectrometer, which is known as GC-MS, a highly effective technique that is sensitive even to trace amounts of sample.

The detection limit is a strength of GC-based analytical methods. Further, the separation-based operation makes GC a superior technique when it comes to the identification of species in a mixture. At the same time, the measurement principle is also responsible for its limitations in many applications: the time resolution. Sample collection and separation are inherent to making this technique rather slow and labour-intensive. In response, on-line GC–MS has been developed to study the conversion of furans to aromatics over zeolites.[97–99] The on-line approach allowed automated sample collection and an increase in sampling time. However, the time resolution is still limited to several minutes. The rather low time resolution is inherent to separation-based methods and it is of particular interest to circumvent this disadvantage to enable studies of dynamic processes, e.g., composition variations in process streams and catalyst activity, selectivity, and fast deactivation phenomena.[100] It would further be advantageous to automate the on-line product stream monitoring.

Both MS and FTIR spectroscopy can conveniently operate in the order of seconds. However, both come with their own challenges that are discussed in the following.

3.1.2 Mass Spectrometry

Mass spectrometry is widely applied for the identification and monitoring of pure samples and complex mixtures. Because MS uses a vacuum, the sample needs to be vaporised if not already in gas form. The gaseous sample molecule is then ionised to form charged particles. For ionisation, several techniques exist, resulting in a parent ion and depending on the ion source, a range of fragments. Electron ionisation (EI) applies an electron beam to the sample. The comparably high energy of the electron beam can break chemical bonds, leading to a high degree of fragmentation of the sample molecules, making it a hard ionisation technique. The generated ions are then directed through an analyser where they are selected depending on their mass-to-charge ratio (m/z). The mass selection is based on the interaction of the ions with an applied electric field.[2] The selected ion is finally directed to a detector, such as a Faraday cup or a secondary electron multiplier. Here, the ions induce a charge or produce a current, so that the intensity of each ion is recorded. The intensity of different m/z ratios results in a mass spectrum, which can be compared to databases for the identification of the species. This is especially useful for pure compounds, where a high fragmentation pattern can be utilised because the fragmentation pattern is specific for each molecule. On the other hand, many fragments make the analysis of mixtures extremely difficult, especially when different specimens have the same m/z ratio resulting in complex mass spectra with overlapping signals.[87]

2: Various methods for mass selection exist, among them, time-of-flight, sector field, quadrupole, octopole and ion trap mass filters.

When less fragmentation is desired, other ion sources, usually referred to as soft ionisation, are available. Among these are chemical ionisation techniques, such as ion molecule reaction mass spectrometry (IMR-MS). In a separate chamber, a primary atomic gas (G) is ionised via EI to form a primary ion, which is then directed to the sample stream. Here, the primary gas ion (G^+) reacts with the sample molecule (A) to produce a sample ion A^+ via a charge transfer ion-molecule reaction as described in Equation 3.1.[101]

$$G^+ + A \rightarrow G + A^+ \qquad (3.1)$$

Since the primary ions have much lower energy compared to EI, fewer bonds in the sample molecule break upon impact with the primary ion. The obtained fragmentation pattern is thus less complex. Further, because the ionisation potential of the sample molecule must be lower than the ion energy of the gas ion, different sample molecules can be selectively ionised with different primary gas ions. In this work, an IMR-mass spectrometer (V&F Airsense Compact) is used for the on-line analysis of the complex HC stream and for desorption experiments. This instrument offers Hg, Xe or Kr as primary ions.

Table 3.1: Ion potentials of different gases used in IMR-MS compared to EI.

Ionizer	ion. potential /eV
EI	70
Kr	14.00
Xe	12.13
Hg	10.44

Example: Krypton ions (14.0 eV) can separate N_2 (15.6 eV) against CO (13.7 eV) on mass 28.[102]

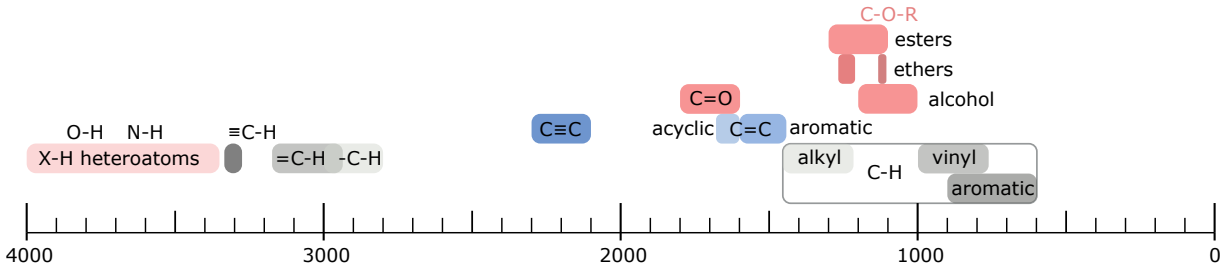

Figure 3.1: Characteristic infrared frequencies of functional groups in organic molecules containing C, O, N, X and H atoms.[107] Reproduced from [87].

3.1.3 Infrared Spectroscopy

IR spectroscopy is another analytical technique that is widely used in analytical and physical chemistry. It is readily applied for the quantitative analysis of hydrocarbon mixtures[103, 104] and as a process analytical tool in the chemical industry[105]. The principle of IR spectroscopy is the measurement of the interaction of infrared light with matter by absorption (or transmission), reflection or emission. Molecules absorb frequencies of light that are characteristic of their structure. Absorption occurs when the frequency of the incident light matches the frequency of the molecular vibration or rotation, which is called resonant frequency. Their energies are affected by the molecular potential energy surface, the mass of the atoms in the chemical bond, and the associated vibronic coupling. These energies are expressed in wavenumbers[3] μ and the infrared spectrum is commonly divided into three regions.[4] Here, I only focus on the mid infrared region, because this is where many functional groups have their characteristic absorption bands. These absorption bands are a result of the vibrations in chemical bonds, which can be described as a harmonic oscillator and have several vibrational modes.[5] As an example, the six normal vibration modes of the CH_2-part of a CH_2R_2 molecule are shown in Table 3.2. An IR active (i.e. observable) vibrational mode must include a change in the dipole moment.[6] IR spectroscopy is thus not suitable to monitor some atoms or molecules, such as hydrogen, nitrogen, oxygen, or argon.

Table 3.2: Presentation of the 6 normal modes of vibrations for the CH_2-part of a CH_2R_2 molecule. Reproduced from [87].

Symmetric	Antisymmetric
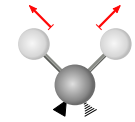 Stretching ν_s	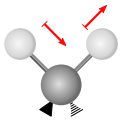 Stretching ν_{as}
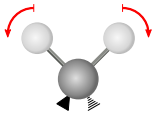 Scissoring δ	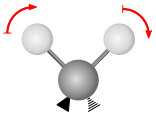 Rocking ρ
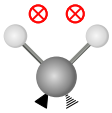 Wagging ω	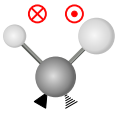 Twisting τ

3: the reciprocal of the wavelength

4: near infrared 4000 cm^{-1} to 12 500 cm^{-1}, mid infrared 400 cm^{-1} to 4000 cm^{-1}, and far infrared region 10 cm^{-1} to 400 cm^{-1}.

5: The number of vibrational modes for a molecule with N number of atoms is 3N – 5 for linear and 3N – 6 for non-linear molecules.

6: Example: N_2 is not IR active while H_2O has 3 degrees of vibrational modes.

Some of the typical group frequencies corresponding to characteristic functional groups are summarised in Figure 3.1.[106] The scope is limited to organic molecules consisting of H, C and O-atoms, but the illustration still shows the complexity of IR-spectroscopy. While the identification of pure molecules based on their unique combination of absorption bands is not always trivial but commonly used, the analysis of a mixture of many different molecules is, however, challenging and requires tedious selection, comparison and deconvolution of the absorption bands.

To quantify the abundance of a molecule, one can rely on the

relationship of absorbance A and concentration c as defined in the Beer-Lambert law. Absorption is usually expressed as absorbance A and is derived from the logarithm of reciprocal transmission (or reflectance) as denoted in Equation 3.3. The transmission T is defined as the fraction of intensity of the incident light I_0 and the transmitted (reflected) light I in Equation 3.2. The magnitude of the absorbance is approximated by the Beer-Lambert law in Equation 3.4, where ϵ is the molecule-specific attenuation coefficient, l the sample thickness and c the sample concentration. From this equation, a linear relationship between the absorbance and the concentration is evident. Hence, the concentration of a sample species can be obtained by measuring its absorbance.

$$T = \frac{I}{I_0} \tag{3.2}$$

$$A = \log_{10} \frac{1}{T} \tag{3.3}$$

$$A = \epsilon l c \tag{3.4}$$

3.2 Developing the on-line analysis

To reach the aim of analysing the effluent stream of catalytic conversion of 2,5-dimethylfuran on-line, several different methods had to be combined. From the initially obtained IR spectra, many of the species present could neither be identified nor quantified by the IR spectra alone. The first reason is that the simultaneous presence of many different compounds makes the corresponding IR spectrum very complex. The second reason is that reference spectra and calibrations for speciation and quantification for some of the compounds are not part of the commercial compound library or not even available as reference spectra in the open literature. For example, in the case of 2,4-dimethylfuran and **2**-**m**ethyl-2-**c**yclo**p**enten-1-**o**ne (2-mcpo), the very first mid-IR spectra are reported, to our best knowledge, in Paper I.[100] From previous studies of the catalytic conversion of furans over zeolites it is known, that a wide range of products is obtained. These include carbon oxides, water, alkanes, and alkenes as well as aromatics including hetero- and polycycles, such as BTX, indene and naphthalenes.[90, 94, 97] Since many of these product species are not *a priori* known, they had to be produced in catalytic experiments to get a realistic coverage of all specimens. GC-MS was then used for the initial product identification.

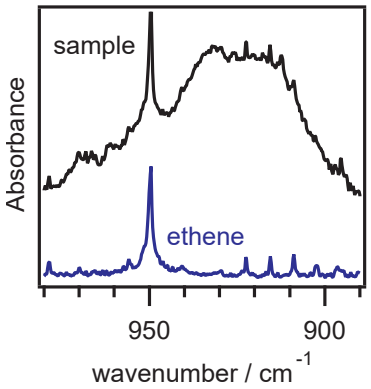

Figure 3.2: Ethene peaks observed in the conversion stream for H-ZSM5 SAR330. Black line: sample spectrum, blue line: reference spectrum.

3.2.1 Initial product identification by GC-MS

Catalytic experiments to create the realistic product species from 2,5-dimethylfuran were carried out in a chemical flow reactor that is described in detail in Paper I.[100] After ca. 30 min of time on stream (TOS), products in the effluent stream were collected on adsorbent tubes. For this purpose, the original product stream had to be diluted by a factor of 10, to not overload the adsorbent

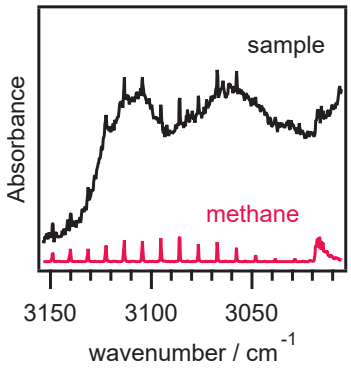

Figure 3.3: Methane peaks observed in the conversion stream for H-BEA SAR38 at 500 °C.

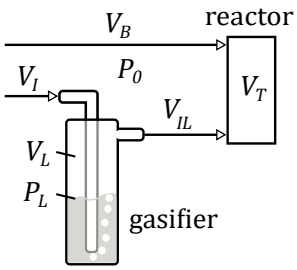

Figure 3.4: Volume flows using the gasifier setup. Reproduced from [87]

V_I : Volume of the inlet flow rate of the carrier gas before going through the gasifier.
V_{IL} : $= V_I + V_L$ Volume of the combined flow rate after the gasifier.
V_L : Volume of the vaporised liquid reactant.
V_B : Volume of the balance gas.
V_T : $= V_B + V_I$ Volume of the set total flow rate.
V_T : $= V_B + V_I$ Volume of the set total flow rate.
V'_T : $= V_T + V_L$ Volume of the actual total flow rate including the vaporised liquid.
p_L : Vapour pressure of the liquid reactant.
p_0 : atmospheric pressure.
C : Volume concentration of the vaporised liquid reactant.

tubes. The collected products were then analysed via GC-MS. Their relative abundance was also determined as equivalents of toluene, which is summarised in Table 3.3. In agreement with the literature, BTX aromatics, indene and naphthalenes are identified as products, with similar relative abundance. In addition, furan derivatives with different methylation of the reactant 2,5-dmf are found that are not commonly described as products. Among these, 2,4-dimethylfuran has a large proportion. Further products are some 5-membered carbon rings, such as 2-mcpo and 3-methyl-2-cyclopenten-1-one (3-mcpo), cyclopentene, and cyclopentadiene as well as the 7-membered ring 1,3,5-cycloheptatriene.

However, these products do not represent the whole picture, but rather only the "heavy" fraction of all products. Light gases such as carbon oxides, formaldehyde, methane, olefins and water can not be collected and analysed in this way. Instead, recorded IR spectra were thoroughly compared and matched to reference spectra, to identify some of the remaining species. The spectra of the sample mixture and the matched reference spectra of ethene and methane are for example shown in Figures 3.2 and 3.3. The full list of identified products is summarised in Table 3.3.

3.2.2 Calibration for quantification

Besides identification, it is also of interest to quantify the products during the dynamic catalytic experiment conditions. For this purpose, the commercial FTIR spectrometer (MKS MulitGas 2030) includes a commercial reference compound library. This library contains reference spectra and corresponding concentrations of many organic and inorganic species. However, many compounds of interest for this work are not included. As a consequence, the missing compounds' spectra at different concentrations were systematically recorded and calibration files were created. This includes the tedious selection of primary analysis bands, which has to be chosen with meticulous care so that interference of compounds with similar absorbance bands does not occur or is at least minimised.

How the spectra of liquid reference compounds of specific concentrations were obtained, has been described in my Licentiate thesis previously.[87] Briefly, commercially acquired pure chemicals were vaporised using a gasifier setup as pictured in Figure 3.4. The concentration (C) of a vaporised liquid can be calculated from its vapour pressure (p_L) and the partial volumes (V_x) of the carrier gas as described in Equation 3.5 and Equation 3.6.

$$V_L = \frac{p_L}{p_0} V_{IL} = \frac{p_L}{p_0}(V_I + V_L) \implies V_L = V_I \frac{p_L}{p_0 - p_L} \tag{3.5}$$

$$C = \frac{V_L}{V_T'} = \frac{V_L}{V_T + V_L} = \frac{V_I \frac{p_L}{p_0 - p_L}}{V_T + V_I \frac{p_L}{p_0 - p_L}} = \frac{V_I p_L}{(p_0 - p_L)V_T + V_I p_L} \tag{3.6}$$

In addition, concentrations were calculated based on the mass of liquid m_L that was vaporised. Here, m_L is the mass difference of the gasifier before (m_b) and after (m_a) the evaporation duration (Equation 3.7). This was done to validate the vapour pressure-based calculation and was necessary for compounds where vapour pressures were not available. The amount of substance (n_L) is derived from its molar mass M_L and mass (Equation 3.8). Together with the ideal gas law, Equation 3.9, the concentration is then obtained from Equation 3.10.

$$m_L = m_b - m_a \tag{3.7}$$

$$n_L = \frac{m_L}{M_L} \tag{3.8}$$

$$pV = nRT \tag{3.9}$$

$$C = \frac{n_L}{n_G} = \frac{\frac{m_b - m_a}{M_L}}{\frac{p_0 V}{RT}} \tag{3.10}$$

To check whether or not the mass-based and vapour pressure-based concentrations coincide, the obtained concentrations are plotted versus the flow rate of carrier gas through the gasifier. The plot is shown in Figure 3.5, confirming a good match between the methods. Small deviations in the mass-based concentrations can be explained by initial overshoots of the mass flow controller (MFC) of the carrier gas, leading to concentrations that are slightly higher than those based on the vapour pressure. To minimise the impact of this overshoot, spectra were recorded every minute over a time span of several hours. Averaging all spectra over a long time span also helps account for short-lived fluctuations in the feed and to obtain a good signal-to-noise ratio.

Next, the averaged obtained spectra were assigned to their corresponding concentrations. According to the *Beer-Lambert* law (Equation 3.4) stated before, a linear correlation between the concentration and the absorbance (here integrated absorbance/IR intensity) can be expected. Figure 3.6 shows the linear relationship for four of the calibrations well. 2,5-dmf, 2-mcpo and 3-mcpo, have a linear relation for all data points including the origin. 2,4-dmf has a linear relation for the measured concentration, however, the linear regression does slightly deviate from the origin. As a

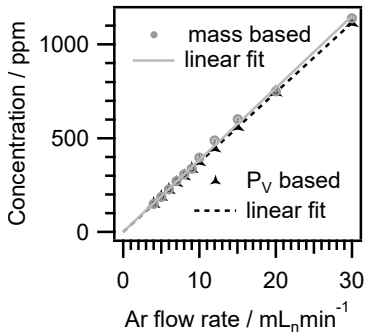

Figure 3.5: Validation of the feed concentration: The mass-based concentration and the theoretical gas concentration based on the vapour pressure P_V as a dependency of the flow rate of the carrier gas show a good match.

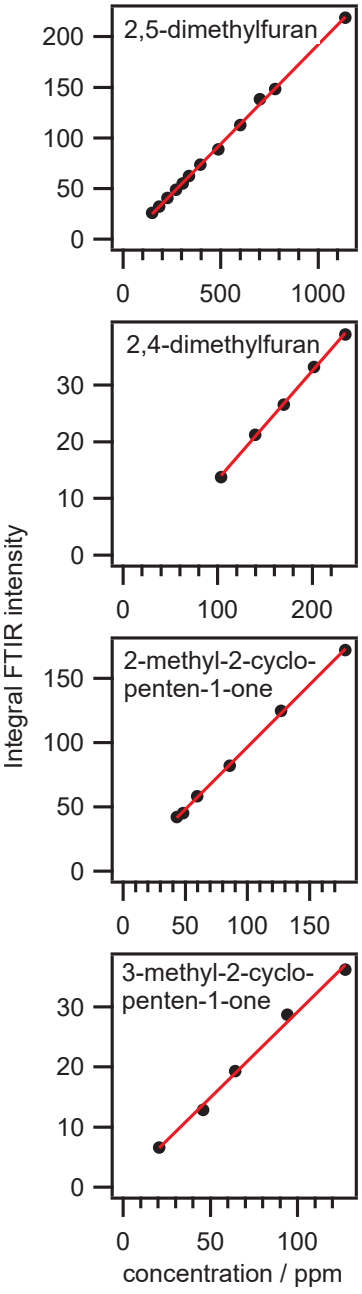

Figure 3.6: Absorbance vs gas concentration and its linear fit for 2,5-dmf, 2,4-dmf and 2- and 3-methyl-2-cyclopenten-1-one.[100]

consequence, the real concentrations of 2,4-dmf might be somewhat underestimated. One plausible explanation could be a small undetected leak during the calibration procedure. Despite this, since the linear relationship between the data points holds, the trends describing concentration changes and comparisons between different catalysts are still valid.

Finally, from the obtained spectra a primary analysis band has to be defined for each species. These primary analysis bands often resemble characteristic absorption bands in the IR spectrum. To account for cross-talk and interference of different species in a mixture and to avoid false positives, the selection of analysis bands has to be made with care and tested against spectra from a mixture. The concentrations of the individual species in the sample mixture are determined from the measured absorption spectra. The software included in the FTIR spectrometer accounts for gas temperature and pressure variations with in-built functions. Concentrations of individual species are calculated by a multivariate analysis using the predefined primary IR bands and a classical least square algorithm.

3.2.3 Matching MS and IR for robustness

Mass spectrometry is used to monitor species that cannot be analysed by IR spectroscopy such as argon and oxygen. These compounds are IR inactive because their vibrations do not possess a change of dipole moment. Further, where reference spectra or pure compounds could not be readily obtained, because of their unstable nature, species like cycloheptatriene or 3-methylenecyclopentene could at least be partially analysed via MS. Table 3.3 summarises on which m/z value various species are identified, and which ionizer (e.g. Xe or Hg) is used.

The simultaneous use of MS also increases the robustness of the product stream analysis by combination with IR spectroscopy, since both analytical tools are independent of each other. For instance, the concentration of ethene from IR is shown in Figure 3.7 together with its corresponding MS intensity signal (m/z = 27). Both signals match very well, which tells us two important things:

1. The correct compound is analysed.
2. The analysed compound shows the correct trend of concentration changes.

In the same way, the IR signal of 1,3-butadiene matches very well with the m/z signal 39 (Hg ionizer), a fragment of 1,3-butadiene as shown in Figure 3.8. Looking at 2,5-dimethylfuran in Figure 3.7, the situation is a bit more complex. At first, the IR and MS signal matches well in relative intensity. Both follow the same increasing

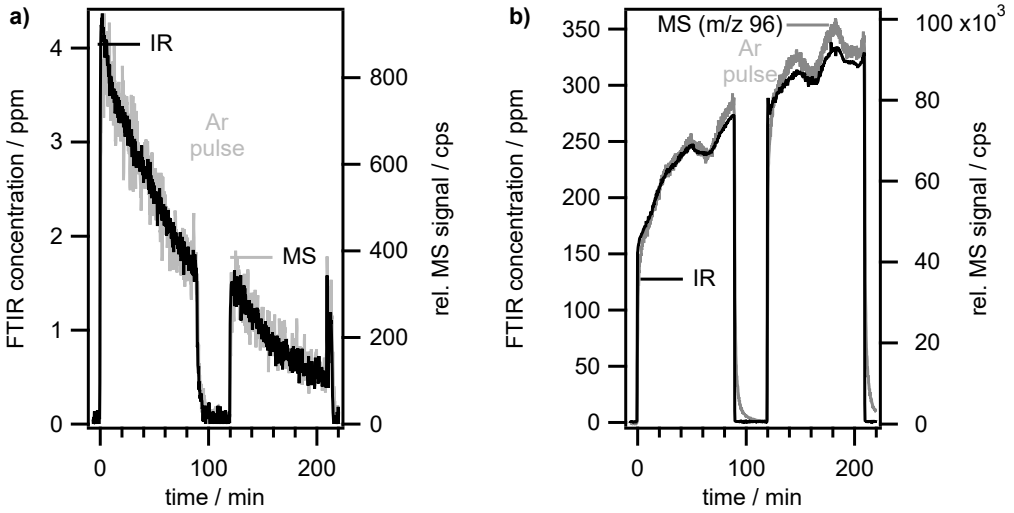

Figure 3.7: Comparison of FTIR and MS: Signal match of IR and MS for **a)** ethene (m/z 27) and **b)** 2,5-dimethylfuran (m/z 96).[100]

trend and show the same fluctuations in the signal. The fact that these fluctuations are recognised by both instruments, indicates that this is not an instrumental issue, but rather originates from the reactant or carrier gas feed. However, some deviation can be observed at later TOS. A closer look at Table 3.3 reveals that besides 2,5-dmf, also 2,4-dmf, 2-mcpo and 3-mcpo are detected at m/z 96. This is because all four molecules have the same number of atoms of the same type, which means they are structural isomers. However, since these atoms are arranged in different ways, their IR spectra are different and can easily be distinguished. It seems that during the catalytic reaction studied here, the reactant 2,5-dmf is increasingly isomerised with TOS. This phenomenon is discussed in more detail in section 4.3.3.

Besides IR spectroscopy, also MS has the potential to distinguish the isomers. This distinction can be made by either using different ionisers or by exploiting the different fragmentation patterns of these isomers as it is reported in Paper I.[100]. The principle is exemplified on 2,5-dmf and 2,4-dmf in Figure 3.9. Here, the mass spectra of both compounds are shown with Xe and Hg as ionizers. The first observation is that the spectra show a higher fragmentation when using Xe as the primary ion as compared to Hg. This result is expected because Xe has a higher ion potential, the ion-molecule reaction transfers thus more energy during impact and more fragments are obtained. The second observation is a fragmentation pattern, that is distinct for both 2,5-dmf and 2,4-dmf. For example, when using Hg, both compounds show the fragment m/z 81, which is attributed to the loss of one methyl group. Only 2,4-dmf creates the fragment m/z 68, attributed to the loss of two methyl groups. This means that 2,4-dmf can be distinguished from 2,5-dmf by monitoring m/z 68. However, other compounds in the

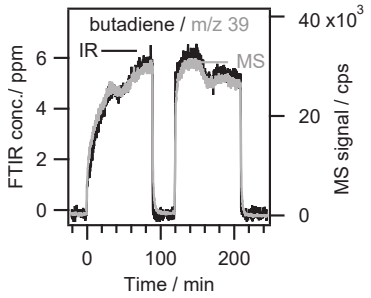

Figure 3.8: Comparison of FTIR and MS: Signal match for 1,3-butadiene and m/z 39.

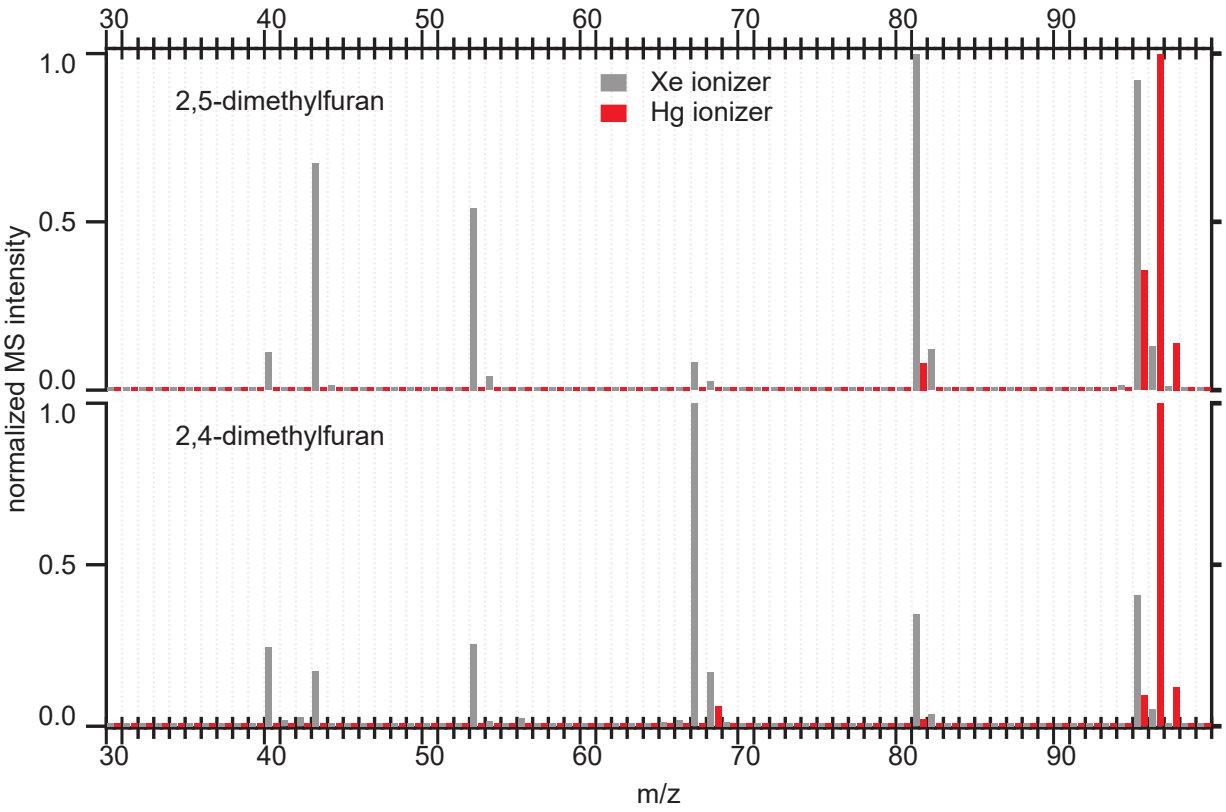

Figure 3.9: Mass spectra of 2,5-dmf and 2,4-dmf using ion-molecule reaction ionisation with Hg and Xe.[100]

mixture such as 2-methylfuran could result in the fragment m/z 68 as well, making this approach dependent on carefully ruling out all other possibilities.

3.2.4 Orientation and critical assessment

To put the method into perspective and make a critical assessment it is also necessary to point out limitations. As stated above, the sole detection of a certain m/z is no guarantee of the signal relating to only one species when using MS, so isomer distinction is difficult. In a similar way, the automated processing of the IR spectra can lead to false positives or negatives, when IR bands are overlapping.[104, 108] One example here is the olefin signal during the presence of ammonia. Ammonia is a strong absorber between 900 cm^{-1} to 970 cm^{-1}, the same region where olefins have some of their characteristic IR bands, which means signal overlapping.[107] This leads to interference during the spectra processing. As a result, the calculated concentrations of olefins can be negative. The issue is exemplified in Figure 3.10 with butadiene and ammonia. The measured sample spectra and the prediction based on the reference spectra show a small difference, which is shown as the residue. Butadiene has its primary absorption band at 909 cm^{-1}, exactly where the residual shows a spike. The software algorithm fits the

Table 3.3: Information about the analysed molecules of the hydrocarbon gas stream. The m/z values are those used in the MS analysis with Xe = 12.13 eV (for CO, CO_2, O_2, Ar) or Hg = 10.44 eV (rest) as ionizers. Based on a previously described method [100] with additions and adaptions.

Compound	Formula	M $\frac{g}{mol}$	GCMS /%	MS m/z	IR band $/cm^{-1}$
C_7+-rings and polycyclic compounds					
1,5-dimethylnaphthalene	$C_{12}H_{12}$	156	0.1	156	
2-methylnaphthalene	$C_{11}H_{10}$	142		142	785.38 – 831.18
1-methylnaphthalene	$C_{11}H_{10}$	142	0.1	142	
Naphthalene	$C_{10}H_8$	128	0.1	128	758.62 – 807.32
Indene	C_9H_8	116	0.2	116	2811.26 – 3176.23
1,3,5-cycloheptatriene	C_7H_8	92	1.0	92	
C_5-rings					
3-methylene-cyclopentene	C_6H_8	80	0.2	80	
5-methylcyclopenta-1,3-diene	C_6H_8	80	1.0	80	
2-methyl-cpo	C_8H_8O	96	0.7	(96), 68	1668.88 – 1809.90
3-methyl-cpo	C_8H_8O	96	0.2	(96), 68	1701.42 – 1811.83
Furans					
2,3,5-trimethylfuran	$C_7H_{10}O$	110	0.1	110	
2,5-dimethylfuran	C_6H_8O	96	75	96, (81)	1168.43 – 1282.69
2,4-dimethylfuran	C_6H_8O	96	14	(96), 68	1074.17 – 1174.70
2-methylfuran	C_5H_6O	81	0.7	81	1117.57 – 1176.87
BTX					
Benzene	C_6H_6	78	6.0	78	606.51 – 726.80
Toluene	C_7H_8	92	0.9	92	689.44 – 769.95
o-xylene	C_8H_{10}	106	0.2	106	702.45 – 779.59
p-xylene	C_8H_{10}	106		106	735.32 – 867.92
Olefins					
Ethene	C_2H_4	28		(28), 27	900.12 – 1000.16
Propene	C_3H_6	42		42, (41)	900.61 – 1019.69
1,3-butadiene	C_4H_8	54		(54), 39	822.26 – 977.02
C_1					
Methane	CH_4	16		-	3000.25 – 3176.23
Carbonmonoxide	CO	28		28	2146.16 – 2159.90
Carbondioxide	CO_2	44		44	2223.57 – 2280.94
Formaldehyde	CH_2O	30			2698.93 – 2822.36
Water	H_2O	18		18	1416.97 – 1502.31
Ammonia	NH_3	17		16	903.98 – 977.27
Oxygen	O_2	32		33	
Argon	Ar	40		40	

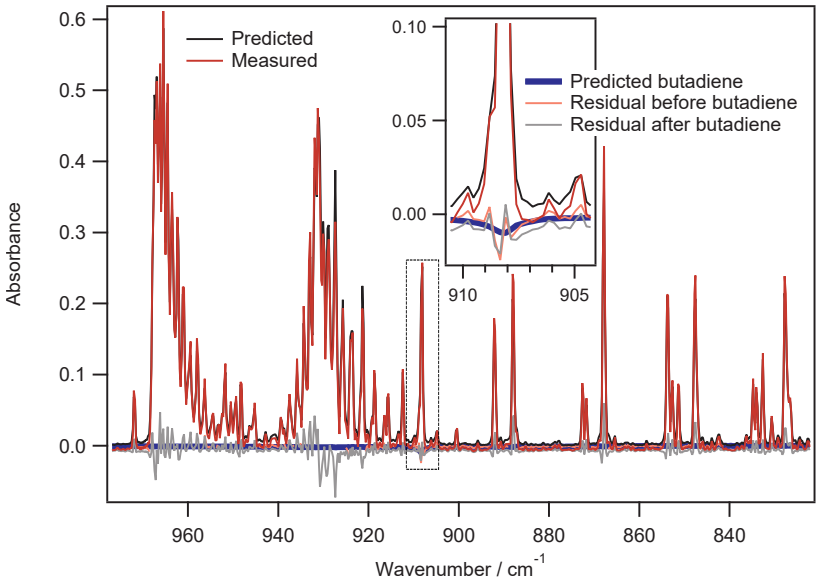

Figure 3.10: Measured, predicted and residual spectra showing false negative predicted spectra during the quantification of the butadiene signal due to interference with the ammonia band around 908 cm^{-1}.

butadiene reference spectra into the residual to predict a butadiene concentration of −4 ppm. A separate check of the goodness of fit reveals that the presence of butadiene is unlikely, however, this must be done manually. A likely origin of the difference between the measured sample and reference spectra could be attributed to noise, which could be tackled by improving the quality of reference spectra or signal-to-noise ratio by averaging several measured sample spectra.

In a similar way, false positive concentrations are of concern. If an IR band of an unidentified species is similar to that of a reference compound, it might be falsely fitted into the remaining residual. Such an unidentified species is for example present in the residual of Figure 3.11 with a peak at 926 cm^{-1}. This is tackled by screening the measured spectra and manually checking them against the full absorption spectra of reference compounds, but also by utilising the corresponding MS signal.

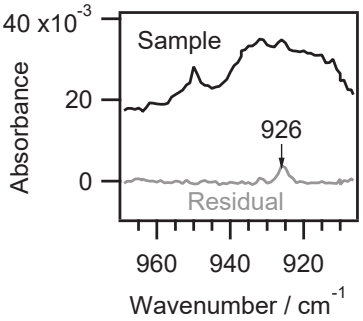

Figure 3.11: Residual from the IR spectra processing, showing unidentified species at 926 cm^{-1}.

Post-processing of recorded IR spectra is possible to identify previously unknown species or obtain more accurate concentrations once the method is refined and updated. While IR is better suited for the distinction of isomers, MS allows analysing of non-IR active molecules. Both instruments offer highly automated data collection and high time resolutions, however, the MS signal can show a certain "drag" of the signal, especially with sticky molecules, such as ammonia or 2,5-dimethylfuran (compare Figure 3.7b). Since no manual sample collection and physical separation of individual species is necessary, the time resolution that can be obtained,[7] is much higher than that of separation based methods such as GC, even when applied in on-line mode (typically 0.05 min^{-1} and up to 0.16 min^{-1})[90, 97]. This allows for example the detection of fluctuations in the feed gas as observed in Figure 3.7b and the

7: typically 4 min^{-1} to 8 min^{-1}, with the potential of 1 s^{-1} at the cost of signal-to-noise ratio.

Table 3.4: Summary of advantages and limitations of some analytical methods.

Method	Advantages	Limitations
GC + detector	· separation · identification	· time resolution · sampling is averaging · manual and labour-intensive sampling · light species are not readily analysed
IR	· time resolution · fast, no "drag" · automated data collection · post-processing of spectra · isomer distinction	· time consuming calibration procedure · complex spectra · some reference compound/spectra not available · difficult to find suitable primary analysis band · false positives and negatives
MS	· non-IR active compounds · fast, but "drag" · automated data collection · time resolution	· complex without separation technique · isomer distinction difficult · m/z can correspond to several species
IR + MS	· increased robustness · almost all species analysed	· two instruments needed

observation of transient phenomena.[8]

8: see also pre-oxidation of Cu in Paper II.

The here developed on-line analysis method is suitable to analyse the complex product stream stemming from the catalytic conversion of bio-derived 2,5-dmf to answer hypothesis I. The method is thus a case study that shows the potential but also the need for future development of analytical methodology for catalysis, which is experiencing a shift to bio-based feedstocks. Certain limitations remain, which is an opportunity from the perspective of future research and development. Some recent examples that show ongoing improvements are new modelling methods, such as "Adaptive Step Sliding Partial Least Squares",[109] the use of deep learning[110, 111] and machine learning for next-generation chemometrics[112–114].

In summary, both IR spectroscopy and MS have their strengths and limitations, which are collected in Table 3.4. Their combined use for on-line composition analysis increases robustness and allows for the analysis of most species in the product stream. For most catalytic experiments of this thesis work, the carbon mass balance is typically around 90% or higher, which is comparable to GC-MS analyses of similar CP processes[90]. Since the method is on-line, catalytic experiments can be combined with temperature programmed experiments, such as temperature programmed oxidation (TPO), which is necessary for the analysis of coke and to calculate a carbon mass balance. Moreover, temperature programmed desorption experiments (TPD) with a continuous heating rate are possible, which are discussed in Section 3.3.

3.3 Temperature programmed experiments

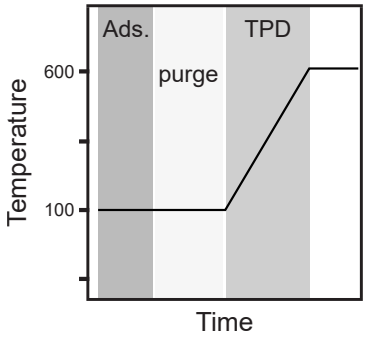

Figure 3.12: An illustration of a temperature programmed experiment.

Temperature is a good discriminator for chemical processes and thus temperature programmed (TP) experiments are a great way to learn about the interaction of molecules with the catalyst. TP experiments can reveal specific characteristics about a material, for example, NH_3-TPD is a well-established method to determine the total acid site density of zeolite catalysts.[115] For such a measurement, the principle is straightforward: a probe molecule, such as NH_3 is pre-adsorbed onto the catalyst at a certain temperature (e.g. 100 °C) as simplified in Figure 3.12. Physisorbed species are usually flushed out during a purging period. The reactor is then heated continuously (e.g. 10 °C min^{-1}) until it reaches the target temperature (e.g. 600 °C). During this temperature ramp, the chemisorbed species desorb when reaching a certain temperature and thus overcoming the energy barrier. The desorbed species are then detected and quantified.[9] Thanks to the on-line method, NH_3-TPD could be carried out before, between and after catalytic conversion reactions with 2,5-dmf, all in the same reactor, with the same instrumentation. This is of advantage from several aspects: the catalyst sample does not have to be manually transferred which is a risk for sample loss, contamination or moisture adsorption. But also the speciation and quantification of products during TPD of pre-adsorbed 2,5-dmf are possible. Finally, the coke can be removed, analysed and quantified by TPO to regenerate the catalyst.

9: For example via TCD, MS or IR.

3.3.1 NH_3-TPD

In this thesis work, NH_3-TPD is used to determine the acid site density of various fresh zeolite and zeotype catalysts.[10] The acid sites in zeolites play an important role in catalytic reactions and are hence also the active sites. NH_3-TPD profiles can show several peaks, which are a result of different types of acid sites. These types are distinguished by their strength, and show up as peaks in the TPD profile at different desorption temperatures. In this work, TPD profiles were analysed by fitting Gaussian functions to identify desorption temperatures and quantify the acid site density of different sites, which are commonly grouped into weak and strong, and sometimes additionally into medium and extra framework acid sites. This principle is illustrated in Figure 3.13

10: More info about the catalysts in Sections 4.1 and 4.2

During catalytic reactions with hydrocarbons, these active sites in zeolite catalysts are often prone to deactivation by coking. It is thus not only of interest, how many active sites are available in the fresh catalyst, but also how their abundance and nature changes over the reaction time.

A prerequisite to perform NH_3-TPD on a coked catalyst sample,[11] is that the NH_3 molecule does not strongly interact or even react with the coke. In fact, it was previously reported that coke mainly reduces the number of acid sites rather than affecting their strength and distribution.[116] Also in this work, no reaction products between coke and NH_3 were detected with the on-line analysis. Only after almost all NH_3 had desorbed, some carbon oxides were released, which is attributed to the pyrolysis of coke at high temperatures (≥500 °C).

11: that means, the access to active sites is blocked by carbonaceous deposits

NH_3-TPD is used to determine the acid site density of fresh catalysts in Paper II, and for both fresh and coked catalysts in Paper III and IV. It is found that available acid site density is significantly reduced after the catalytic conversion experiments. However, some catalysts, especially those with high initial acid site density, such as high aluminium containing zeolite (ZSM-5(22)) were completely deactivated after conversion experiments, while a major portion of acid sites can still be detected via NH_3-TPD. This could be attributed to some of these acid sites being accessible to the small NH_3 molecule, but not the bigger 2,5-dmf molecule. Future studies could thus make use of other probe molecules like pyridine that are bulkier and thus allow to distinguish different acid sites.

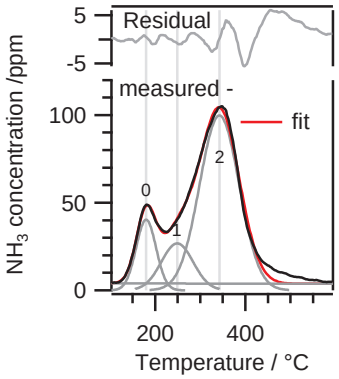

Figure 3.13: Example of fitting an NH_3-TPD signal obtained from a H-ZSM-5(38) catalyst sample.

In Paper V, NH_3-TPD is used extensively to track the amount of acid site density in between catalytic conversion periods, which aimed to understand which type of acid sites are responsible for which type of reactions. This is discussed in more detail in section Section 4.4.

3.3.2 TPD of pre-adsorbed 2,5-dmf

The speciation of desorption products during TPD of pre-adsorbed 2,5-dmf is carried out with several catalysts as described in Paper V, but this technique has also been used in Paper II. 2,5-dmf is pre-adsorbed on the catalyst at a relatively low temperature, e.g. 100 °C which is above the boiling point of 2,5-dmf (93 °C). The reactor is then flushed with Ar for at least 20 min to remove physisorbed species. It's noteworthy that after adsorption and upon increasing the temperature, almost no 2,5-dmf desorbs from the zeolite H-ZSM-5 as shown in Figure 4.15. For zeolite beta, some desorption of 2,5-dmf at low temperatures is detected as described in Paper II (SI). Since the pore size of zeolite beta is larger than that of ZSM-5 (compare Table 4.1), some 2,5-dmf molecules might be trapped between two occupied acid sites, without themselves being chemisorbed. The trapped ones might be released upon heating, while those 2,5-dmf molecules occupying acid sites do not desorb. The chemisorbed 2,5-dmf molecules are in fact adsorbed so strongly, that they rather react to other

Table 3.5: Temperatures of maximum desorption from TPD of pre-adsorbed 2,5-dmf from a H-ZSM-5(38) catalyst.

Species	T / °C
water	270
CO_2	277
CO	332,374
p-xylene	353
toluene	356
benzene	358
ethene	367
propene	363
naphthalene	371
indene	392
2-methylnaphthalene	394
methane	482

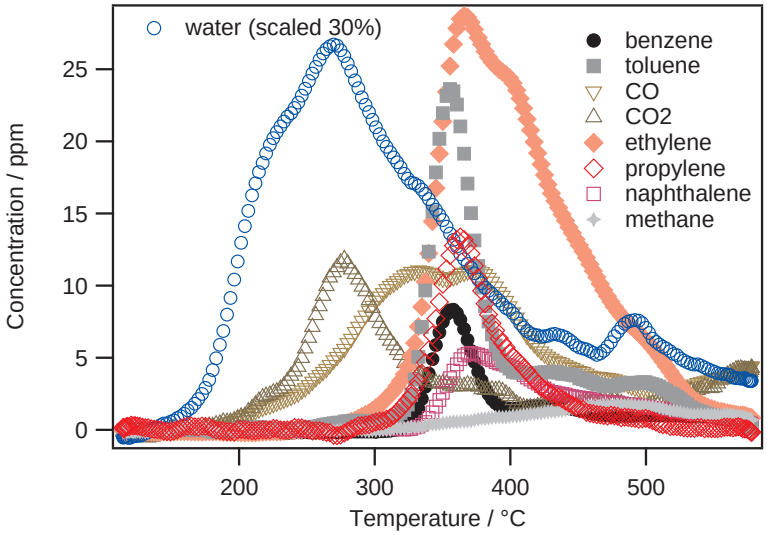

Figure 3.14: Temperature programmed desorption from pre-adsorbed 2,5-dmf using a H-ZSM-5(38) catalyst (particle size 300 μm to 355 μm). The signal has been smoothed for visual clarity with a Savitzky-Golay (17 points) algorithm.

species when increasing the temperature. This is indicated by first detecting water and CO_2 at 270 and 277 °C respectively as shown in Figure 3.14 and summarised in Table 3.5, suggesting early dehydration and decarbonylation reactions. Besides some CO, no other species desorb before reaching 350 °C. At this point, BTX desorb in the order xylene, toluene and finally benzene. Similarly, propene desorbs before ethene at slightly higher temperatures. No desorption of 1,3-butadiene is detected. In Paper II, a species with m/z 58, which is assigned to butene, desorbs before propene (m/z 42) when using H-BEA(37). In the same work, I also pointed out the desorption correlation between certain olefins and BTX aromatics. However, such a correlation does not necessarily mean causation. For example, while the benzene signal and desorption temperature often correlate with ethene, benzene is not produced from ethene itself as discussed in section 4.5.2.

At around 400 °C, the desorption of heavier polycyclic aromatics, such as indene and naphthalenes is detected Finally, methane is detected at the highest temperature (482 °C), which might be attributed to the formation and pyrolysis of coke, breaking apart methyl groups and release them in form of methane. It is noteworthy, that no desorption of isomer products such as 2,4-dmf is detected.

3.3.3 Temperature programmed oxidation

The last temperature programmed experiment using the on-line analysis, is temperature programmed oxidation (TPO). During continuous catalytic and adsorption experiments with hydrocarbons, some carbonaceous deposits remain on the catalyst surface. These deposits are often the reason for the deactivation of active sites and are referred to as coke. The deposits can be removed from

the catalyst surface through an oxidative treatment (combustion) at elevated temperatures to regenerate the catalyst.

Studying coke on the catalyst can give many insights. It might be interesting to know where coke is formed, for example inside the channels or on the external surface in the case of zeolites. The coke can be of different compositions and be more or less condensed. The coke can be active or inactive at promoting reactions and can be analysed *in situ* for instance with IR spectroscopy.[117, 118] However, the analyses of the TPO results are dependent on many factors, for example, the heating rate, the oxygen concentration, how the coke is formed *et cetera*.[119]

One important function TPO plays in this work, is to determine how much coke is deposited on the catalyst. Thanks to the online analysis, the amount of coke can readily be determined by the detection and quantification of carbon-containing products of the TPO. The majority of species are CO and CO_2, but also formaldehyde, ethene and aromatics are detected, although to a lesser extent. Compared to other analysis methods, the here developed on-line analysis allows the use of the same instruments and reactor and thus sequential experiments. It also allows for the detailed analysis of oxidation products, for example, compared to thermo gravimetric analysis (TGA), which only determines the mass loss. The carbon deposited on the catalyst can be a relevant fraction of the total reactant feed and its quantification is hence necessary to calculate a carbon mass balance.[12] The carbon mass balance is an important measurement to put conversions or selectivities into perspective. In Paper I, carbon mass balances for experiments at different temperatures closed at 89, 93 and 97 % at 500, 400 and 300 °C, respectively. Of the total amount of detected carbon up to 20% is stored as coke on the catalyst.

12: Carbon mass balance means the number of carbon atoms from all detected product species, such as BTX but also coke, divided by the number of carbon atoms that were fed into the reactor as a reactant.

In Paper III, three catalyst samples were compared with respect to how much coke they had accumulated in a 10 h conversion experiment. A Ga-silicate sample had stored 7.7 wt% worth of coke (assumed as carbon only, not considering hydrogens) of the total catalyst mass, whereas an H-ZSM-5(22) sample accumulated 6.7 wt%. A silicalite-1 did not store any significant amount of coke. The first two samples show also differences in their release of CO and CO_2 during the TPO of the coke depositions. The Ga-silicate released more CO (1.67 $mmol/g_{cat}$) compared to the H-ZSM-5 sample (0.65 $mmol/g_{cat}$) but less CO_2 (3.14 $mmol/g_{cat}$ vs 4.08 $mmol/g_{cat}$) during the TPO. Finally, the peak maxima for the CO and CO_2 release for the Ga-silicate sample are lower than those of the ZSM-5 sample (559 and 553 vs 587 and 578 °C respectively).

In Figure 3.15 the product signals during TPO of coke for an H-

13: Experiments from Paper V.

14: The latter is expected to have a higher number of hydroxyl groups due to the higher Al content.

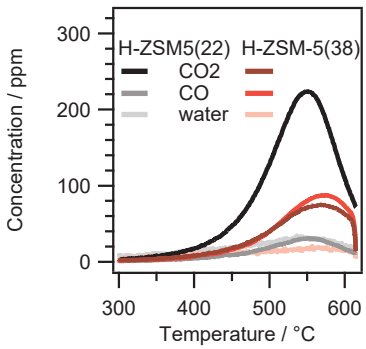

Figure 3.15: Temperature programmed oxidation of carbonaceous deposits of catalysts H-ZSM5(22) and H-ZSM5(38), showing signals of CO, CO_2 and water.

ZSM5(22) and an H-ZSM5(38) sample are shown.[13] The heating rate was 10 °C min^{-1} and the oxygen concentration was 20%. The desorption peaks for H-ZSM-5(38) for all TPO products, CO, CO_2 and water are detected at slightly higher temperatures than for the H-ZSM5(22) sample. The catalyst sample with a higher Al content, H-ZSM5(22), is more selective to CO_2, but less selective to CO than H-ZSM5(38). Coke might react with surface hydroxyl groups to carbon oxides (even in the absence of oxygen),[120] which might explain the higher selectivity towards CO_2 of the H-ZSM5(22).[14] In fact, the latter sample even produces more water than H-ZSM5(38).

It is also observed that an H-ZSM-5(22) sample, that had stored a lot of coke, could not be completely regenerated, even under conditions that would regenerate another H-ZSM-5 catalyst. Catalytically active acid sites were not recovered and the sample remained mostly inactive for conversion of 2,5-dmf. It is found that the removal of coke sometimes needs more extreme conditions, especially when the catalyst had a high initial content of coke.[121] This suggests, that some coke remained mainly in the internal channels. This is of particular concern, as extreme temperatures and oxidation conditions to remove the last amount of coke could cause permanent deactivation of the catalyst by loss of active sites.[121]

Applying the on-line analysis for catalyst evaluation and design

4

In this chapter, the application of the previously described on-line analysis is discussed. In contrast to the previous chapter which addresses how the method was developed and can be utilised, this chapter focuses on the observations that were made during catalytic experiments to evaluate the catalysts. For that purpose, the here used catalysts, zeolites and zeotypes are introduced. To make meaningful conclusions about the interaction of the reactant with the catalyst, also the structure and composition of the material must be known. Important concepts are briefly introduced and summed up, while experimental details and more thorough analyses can be found in the corresponding Papers II-V. Since discussing all details is beyond the scope of this thesis, the chapter focuses on combining the results and conclusions from the papers. The reaction products and their dynamic changes in distribution and selectivity as well as catalyst deactivation behaviour are addressed. The understanding of reaction phenomena and the role of the active site allows for targeting increased aromatic production by rational experimental and catalyst design.

4.1 Zeolites and Zeotypes

Zeolites are relevant catalyst candidates for the successful production of aromatics from furans. These materials have been used both in the catalytic pyrolysis and Diels-Alder cycloaddition dehydration pathway leading to *p*-xylene and other BTX.[76, 94] But not only here, zeolites also play a crucial role as solid acid catalysts for many industrial processes, and have been studied extensively for the traditional production of aromatics via petroleum refining.[122] Another important aspect is that these materials are environment-friendly.[123]

Zeolites are microporous, crystalline aluminosilicates with a three-dimensional framework structure and are catalyst materials of choice due to relevant favourable characteristics such as (thermal) stability and tunable properties like acidity and shape selectivity.[124] These properties are a result of the microporous structure. This structure is formed by an assemble of TO_4-tetrahedrons,[1] which are the primary units of the zeolite structure. The corner-sharing tetrahedrons are organised to form channels, cages and cavities, creating more than 200 types of framework structures that are known today.[125] For a large number of structures, a

1: Where T atoms are Si, Al, Ga *etc.* The material is called Silicalite-1 if all T atoms are Si, a zeolite, when some T atoms are Al and most T atoms are Si atoms, or a zeotype if it is another atom than Al.

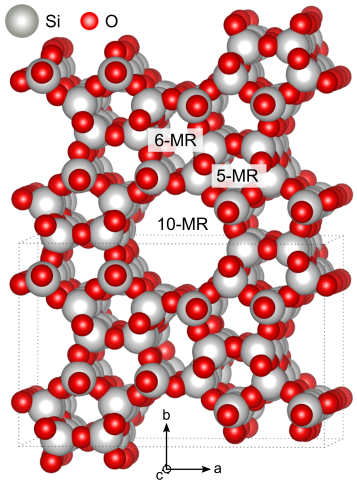

Figure 4.1: Visualisation of the MFI type framework structure showing different channels. Reproduced from [87].

Table 4.1: Some characteristics of chosen zeolites.[128]

zeolite	code	ring	size [Å]
Y	FAU	12	7.4
ZSM-5	MFI	10	5.1
		10	5.3
beta	BEA	12	6.6
		12	5.6

three-letter code assigned by the International Zeolite Association marks the framework structure types.[125] Two of these framework structures that are of relevance here are the MFI and BEA framework structures. The latter is characterised by 10, 6, 5 and 4-membered rings (MR) as shown in Figure 4.1. Depending on the size and shape of these rings, various pore sizes make the zeolite shape- and size-selective to certain molecules, which is why zeolites are also known as molecular sieves.[126]

Some of these zeolites, namely zeolite Y, ZSM-5 and zeolite beta are shown with their corresponding three-letter code, ring and pore size in Table 4.1. The maximum pore diameter of these materials is especially relevant because it matches the kinetic diameter of BTX as well as furans.[127] A study investigating the shape selectivity of zeolite catalysts found that ZSM-5 (MFI type) is the most suitable candidate for high aromatic yields.[127]

Besides their microporous structure, responsible for the high surface area and shape selectivity, the materials must also host catalytically active sites to be catalysts. These active sites are acid sites and can be of different natures.

When T is an Al atom in the above described TO_4-tetrahedron, a net negative charge is induced, which is balanced by a counter ion. If the counter ion is a proton, the zeolite becomes acidic. More specifically, the species Si–O(H)–Al is known as a Brønsted acid site (BAS). The number of acid sites then correlates with the amount of Al in the zeolite. This means a high Al content – or low silica to alumina ratio (SAR) corresponds to a high acid site density. With other metals than Al in the tetrahedron, zeotypes offer the possibility to adjust the acid site strength, but also the microenvironment in the pore caused by the atomic radii and electronegativity. For example, based on different T atoms in the MFI framework the following series in acid strength was outlined: Silicalite-1 < B-silicalite < Fe-Silicalite < Ga-silicalite < Al-silicalite (=ZSM-5).[129, 130]

The counter ion can also be a metal, such as Na, Ga or Cu forming Lewis acid sites (LAS). The role of Cu was studied in Paper II in form of a Cu-ZSM-5 and is discussed in section 4.4.2. LAS can also be formed through dehydration, the loss of an Al-bound hydroxy group at high temperatures.

However, these are not the only parameters that impact the acid sites. The acid site strength is for instance also dependent on the framework structure,[2] and the exact location of the Al (or another T atom) in the framework. For instance, MFI has 12 crystallographically distinct T sites while BEA has 9.[123] Hence, the catalytic properties do not only depend on the T location, but also on its neighbours and their distribution, e.g. in the MFI type, Al atoms

2: H-MFI (133–177°) zeolites are stronger acids than H-FAU (133–147°) because of the bond angle.[123]

can be in channels or intersections.[123] This complexity makes the materials synthesis, characterisation and analysis challenging, and further studies are needed to "achieve complete control over tailoring the acidic properties of any zeolite material".[123]

4.2 Catalyst characterisation

This section briefly summarises the catalysts studied in this work. Some of their physico-chemical properties, in which Papers they were used, and where additional sample characterisation can be found in the literature are summarised in Table 4.2. The beta zeolite, H-BEA(37)[3] (Zeolyst) and ZSM-5 zeolites (AkzoNobel) were commercial products. Ion exchanged Cu-ZSM-5(22) was prepared by Xueting Wang.[131] Ga-silicate and Silicalite-1 samples were provided by Simone Creci[130, 132, 133] and synthesised by a sol-gel method followed by hydrothermal crystallisation[134] to obtain MFI-type zeotypes where Ga is in the framework.

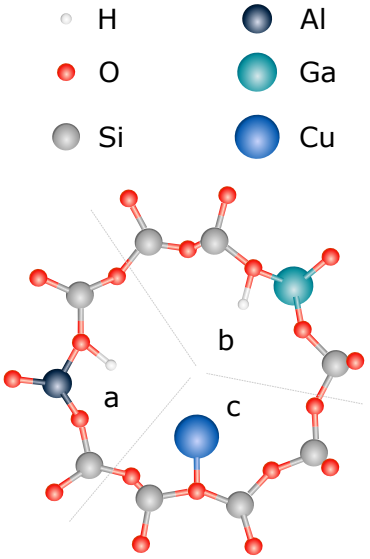

Figure 4.2: Visualisation of zeolite modifications, a) BAS created by framework Al, b) BAS created by framework Ga, c) ion exchanged Cu.

A detailed description of the instrumentation, experimental procedures and discussion of catalyst characterisation can be found in the corresponding Papers. Briefly, X-ray fluorescence (XRF) spectrometry was used for chemical analyses and to determine the elemental composition of the materials. The SiO_2/M_2O_3 ratio, where M is Al or Ga, as well as the amount of ion-exchanged Cu, was calculated from the XRF results considering the amount of water stored on the materials. Minor impurities such as Na in Silicalite-1 or Fe in ZSM-5 catalysts were found on a ppm level and are summarised in the SI of the corresponding Papers. These impurities likely stem from precursor materials during the synthesis, however, due to their low concentrations no relevant effect on catalytic conversions is expected. Thermal gravimetric analysis (TGA) was used to evaluate the thermal stability of the materials and derive the amount of water absorbed at room temperature. In summary, materials with higher acid density showed an increased mass loss between RT and 200 °C, readily explained by the increased capability to store airborne moisture, which evaporates upon heating. Upon further heating, no significant mass loss was observed, indicating the high thermal stability of the materials. Crystal phases were analysed by X-ray powder diffraction (XRD), confirming the BEA and MFI framework structure of the catalysts. The absence of other peaks suggests that no additional crystalline phases of long-range order are present. N_2-physisorption was used to analyse porosity and determine surface areas. Isotherms are all of class IV, typical for microporous materials. Silicalite-1 also has a type H1 hysteresis, indicating the presence of well-defined channels of uniform sizes and shapes.[135] H-ZSM-5(355), Cu-ZSM-5(22)

3: The number in brackets indicates the SiO_2/Al_2O_3 ratio.

and H-BEA(37) show a type II hysteresis associated with capillary condensation. In addition, Silicalite-1, Ga-silicate and H-ZSM-5(38) show a type IV hysteresis in the lower range indicating the presence of both micro- and mesopores, often found for aggregated crystals of zeolites.[136] Surface areas (SA) and micropore volumes were determined by the BET method and t-plot method respectively, following consistency criteria and show values typical for microporous zeolites.[137] The morphology of some of the samples is described in previous works using scanning electron microscopy (SEM). Ga-silicate shows interconnected crystals, indicating the presence of mesopores.[132] Irregular structures on the external facets could suggest the potential migration of some Ga species during the post-synthesis calcination.[132]

Table 4.2: Physico chemical properties and additional characterisation availability of the catalysts studied in this work.

Sample	SiO_2/	Cu,Ga	SA	SA_{micro}	SA_{ext}	V_{micro}	Acid site density[a]		Used in	Ref.
Framework	M_2O_3	%	$\frac{m^2}{g}$	$\frac{m^2}{g}$	$\frac{m^2}{g}$	$\frac{cm^3}{g}$	$\frac{mmol}{g}$		Paper	info
BEA							*monolith*[b]	*powder*[c]		
H-BEA(37)	37		648	620	28	0.255	0.230		I, II	
MFI										
H-ZSM-5(355)	355		433	420	12	0.198	0.118		II	[138]
H-ZSM-5(38)	38		403	394	9	0.166	0.300	0.417	II, V	[138]
Cu-ZSM-5(22)	22	2.8	367	348	19	0.140	0.647		II	[131]
H-ZSM-5(22)	22		412	386	26	0.158		0.767	II, III, V	[131, 138]
Silicalite-1	-		395	386	9	0.175		0.002	III	[130, 133]
Ga-Silicate	67	3.1	365	338	27	0.145		0.179	III, IV	[130, 132]

[a] Acid density determined by NH_3-TPD:
[b] In the range 150 °C to 550 °C for catalysts coated on monolithic cordierite substrate (Paper II).
[c] Temperature range of 100 °C to 600 °C for catalyst powder with a particle size of 300 μm to 355 μm (Paper III-V).

4.2.1 DRIFTS

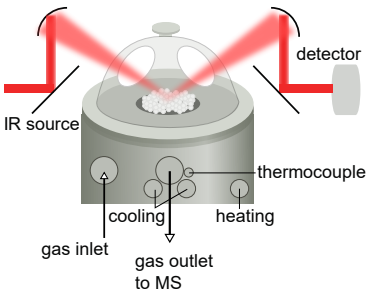

Figure 4.3: DRIFTS setup showing the reactor cell and the incoming IR beam, that is diffusely reflected by the powdered catalyst before being directed to the detector.

In section 3.1.3 infrared spectroscopy was introduced and I explained how the technique can be applied for the analysis of a gaseous mixture. However, IR spectroscopy can of course also be applied to solids, such as catalyst materials. In this specific case, diffuse reflectance infrared Fourier transform spectroscopy (DRIFTS) is used to study the surface species of the catalyst. The principle and the reactor setup are illustrated in Figure 4.3. An IR beam hits the sample and makes the chemical bonds vibrate at certain frequencies. Due to the interaction of the incident light with the rough sample's multiple surfaces the samples, the diffusely reflected light is especially sensitive to surface species. For example, DRIFT spectra confirm the Ga-O(H)-Si vibration in the Ga-silicate sample, and it is thus concluded that Ga is inside the framework.[132] Spectra reported in the SI of Paper II[139] indicate the presence of octahedral extra-framework Al for the H-ZSM-5(22) sample at 3778 cm^{-1}.[123]

DRIFTS can also be used for *in situ* and *operando* measurements, where the catalyst is studied when exposed to a stimulus or under reaction conditions. In Paper II, adsorption and TPD studies of 2,5-dmf are discussed. The studied spectra for H-BEA(37) in Figure 4.4 show a peak at 3733 cm^{-1}, indicating the interaction of the adsorbent with internal silanols. Peaks at 3746 cm^{-1} and 3742 cm^{-1} for both H-BEA and ZSM-5 samples are attributed to external silanols.[140, 141]

Vibrations assigned to strongly acidic bridged hydroxyl groups (BAS) are observed around 3611 cm^{-1} to 3612 cm^{-1}.[142] However, for the Cu-ZSM-5 sample, no such strong BAS interaction could be observed confirming the absence of BAS due to the ion exchange.

Upon temperature increase, the evolution of the bands between 3000 cm^{-1} to 2900 cm^{-1} is assigned to aliphatic C-H stretching vibrations, while the signals between 3200 cm^{-1} to 3000 cm^{-1} are attributed to aromatic and olefinic C-H stretch vibrations.[143] More details are discussed in Paper II.

However, another observation from DRIFTS studies, that is worth mentioning are relatively strong bands at 1726 cm^{-1}, 1715 cm^{-1} and 1684 cm^{-1} for H-ZSM-5(22), H-BEA(37) and Cu-ZSM-5(22) respectively. These signals strongly indicate a C=O stretch vibration of ketones.[144–147] Ketone vibrations in the gas phase are usually expected between 1750 cm^{-1} to 1730 cm^{-1}, however, upon interaction with the zeolitic BAS, a shift to lower wavenumbers is observed. Moreover, ketone and Cu interaction are even stronger, leading to a C=O bond weakening to even lower frequencies at 1680 cm^{-1} to 1690 cm^{-1}.[144] These interactions suggest ring-opening reactions of the adsorbed 2,5-dmf upon adsorption, which are of relevance for discussion later in this chapter.

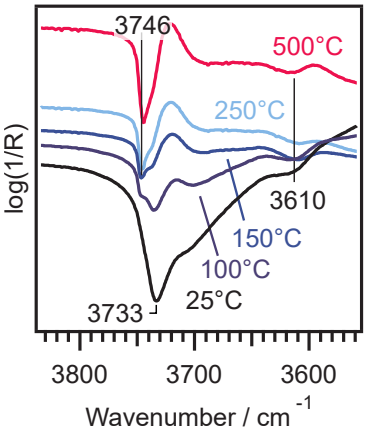

Figure 4.4: Background substracted DRIFT spectra of pre-adsorbed 2,5-dmf on H-BEA(37) and signal evolution upon temperature increase.[139]

4.3 Reaction products

The catalytic conversion of 2,5-dmf produces a wide range of products. The product distribution and selectivity are dependent on many factors, such as the reaction temperature, the catalyst framework structure, acidity, deactivation *etc.* Commenting on all observations and specific numbers is far beyond the scope of this chapter, meanwhile, these can be found in the corresponding papers. Here, I summarise and highlight the most important trends and group the products into BTX, olefins, isomers and others (compare Figure 4.5).

In Paper II, four catalysts are evaluated for the valorisation of 2,5-dmf at 300 °C, 400 °C and 500 °C: H-BEA(37), H-ZSM-5(38) of similar Al content, H-ZSM-5(355) with a lower Al content, and a

It must be noted that catalysts in Paper II were evaluated as powder samples (160 mg) deposited on a cordierite monolithic substrate (Corning, 400 cpsi, 188 channels, length = 15 mm, Ø= 13 mm) by a dip coat process.[139] A picture of the catalyst on the monolithic substrate is shown in Figure 4.9
Otherwise, catalysts were evaluated as powder samples (ca. 65 mg) of 300 μm to 355 μm particle size, hold in place by quartz wool plugs.
In both cases, no pressure drop during catalytic reactions was observed.

Cu-ion exchanged Cu-ZSM-5(22). In Paper III, a pure silicalite-1, Ga-silicate with Ga in the MFI framework and H-ZSM-5(22) were studied. In this way, the BEA and MFI framework structure can be compared, as well as the effects of acid site density, acid site strength and the effect of ion-exchanged Cu in a zeolite, which has been explored for cycloaddition reactions before.[148] Silica, alumina and silicalite-1 did not result in any relevant conversion or product formation, which highlights the importance of the combination of microporous structure and the presence of acid sites. The following describes the results during continuous production, which means the catalyst is continuously exposed to the reactant 2,5-dmf at isothermal conditions, which is distinct from results discussed in section 4.5.3.

4.3.1 BTX

In general and for all studied catalysts the selectivity to BTX is highest at initial exposure to the reactant and then declines over a time span of minutes to hours of TOS to reach zero. This decline is attributed to the deactivation of certain active sites caused by the formation of coke.

Different temperatures were studied in Paper II. The conversion decreases with lowering the temperature. At 500 °C the selectivity to benzene is highest among BTX, with a general trend of B > T > X. At lower temperatures, toluene or xylenes might be favoured over benzene, however, their selectivities are usually quite low and in the range of single-digit percentage region, hence comparable to other CP studies.[97, 149] Among the four above-mentioned catalysts, the highest initial benzene selectivity of 18% was achieved with Cu-ZSM-5(22) (based on a 2,5-dmf feed of 386 ppm and a conversion of 53%). In comparison, H-ZSM-5(38) had 8% while H-BEA(37) 4%. This indicates that introducing Cu can target increased benzene production. However, with Cu, the catalyst sample experiences faster deactivation and shows increased carbon oxide selectivity as discussed in section 4.4.2 and visible in Figure 4.6. At 400 °C the H-BEA(37) sample seems to favour the larger toluene (1.3%) and xylene (3.1%) aromatics, possibly due to the slightly bigger pore size compared to the MFI framework structure. Noteworthy, at 300 °C, no benzene formation takes place, but some toluene is detected for H-BEA(37) and trace amounts of xylene for H-ZSM-5(38).

4.3.2 Olefins

Olefins, including ethene, propene and 1,3-butadiene follow similar trends as described for BTX, while overall concentrations and

selectivities are lower than those for BTX. In Paper II, I described certain correlations between ethene and benzene, propene and toluene, and 1,3-butadiene and xylene. Olefin availability was linked to the formation of BTX, however, it is now clear that BTX are not formed from ethene alone, nor does additional ethene facilitate BTX formation as discussed in section 4.5.2. Since tests with other olefins were not carried out, future studies should also evaluate the effect of propene and butadiene on aromatisation. The simultaneous evolution of olefins and BTX can however still be connected, for example by originating from the same cracking, oligomerisation and aromatisation reactions as described in Figure 4.18.

4.3.3 Isomers

Three structural isomers of the reactant 2,5-dmf were identified during catalytic reactions. These isomers are discussed in more detail in Paper II and Paper IV. It is noteworthy, that all studied catalysts do not favour the isomer products at initial exposure to 2,5-dmf. Instead, they are preferably produced with increasing TOS, once the formation of BTX and olefins declines. This selectivity change from olefins and aromatics to 2,4-dmf, 3mcpo and 2mcpo must thus depend on a change in active site availability. This means, with increasing TOS, the catalyst might lose certain active sites that are responsible for cracking and aromatisation reactions, while active sites that are responsible for isomerisation remain or emerge. The cause of this change is suggested to be the formation of coke and is discussed in more detail later on.

There are indications that Cu suppresses the isomerisation since selectivities are lower than its H-form derivatives, which suggests that isomerisation reactions are less likely to happen in the absence of BAS. The BEA framework seems to favour 3-mcpo over 2-mcpo, in contrast to all MFI structures including the Ga-silicate that favour 2-mcpo over 3-mcpo.

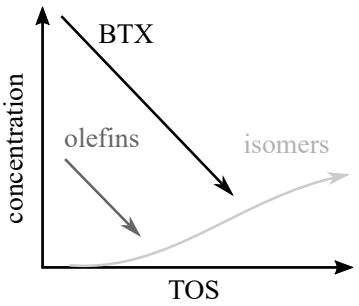

Figure 4.5: A simplification of the product trends during continuous catalytic valorisation of 2,5-dmf over zeolites: BTX and olefins decline with TOS, while isomer concentration increases.

4.3.4 Others

Among the many products described in Table 3.3, some of the most relevant are discussed in the following. Small amounts of 2-methylfuran and 2,3,5-trimethylfuran were identified, which are likely reaction products of the reactant 2,5-dmf undergoing transalkylations. Such reaction phenomena are well known for zeolites and xylenes and are exploited on an industrial scale to increase *p*-xylene yields.[122]

Carbon oxides detected during all catalytic reactions indicate decarbonylation reactions, removing CO and CO_2 from the reactant and providing hydrocarbon intermediates for further cracking, oligomerisation and aromatisation reactions. The heavier aromatics indene, naphthalenes and other polycycles are formed in relatively smaller amounts, however, these are suggested precursors of graphite-like coke.[90] Some of these molecules might lose a methyl group and release methane, mostly at temperatures above 500 °C. Water is always detected as a dehydration product and can indicate the overall cracking activity of the catalyst, but less so the isomerisation activity.

4.4 Understanding selectivity changes and deactivation

The above-described differences and changes in product distribution and selectivity sparked interest in how the reactant interacts with the catalyst. How and where does deactivation take place? Are different active sites involved? If so, which active sites are responsible for which reactions? Which modifications of the catalyst or the experimental design can target increased selectivity to certain products?

4.4.1 Observing transient phenomena

The high time resolution of the developed on-line analysis method makes it especially suitable to observe transient phenomena. It can also be conveniently operated under dynamic reaction conditions, such as temperature programmed experiments. Because a wide range of species can be analysed simultaneously, the method is especially suitable to combine catalytic experiments with TPD to monitor the state of active sites. To make meaningful conclusions about the molecular interactions of surface species, results from catalytic experiments are combined with *in situ* DRIFTS.

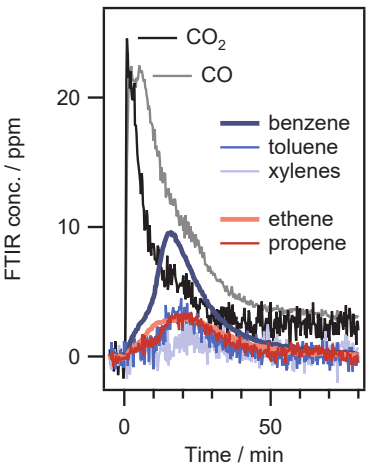

Figure 4.6: Concentrations of CO, CO_2, BTX, ethene and propene during a 2,5-dmf pulse over Cu-ZSM-5(22) at 400 °C, showing a pre-oxidation effect of Cu.[139]

4.4.2 Pre-oxidation phenomena caused by Cu

During the study of the Cu-ZSM-5(22), the CO_x, BTX and olefins signals were distinct from the other tested catalysts. The peak maximum was not exactly at the start of 2,5-dmf exposure but shifted for a few minutes TOS. At the same time, the initial CO and CO_2 selectivities are higher and their decrease coincides with the increase of BTX and olefins as shown in Figure 4.6. In separate ad- and desorption studies with *in situ* DRIFTS, surface species

formed on the catalyst were probed. Figure 4.7 illustrates that with increasing temperature a peak at 2156 cm^{-1} starts to emerge at ≥180 °C. This band is assigned to C=O stretching vibrations from CO on Cu-species $\nu[Cu^{+}-CO]$.[131, 150] and is supporting evidence for the previously postulated decarbonylation pathway of 2,5-dmf.[97] The enhanced oxidation behaviour of Cu-ZSM-5(22) is assumed to originate from the oxidative pretreatment of the catalyst, which is done to remove any possible carbon deposits. The Cu-centres in the zeolite function as oxygen storage and as an oxidation catalyst once exposed to the carbon-rich reactant.[139, 151]

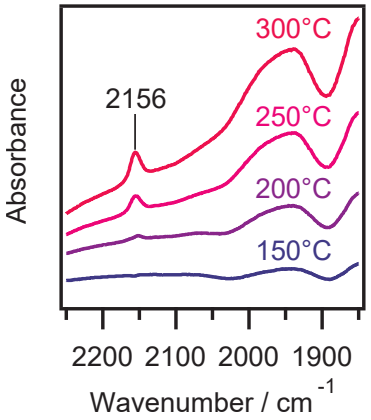

Figure 4.7: Observation of C=O stretch vibration on Cu at 2156 cm^{-1} in a DRIFTS experiment. Difference spectra, background at 25 °C.[139]

The observation of this phenomenon, which happens within a few minutes, is possible because of the high time resolution of the on-line analysis and the simultaneous monitoring of both carbon oxides and hydrocarbons.

4.4.3 Cycling Temperature

In an experiment part of Paper V and also described in Mestre's Master thesis,[138] the temperature was cycled consecutively from 100 °C to 582 °C (10 °C min^{-1}) while exposing the catalyst H-ZSM-5(38) continuously to 2,5-dmf. The dynamic response of reactant and product concentrations are plotted in Figure 4.8. The production onset temperature and the maximum production temperature of the 1st cycle are summarised in Table 4.3. At the initial 100 °C the reactant 2,5-dmf is not converted. Only upon increasing the temperature, its concentration starts to decrease, indicating the first conversion process. When it comes to the three isomers, 2,4-dmf, 2-mcpo and 3-mcpo, two main differences must be pointed out:

Table 4.3: Onset and maximum production (conversion in case of 2,5-dmf) temperature for the 1st cycle (100 °C to 582 °C, 10 °C min^{-1}) during continuous 2,5-dmf exposure of H-ZSM-5(38). Compare Figure 4.8.

	Temperature / °C	
	onset	max
2,5-dmf	117	579
2,4-dmf	233	582
2-mcpo	319	501
3-mcpo	361	582
ethene	240	447
benzene	345	565
toluene	341	418

1. In contrast to experiments, where the catalyst is exposed to the reactant at high temperatures from start, e.g. 400 °C and isomers only evolve after BTX decline with increased TOS, the onset of isomers here is *before* BTX detection (compare Section 4.3).

2. In experiments, where 2,5-dmf is pre-adsorbed onto the catalyst, and then heated without additional 2,5-dmf exposure, *no* isomers are detected (compare 3.3.2). However, in this procedure, toluene is formed before benzene likewise to continuous production at a steady temperature and to pre-adsorption-TPD experiments.

These observations suggest that depending on the adsorption conditions and the initial temperature, the order and nature of product formation and distribution are fundamentally different and need to be examined further.

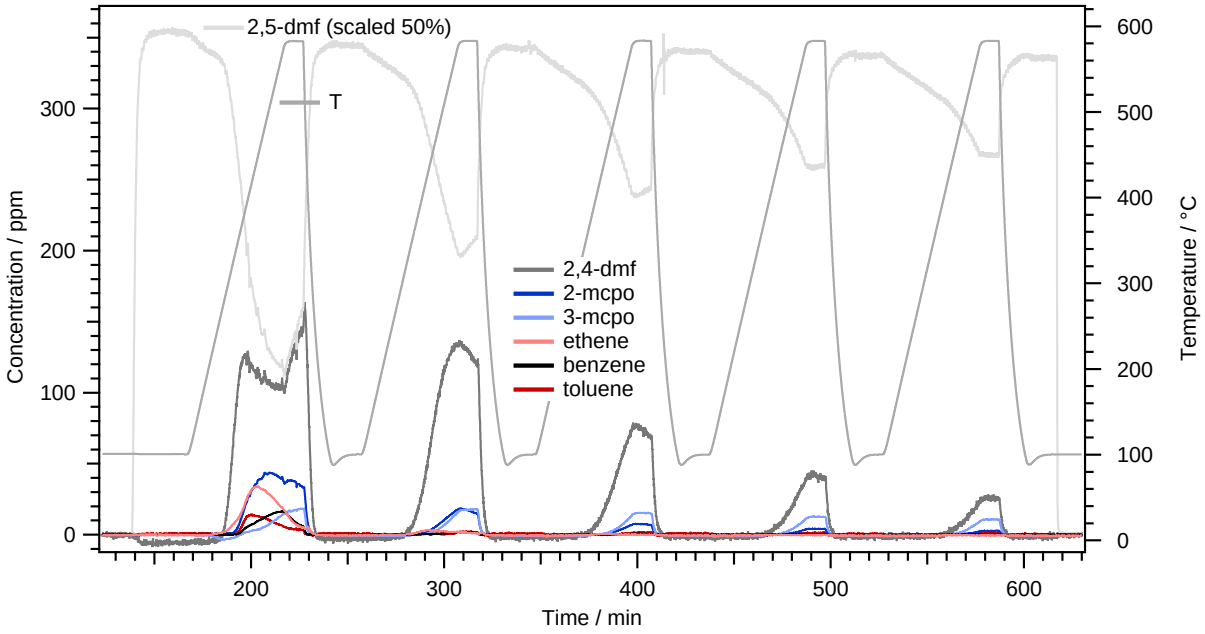

Figure 4.8: Dynamic product evolution during consequential temperature cycles (100 °C to 582 °C, 10 °C min^{-1}) of continuous 2,5-dmf exposure of H-ZSM-5(38).

4.4.4 Coking

Figure 4.9: Depiction of a fresh (colourless) and a spent (coked, black) catalyst coated on a monolith substrate.

4: or blue for Cu-ZSM-5.

During the catalytic conversion of 2,5-dmf, the catalyst deposits graphite-like coke on its surface and pores. This can often be observed visually by a black, soot-like residue on the spent sample in contrast to a fresh sample that is colourless[4] as artistically portrayed in Figure 4.9. Precursors of coke are supposed to be heavier, polycyclic aromatics, such as (substituted)indene and naphthalenes.[90] Figure 4.10 shows the MS signals of such aromatics, with an obvious trend of later detection, the bulkier and heavier the aromatics are. For instance, xylene formation is detected right at the start of 2,5-dmf exposure to the H-ZMS-5(355), while naphthalene is detected some minutes after and methylnaphthalene even after that. The detection of these coke precursors at longer TOS indicates increased coke formation, which is also observed with increasing catalyst deactivation.

This coke can be analysed in many different ways. In section 3.3.3, I already presented the analysis of temperature programmed oxidation for two different catalysts based on temperature-dependent CO and CO_2 release. In Paper III, the amount of coke stored on three different catalysts was examined. Silicalite-1 did not accumulate coke, because the absence of strong acid sites does not lead to any relevant conversion of the reactant to products and precursors of coke. In the following, the discussion focuses on how coke affects the active acid sites. Since the distinct trends in product distribution depending on TOS have been pointed out,

they must be connected to the availability of different active sites, which shall be evaluated in the following.

4.4.5 Ammonia-TPD

NH_3-TPD was introduced in section 3.3.1 as a method to determine the total amount of acid sites in zeolites. In Paper III, NH_3-TPD was used to evaluate the acid sites of fresh and spent ZSM-5 and Ga-Silicate catalysts. In Paper V and discussed in the following, NH_3-TPD was used to monitor the acid site density of the fresh catalyst, but also the increasingly coked catalyst by intermittent NH_3-TPD experiments of consequential 2,5-dmf conversion experiments. Figure 4.12 displays the experimental sequence and some of the product concentrations emerging from the consequential 2,5-dmf pulses. As can be seen, the product concentration profiles' progressions are not affected by the intermittent NH_3-TPD experiments. BTX and olefins are initially preferred products, but once they decline, isomerisation takes place before the catalyst deactivates completely.

In Figure 4.11, the corresponding intermittent NH_3-TPD profiles are presented. An obvious trend of decreasing available acid site density relates to the build-up of coke. It seems that weak acid site density (≤250 °C) is decreasing initially (NH_3-TPD#0-2), but remains stable later on (NH_3-TPD#2-4). This coincides with the decrease of BTX and olefins, while the later decrease of strong acid sites correlates with decreasing isomerisation. However, this does not necessarily mean that weak acid sites are responsible for aromatisation. On the contrary, it was found in Paper III, that even though a majority of acid sites were still available after a 10h conversion experiment, the catalyst H-ZSM-5(22) was completely inactive. On the other hand, a Ga-silicate had lost most strong acid sites but was still active for the isomerisation of 2,5-dmf, which is discussed in Section 4.6 and the topic of Paper IV.

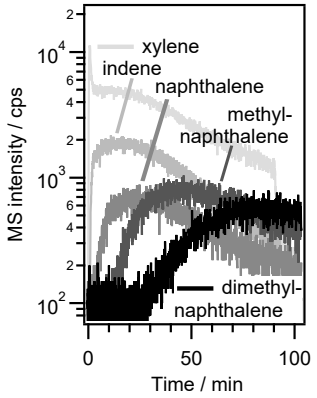

Figure 4.10: MS signals of xylene and heavier aromatics which might be precursors of coke formation.

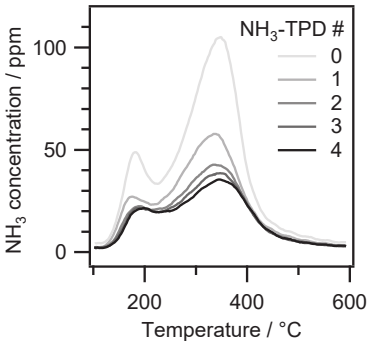

Figure 4.11: Intermittent NH_3-TPD during consecutive 20 min 2,5-dmf pulses. #0 corresponds to the fresh catalyst (H-ZSM-5(38) 300 μm to 355 μm).

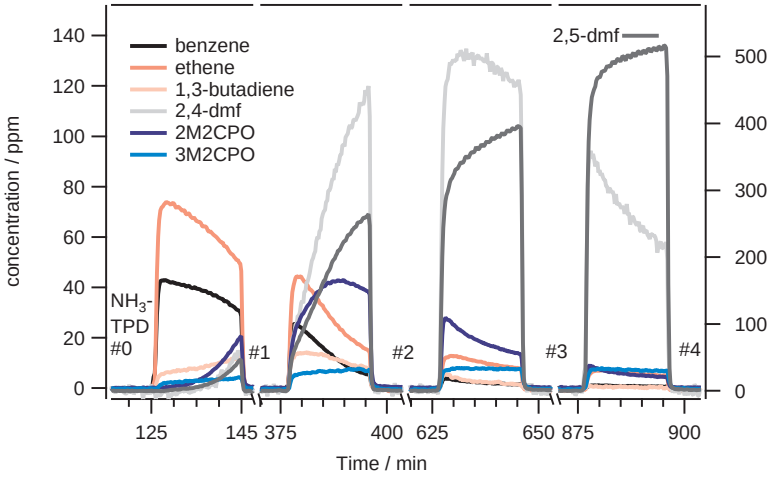

Figure 4.12: Concentration profiles of various species during 20 min 2,5-dmf pulses intermitted by NH_3-TPD (see Figure 4.11); catalyst: H-ZSM-5(38) 300 μm to 355 μm.

4.5 Targeting increased aromatics production

To increase the attractiveness of BTX production from biomass molecules, it is desirable to increase BTX yields. In this chapter, the most important findings that could contribute to enhanced BTX yields are addressed.

The comparison of continuous production with adsorption and subsequent TPD experiments described in section 3.3.2 revealed distinct differences in product distribution. One way to increase BTX yield could be to exploit the experimental procedure and process design as described later on.

Another way is the modification of the catalyst. As discussed above, using Cu-ions in the zeolite could increase initial aromatics yield at high temperatures. However, the same catalyst also suffers from faster deactivation and higher carbon oxide selectivities, which are both undesirable. It is hence interesting to study the impact of other metals in the zeolite as well. Among several, Ga was found to be a promising candidate.[152] Ga-promoted zeolites were studied for the enhancement of aromatics production for both furan[149] and 2,5-dmf[97]. The study using furan as the reactant found that aromatics selectivity increases when Ga is ion-exchanged. When Ga is incorporated into the framework, benzene selectivity increases, but overall aromatics selectivity is lower and the catalyst suffers from increased coking.[149] With 2,5-dmf as the reactant, Ga-ion exchanged zeolite shows higher aromatics selectivity, but the catalyst experiences faster deactivation and lower cumulative yields.[97] A study that used beech wood as feedstock found that Ga-containing ZSM-5 zeolites could increase *p*-xylene selectivity.[153]

From the TPD experiments with 2,5-dmf, it was observed that once adsorbed, 2,5-dmf does not desorb anymore. The modification

of acid site strength by using Ga instead of Al in the framework would thus allow a better understanding of the role of Ga in the framework and its effect on the valorisation of model compounds such as 2,5-dmf.

4.5.1 The effect of Ga in the framework

As described in section Section 4.2, Ga-silicate samples were synthesised by a sol-gel method followed by hydrothermal crystallisation to obtain MFI-type zeotypes where Ga is in the framework.[130] Figure 4.13 shows the conversion and product selectivity of benzene, toluene, olefins and isomers for two different catalyst samples, namely H-Ga-silicate(68) and H-ZSM-5(22). Some major differences can be observed: The conversion of the ZSM-5 sample is initially high but drops rapidly after 60 min to 90 min TOS. The Ga-silicate sample, on the other hand, shows a much slower decline in conversion. In fact, the latter is active for aromatisation for more than 4 h TOS and remains active for isomerisation beyond 10 h. A study on hierarchical zeolites discussing the effect of different intracrystalline pore dimensions on catalyst deactivation behaviour in the MTO reaction found that meso- and macropores suppressed deactivation behaviour in a similar way.[154] One could speculate that this has also an effect on the different samples here, however, the characterisation shows, that both ZSM-5 and Ga-silicate samples show similar isotherms and hystereses, indicating that there must be another factor that favours the prolonged activity. The weakened acid strength of the Ga-silicate might indeed lead to slower deactivation by being more selective to desired products and less to deactivating coke.

The second distinction is product distribution. For the Ga-silicate, the selectivity to benzene is significantly higher, however, toluene, xylene and olefin selectivity is lower compared to ZSM-5 samples.[5] A similar observation in selectivity changes has been made by Cheng *et al.* when studying the effect of Ga during furan conversion.[149]

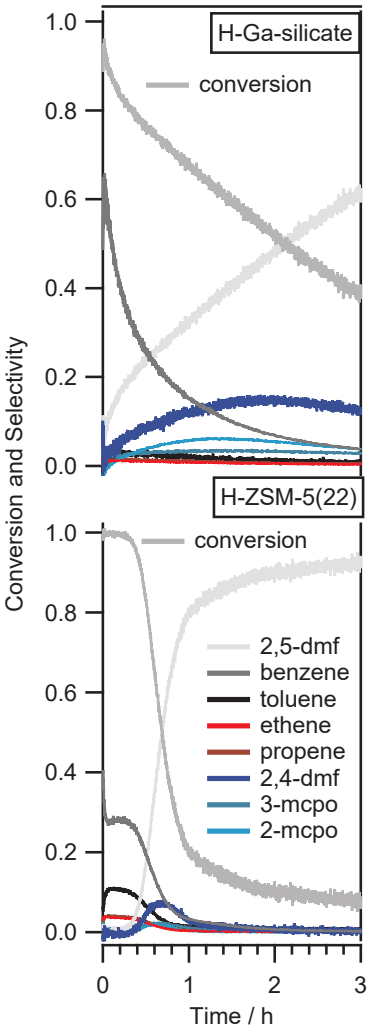

Figure 4.13: Conversion and product selectivity comparison between H-ZSM-5(22) and an H-form Ga-silicate sample.

4.5.2 The effect of ethene

The Diels-Alder cycloaddition of 2,5-dmf and ethene and subsequent dehydration is a desirable route to make *p*-xylene. If this reaction pathway takes place during the here studied conditions under a continuous flow of 2,5-dmf, adding an additional ethene feed should promote this path and thus increase the otherwise low *p*-xylene selectivity.

5: Although the Si/Al ratio is quite different from the Si/Ga ratio, the same trends in deactivation have been observed for ZSM-5 with lower and higher Si/Al ratios than the Ga-silicate sample, indicating that the deactivation behaviour might not be dependent on the Si/Al ratio. Compare also Figure 4.12 and Paper II.

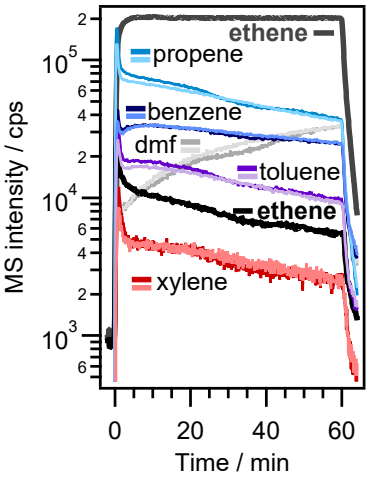

Figure 4.14: MS signals showing the effect of co-feeding ethene (light colours) on BTX production for a Ga-silicate catalyst at 400 °C. Compare also Paper III.

For this purpose, it was first tested, what happens if the catalyst is exposed to ethene alone at the target reaction temperature. For example, tests with ZSM-5(355) feeding ethene at 460 °C show no aromatics production and only trace amounts of propene are detected via MS. With Ga-silicate and at 500 °C, trace amounts of propene, benzene and toluene were detected, however, no *p*-xylene is formed as described in Paper III. This means a hypothetical increase in *p*-xylene formation from 2,5-dmf plus ethene cannot originate from ethene alone.

Second, it was tested, if *p*-xylene formation increases when both 2,5-dmf and ethene are used as reactants compared to using either 2,5-dmf or ethene alone. Figure 4.14 shows no increase in the xylene signals, which suggests, that ethene has no relevant effect on aromatics formation and behaves instead as a spectator. This can be said for both ZSM-5 and Ga-silicate catalysts. It can thus be ruled out, that Diels-Alder cycloaddition and dehydration reactions take place under the studied conditions, which is further supported by work from Uslamin *et al.*[98]. Experiments and observations regarding this question are discussed in more detail in papers II and III.

4.5.3 Increasing *p*-xylene formation

It would be desirable to steer the selectivity within the aromatic distribution to the ones that are of most need and value, of which *p*-xylene is of particular interest. In high-pressure batch reactors, very high selectivities of *p*-xylene have been achieved,[79, 92] although the same cannot be claimed for CP approaches. The latter is especially desirable because it is solvent free and can be operated continuously at atmospheric pressure, while also offering much faster reaction times.[6] During this thesis work and the Master project of Pol Mestre,[138] it is observed that *p*-xylene is formed in much higher amounts in a specific experimental procedure:[7]

At a relatively low temperature, e.g. 100 °C, 2,5-dmf is adsorbed onto the H-ZSM-5 catalyst and purged in argon to remove any physisorbed species. Then the sample is heated in inert argon atmosphere (e.g. 10 °C min^{-1}). Surprisingly, no 2,5-dmf desorbs anymore after it had been adsorbed.[8] Instead of desorption, certain reactions must take place, which is discussed in more detail later and reaction products desorb at temperatures above 200 °C. The desorption products and their desorption temperatures are summarised in Table 3.5. Among these desorption products is *p*-xylene, with one of the highest concentrations. In fact, the usual trend of selectivity B>T»X[9] is inverted to *p*X>T>B.

6: High-pressure batch reaction using 2,5-dmf and ethene produces *p*-xylene in high yields (≥90 %, however many hours reaction time, unpolar solvents and relatively high pressures (typically 40 bar to 50 bar are required.

7: This is in principle a TPR of pre-adsorbed 2,5-dmf as described in section 3.3.2.

8: The adsorption must thus be stronger than for N-heterocycle equivalents such as pyridine which is commonly applied for TPD and acid site characterisation.

9: Xylene concentrations are so low that they are at the detection limit.

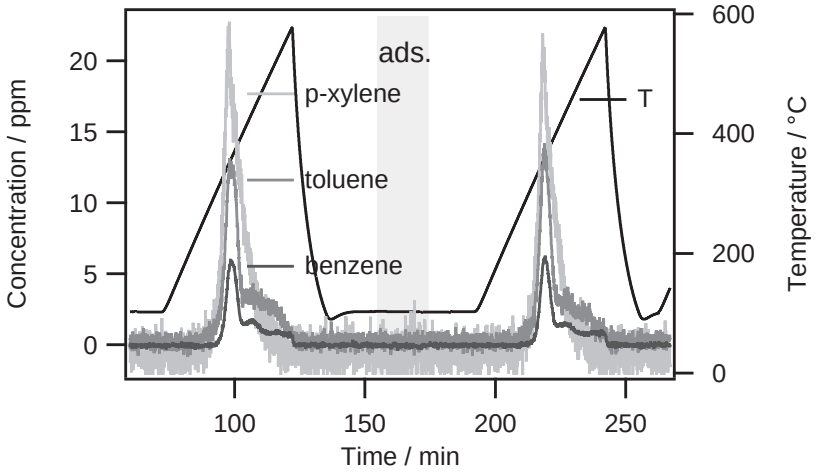

Figure 4.15: Consecutive TPR for *p*-xylene production. A consecutive sequence of 2,5-dmf adsorption and temperature programmed desorption, without catalyst regeneration in between shows continued *p*-xylene, toluene and benzene formation.

Moreover, this adsorption and temperature programmed reaction procedure gives similar results with increased heating rates and can be repeated *without* regeneration of the catalyst, resulting in only slightly lower BTX yields. The BT*p*X signals and temperature profile of two consecutive cycles are plotted in Figure 4.15. The corresponding yields are shown in Table 4.4. The *p*X yield in the 1st TPR was 46 μmol g^{-1} catalyst, more than three times the amount of benzene. For the second TPR, the decrease in BTX was between 4 and 17%, allowing several cycles before the catalyst needs to be regenerated. I also suggest that reaction conditions could be chosen even milder in the future since the temperature of maximum desorption for *p*X is around 350 °C, which is expected to reduce catalyst deactivation further.

Table 4.4: Yields of BTX and olefins obtained during a TPD after 2,5-dmf adsorption in two consecutive experiments without catalyst regeneration and the percentage decrease between the 1. and 2. TPD.

	1. TPD	2. TPD	↘
	Yield / μmol g^{-1}		/%
Aromatics			
*p*X	45.9	37.8	17
T	35.5	32.9	7
B	13.5	13.0	4
Olefins			
Bu	2.8	1.9	31
P	22.8	18.9	17
E	67.5	57.1	15

This is the first time that more of the desired *p*-xylene could be achieved under atmospheric pressure conditions. It is so far unclear what the origin of this phenomenon is. Possibly, the increased contact time at low temperatures favours *p*-xylene production over benzene. Perhaps disproportionation and transalkylation reactions are favoured under these conditions. These transalkylations of BTX are industrially applied to increase *p*X yields and utilise less desired toluene, *o*- and *m*-xylene.[126] To examine the underlying mechanisms I suggest TPR experiments, that stop the temperature ramp at the maximum desorption temperature of *p*X. Possibly the heating rate should also be slow, to distinguish better between the formation and desorption of the various BTX. Since *p*X desorbs at lower temperatures, the corresponding occupied active sites are now free to be investigated. As such, they can be probed with e.g. NH_3 or pyridine, ideally *in situ*, e.g. using DRIFTS, to clarify which acid sites become available. Active sites that host the remaining products, including benzene and toluene, should thus still be occupied.

The effect of ethene

Once again it was tested if ethene would affect aromatics selectivity. If *p*-xylene formation would happen through cycloaddition and dehydration reactions, then feeding additional ethene is expected to have a promoting effect on *p*-xylene selectivity. However, in the following separate experiments, no such effect was found.

1. Pre-adsorption of ethene onto H-ZSM-5(38) before 2,5-dmf adsorption did not increase *p*-xylene production during TPR.
2. Adsorption of ethene onto H-ZSM-5(38) that had 2,5-dmf already adsorbed did not increase *p*-xylene production during TPR.
3. Feeding ethene continuously during the TPR of pre-adsorbed 2,5-dmf did not increase *p*-xylene production.

These observations indicate that no cycloaddition and dehydration take place, meaning that other reactions or factors must be the reason for the inverted selectivity trend compared to the continuous 2,5-dmf exposure.

4.6 Selective isomerisation to 2,4-dimethylfuran

2,4-dimethylfuran possesses a rare 2,4-disubstitution pattern in the 5-membered furan ring. This structure is rather difficult to access by chemical synthesis as discussed in Paper IV. In section Section 4.6, I described that the isomerisation rate of 2,5-dmf increases with TOS, once olefin and aromatic formation declines. This discovery sparked thus interest if this observation could be exploited for the selective isomerisation of 2,5-dmf to 2,4-dmf. Indeed it was found that the Ga-silicate catalyst provides much improved long-term activity for isomerisation compared to the ZSM-5 catalysts. Figure 4.16 shows the conversion of 2,5-dmf and product selectivity, with 40% selectivity to 2,4-dmf, remaining stable after ca. 5 h TOS, while conversion continues to decline slowly. Besides, 2-mcpo and 3-mcpo are formed in lesser amounts. The same catalyst could be regenerated and was active for 48 h TOS, although with decreased overall activity, indicating some deactivation through potential loss of active sites. It is yet not completely understood what the underlying cause of the Ga-silicate catalyst's superiority in terms of activity is. Possibly the reduced acid strength makes it less prone to deactivation. However, also sterical effects caused by the larger Ga atoms compared to Al atoms in the framework could play a role.

As shortly mentioned in section Section 4.3, the BEA framework seems to favour 3-mcpo over 2-mcpo, which could path the way

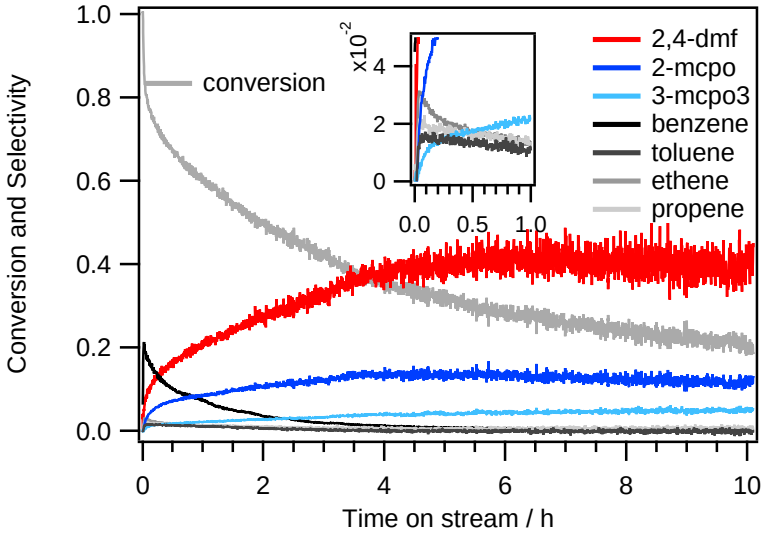

Figure 4.16: Conversion and selectivity of aromatics, olefins and isomers from a 10 h long 2,5-dmf valorisation experiment.

for more selective 3-mcpo production from 2,5-dmf with a Ga-BEA catalyst.

4.7 The role of the acid site and proposed mechanism

With the previously described observations and discussions, I now dare to propose some reaction pathways and mechanisms that 2,5-dmf undergoes upon interaction with the zeolitic catalysts. A schematic summary can be found in Figure 4.18.

The detection of 2-methylfuran and 2,3,5-trimethylfuran by GC-MS suggests disproportionation and transalkylation taking place, analogue to BTX.[126]

Predominantly weak acid sites are suggested to be responsible for isomerisation as shown in Paper III. This conclusion relies on the observation that Ga-silicate was still active for isomerisation, even though it had lost most of its acid sites, and of those mostly strong acid sites as determined by NH_3-TPD. The formation of 2,4-dmf requires an acid-catalysed methyl shift and is believed to be dependent on the sterical confinement provided by the MFI (and partly BEA) framework structure. Isomerisation to 3-mcpo and 2-mcpo requires a ring opening of 2,5-dmf.[10] The ring opening would lead to the suspected observation of ketonic C=O stretch vibrations, which were indicated by *in situ* DRIFTS experiments at 1720 cm^{-1}, 1715 cm^{-1} and 1684 cm^{-1} for H-ZSM-5(22), H-BEA(37) and Cu-ZSM-5(22) (compare Figure 4.17). In fact, adsorption of 2,5-dmf onto the here studied catalysts is not (fully) reversible and the reactant experiences subsequent reactions, such as the

10: The cyclisation of 2,5-hexanedione to either 2,5-dmf or 3-mcpo catalysed by ZSM-5 was described by Dessau.[155]

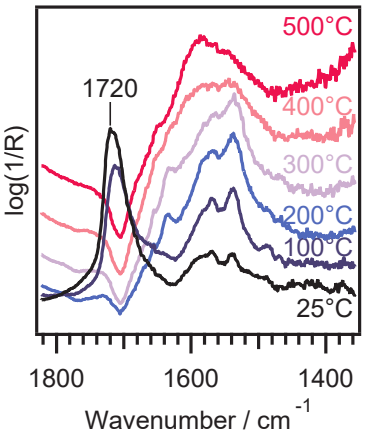

Figure 4.17: Background substracted DRIFT spectra of pre-adsorbed 2,5-dmf on H-BEA(37) and signal evolution upon temperature increase.[139]

ring-opening instead. Other works have also described such ring-opening reactions. 2,5-dmf is hydrated to 2,5-hexanedione which is then dehydrated to 3-mcpo.[156, 157]

Strong acid sites are supposedly mainly responsible for cracking, decarbonylation and dehydration reactions. Decarbonylation is indicated by the detection of carbon oxides and the C=O stretch vibration on Cu in Figure 4.7 was further evidence for such mechanisms. Dehydration reactions are well known for zeolites and are indicated by the detection of relatively large amounts of water in the product stream. These reactions could proceed for example through pathway a) in Figure 4.18 as proposed by Uslamin.[97] The resulting (olefinic) hydrocarbon pool is then subject to oligomerisation and aromatisation, which produces the desired BTX products. Some olefins such as butadiene, propene and ethene were detected in larger quantities. It was also shown, that ethene does not contribute to aromatisation. BTX can further react in a so-called arene cycle, with similar disproportionation and transalkylation as described above, but also additional alkylations are possible.

The formation of polycyclic aromatics stems from the same hydrocarbon and aromatic pool and is believed to be a precursor of coke, which finally leads to catalyst deactivation.

Diels-Alder cycloaddition reactions between 2,5-dmf and ethene and subsequent dehydration to *p*-xylene are not taking place under the here studied conditions. This is in contrast to reactions studied in high-pressure batch reactions, including the use of unpolar solvents such as *n*-heptane.[76, 79] Whereas cycloaddition seems to be facilitated by LAS on the external surface, dehydration is catalysed by BAS.[91] However, no microporous zeolite structure is strictly necessary for aromatisation,[76, 158] in contrast to the CP of biomass and bio-derived compounds. The solvent seems to stabilise certain intermediates and possibly even block the micropores, preventing undesired side reactions. Cycloaddition is also facilitated by high pressures, shifting the equilibrium to the product side.

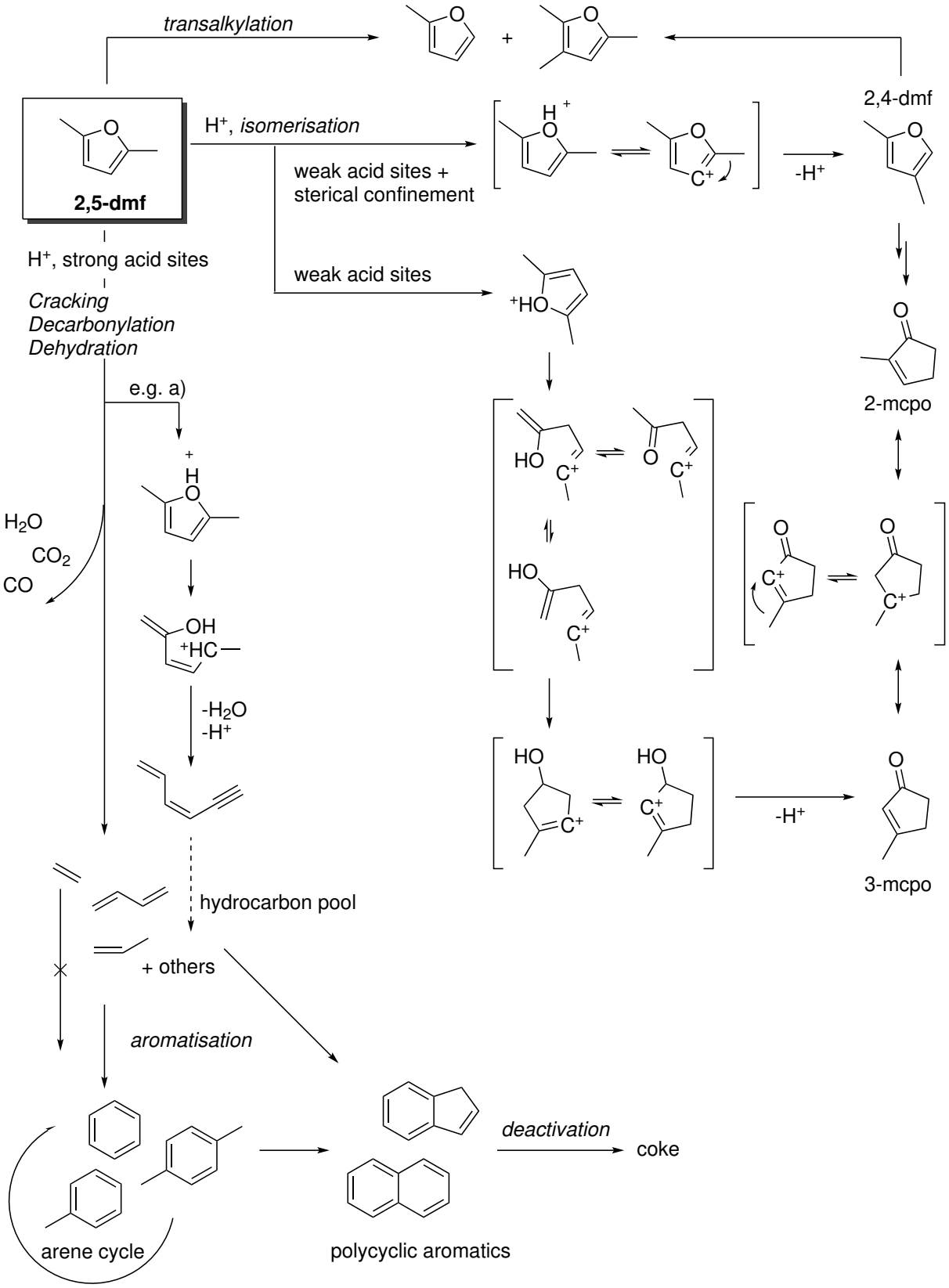

Figure 4.18: Reaction pathways for 2,5-dmf in zeolites undergoing isomerisation, cracking, decarbonylation, dehydration, oligomerisation and aromatisation reactions. The example pathway a) is based on [97].

5 Conclusions and outlook

In this final chapter, I summarise what my studies have shown and conclude the research questions and hypotheses. Then, I discuss the impact of my research and address where understanding is still missing and which questions could be targeted next.

To tackle the societal challenge of reducing fossil resource consumption, making commodity chemicals from a renewable, bio-derived feedstock can make a contribution that sequesters carbon longer than making fuels. This process requires new and better catalysts, whose development relies on the understanding of reactant-catalyst interaction and the structure-function relationship of the catalyst. For the purpose of catalysis research, the need for analytical methodology with high time resolution to study the product stream was identified.

5.1 What have I shown?

First, an on-line gas phase analysis method of a continuous complex hydrocarbon stream with infrared spectroscopy and mass spectrometry has been developed and reported in Paper I. This hydrocarbon stream stems from the catalytic valorisation of 2,5-dmf over zeolitic materials and includes a wide range of compounds, such as aromatics, olefins, carbon oxides, water and other hydrocarbons. The method was successfully applied for the identification and quantification of most compounds of interest. Hypothesis I and II[1] can thus be answered as follows: IR spectroscopy in combination with mass spectrometry is indeed a suitable and practical technique to monitor the complex hydrocarbon stream stemming from 2,5-dmf valorisation. Despite the successful identification of most products (ca. 90% carbon mass balance), some species could not be analysed and calibration plus IR band selection can be tedious. Further limitations, such as false negatives and false positives were discussed and remain a reason for caution. However, spectra can be reevaluated after future refinement. Data collection is highly automated and the method can be operated with a high time resolution ($\geq 8\,\mathrm{min}^{-1}$).

In the remaining Papers II, III, IV and V, the method was applied to a range of catalysts, among them zeolite beta and ZSM-5 to account for different framework structures[2], H-form and Cu-ion-exchanged ZSM-5, and finally, a Ga-silicate MFI zeotype, to account for various modifications of the catalyst with the same framework structure.

1: Hypothesis

- I IR spectroscopy in combination with mass spectrometry is a suitable and practical technique to monitor a complex hydrocarbon stream.
- II The developed method can be applied to catalytic conversion reactions of 2,5-dimethylfuran for a number of known zeolite catalysts.
- III The method improves understanding of the reactions and catalysts that is necessary to ultimately design better catalysts.

2: BEA and MFI

The capability of the on-line method has been shown in a variety of different experiments, that indeed improve the understanding of the reactions and catalysts as proposed in Hypothesis III. In the following, I want to highlight the most important findings:

Catalytic studies under a continuous flow of the reactant at a set temperature allowed the monitoring of product distribution and selectivity changes over time. The catalysts' selectivity towards aromatic products, such as benzene, toluene and xylenes as well as olefins is high at the beginning of 2,5-dmf exposure, but with increasing time on stream, the selectivity shifts towards isomers of 2,5-dmf. Moreover, as discussed in Paper IV, the isomer 2,4-dmf, which has a substitution pattern that is synthetically difficult to access, could be produced selectively for many hours with a Ga-silicate catalyst.

Measurements of the dynamic response of the products were carried out in (NH_3-)TPD, TPR and TPO experiments. The analysis method also facilitates the combination of many such experiments in the same reactor, allowing the preservation of the catalyst and avoiding the risk of sample loss or contamination during sample transfer.

It is suggested, that isomerisation reactions mainly proceed via weak acid sites, while cracking, oligomerisation and aromatisation reactions leading to desired BTX products mainly proceed via strong acid sites. These acid sites, especially the strong ones are, however, also prone to deactivation through the formation of coke. The reduced acid strength in the Ga-silicate sample showed decreased deactivation, resulting in higher yields of BTX aromatics, of which benzene was the most favoured one as described in Paper III.

Finally, it was shown in Paper V that *p*-xylene can be produced much more selectively by pre-adsorption of 2,5-dmf at 100 °C and subsequent TPD of the products. In fact, this procedure inverts the B>T>X selectivity trend in favour of the much-desired *p*-xylene to *p*-X>T>B.

5.2 What is the impact?

The application of the on-line analysis method presented here serves as an example for research purposes and is of high interest for catalysis research because high time resolution is a crucial factor to understand the catalyst structure-function relationship. This case extends the established use of IR spectroscopy and mass spectrometry for small molecules in catalysis research[3] to more complex organic molecules. The potential of on-line analysis

3: such as methane, carbon oxides, nitrous oxide etc. in environmental catalysis of exhaust gas

method based on IR and MS might be especially relevant for evaluating hydrocarbon streams, stemming from biomass and recycled waste plastic. The increased use of data science, machine and deep learning will also facilitate the future development of spectral analysis.

Reducing catalyst deactivation and increasing BTX yields is highly desirable for aromatics production from bio-derived molecules. The potential of a Ga-silicate zeotype catalyst was shown here and its specific catalyst properties might be relevant for future catalyst design and industrial applications, for which Ga-promoted zeolitic materials have already been pointed out as promising candidates.[152]

The discovery that 2,4-dmf can be selectively obtained from the isomerisation of readily available 2,5-dmf through a heterogeneous catalytic process might be especially relevant from the perspective of the emerging bio-refinery era.[159] 2,4-dmf has a rare 2,4-disubstitution pattern in a furan ring, interesting for the synthesis of complex organic molecules, where specific stereoselectivity is required.[160, 161]

P-xylene can be produced much more selectively when 2,5-dmf is pre-adsorbed onto H-ZSM-5 followed by TPD. Although this is not continuous production, it was shown that this procedure can be repeated consecutively with only small decreases in yield before regeneration of the catalyst becomes necessary. This approach might be industrially relevant, by applying cycles of adsorption and rapid heating[4], which could be achieved, for example via microwave-assisted heating.[162]

4: Doubling the heating rate from 10 °C min^{-1} to 20 °C min^{-1} showed similar *p*-xylene yields

5.3 What next?

The insights from this thesis work have opened many new questions, of which a few are addressed in the following discussion. For example, it remains unclear what causes the drastically increased *p*-xylene selectivity from pre-adsorbed 2,5-dmf TPD. To gain a better understanding of the reactions ongoing on the catalyst surface, I recommend further *in situ* and operando studies, for instance using DRIFTS. Moreover, adjusting the experimental procedure and catalyst could optimise *p*-xylene, ideally by suppressing undesired products.[5]

5: Isomerisation can already be avoided using this procedure.

Further improvements regarding catalyst deactivation and BTX yields are desirable. Here, the first studies on a Ga-silicate have been promising and I recommend future studies with various Ga/Si ratios. It is also desirable to understand which Ga species are responsible for which reactions, and where they are located in

the zeolite. (*In situ*) NMR and XAS studies could answer some of these questions. At the same time, other structural modifications that reduce the acid strength, such as Fe-silicate, could be worth investigating.

The isomerisation reactions described here could be investigated for furans with different substituents, as furans gain importance as platform molecules.[6] The scope of isomerisation might also be extended to N-heterocycles and thiophenes, sulfur analogues of the 5-membered furans.

6: E.g. as PET replacement PEF.

Finally, N-heterocycles, such as pyridine could also be used as probe molecules to further investigate the role of acid sites. Pyridine is used for reversible adsorption on the zeolite, whereas it was shown here, that 2,5-dmf adsorbs irreversibly. Competitive adsorption studies could exploit the different adsorption behaviour to probe only certain sites with either pyridine or 2,5-dmf and reveal the character of the acid site.

Acknowledgements

The research presented in this thesis was carried out at the Division of Applied Chemistry at the Department of Chemistry and Chemical Engineering at Chalmers University of Technology, Gothenburg, Sweden between May 2018 and December 2022.

Parts of this work were carried out at the Chalmers Materials Analysis Laboratory (CMAL). The access to instrumentation and assistance is greatfully acknowledged.

This work was funded by the Swedish Research Council for Environment, Agricultural Sciences and Spatial Planning (Formas) through the project "Green aromatics for a bio-based economy" (No. 2017-00420). The financial support is gratefully acknowledged.

I want to express my sincere gratitude to my main supervisor Per-Anders Carlsson for your guidance and support. I appreciate your patience and encouragement, your positive perspectives and your attitude. I value that your supervision style makes research an explorative adventure. I will remember many valuable discussions about research and being a scientist. Tack.

Major thanks also to:

My co-supervisor Anders Lorén, for our experiments, lunches and discussions together. Danke Andreas Schaefer, für all deine Hilfe und Unterstützung.

My examiner Hanna Härelind, for evaluating my research progress, leading the Chemistry Department and creating a nice work environment.

My opponent and defense committee for evaluating my thesis and disputation.

Lasse Urholm and Lennart Norberg for your help with the reactors, and equipment and for fixing many failures.

Xuětíng Wang and Simone Creci for providing catalyst samples.

Lotta Pettersson, Frida Andersson, Anna Oskarsson, and Christian Müller for your efforts, support and hidden administrative work making Applied Chemistry a great place to work at.

Professors and researchers at Chemistry and KCK for your encouragement, perspectives, advice and our discussions.

My special thanks to Felix and Xuětíng for your tireless help especially when I was new. To Guido and Pol thanks for our great collaboration and discussions. To my group members Xuětíng, Yanyue (妍王月), Peter, Per-Anders, Jojo (梦乔), Guido, Felix, Alexander and Andreas.

I am grateful for my time and colleagues in the K BIO PhD student council, the Doctoral Students Guild and Sveriges Förenade Studentkårers Doktorandkommitté. You have been great colleagues to work with during these challenging and meaningful tasks, where also I have developed tremendously.

All my current and previous colleagues at KCK, TYK and the rest of Chalmers for a good atmosphere including all the fikas, sports sessions, after works, games and discussions. I am grateful for my friends in and outside of Chalmers, for your love and for letting me have a good time with you during and after my research studies, when we play board games, practise yoga, spent time in nature, go hiking, biking, climbing. I want to thank those who taught me and are always motivated to join. I consider these **activ**ities crucial for my health just as Juvenal wrote: *sana mens in corpore sano*.

亲爱的雪婷，我要感谢你对我的爱和所有的支持。我很感激我们一起度过的时光，并且更加期待我们不断壮大的家庭的未来。*

Zum Schluss möchte ich meiner Familie danken. Ganz besonders meinen Eltern, für eure Liebe, Unterstützung und die Freiheit meinen Interessen und Vorlieben nachzugehen. Dank natürlich auch meinen Geschwistern. Danke, dass ihr immer für mich da seid.

Christopher Sauer
Göteborg, December 2022

* Translation: Dear Xueting, I want to thank you for your love and all your support. I am very grateful for the time we spent together, and I look forward to the future of our growing family.

Bibliography

[1] Chris D. Thomas et al. 'Extinction risk from climate change'. In: *Nature* 427.6970 (Jan. 2004), pp. 145–148. DOI: 10.1038/nature02121 (cit. on p. 1).

[2] Pieter Tans and Ralph Keeling. *Trends in Atmospheric Carbon Dioxide*. DOI: 10.1029/95JD03410. URL: https://gml.noaa.gov/webdata/ccgg/trends/co2/co2_annmean_mlo.txt (cit. on p. 1).

[3] Global Carbon Project. *Annual CO2 emissions worldwide 1940-2020 | Statista*. URL: https://www.statista.com/statistics/276629/global-co2-emissions/ (cit. on p. 1).

[4] Johan Rockström et al. 'A safe operating space for humanity'. In: *Nature* 461.7263 (Sept. 2009), pp. 472–475. DOI: 10.1038/461472a (cit. on pp. 1, 10).

[5] Johan Rockström et al. 'Identifying a Safe and Just Corridor for People and the Planet'. In: *Earth's Future* 9.4 (Apr. 2021), e2020EF001866. DOI: 10.1029/2020ef001866 (cit. on p. 1).

[6] Hannah Ritchie, Max Roser and Pablo Rosado. 'CO2 and Greenhouse Gas Emissions'. In: *Our World in Data* (2020). https://ourworldindata.org/co2-and-other-greenhouse-gas-emissions (cit. on p. 1).

[7] H.-O. Pörtner et al. 'IPCC, 2022: Summary for Policymakers'. In: *Climate Change 2022: Impacts, Adaptation and Vulnerability*. Cambridge, UK and New York, NY, USA: Cambridge University Press, 2022, pp. 3–33. DOI: 10.1017/9781009325844.001 (cit. on p. 1).

[8] David I. Armstrong McKay et al. 'Exceeding 1.5°C global warming could trigger multiple climate tipping points'. In: *Science* 377.6611 (Sept. 2022), eabn7950. DOI: 10.1126/SCIENCE.ABN7950 (cit. on p. 1).

[9] Benjamin I. Cook et al. 'Megadroughts in the Common Era and the Anthropocene'. In: *Nature Reviews Earth & Environment* (Oct. 2022), pp. 1–17. DOI: 10.1038/s43017-022-00329-1 (cit. on p. 1).

[10] Guangdong Li et al. 'Global impacts of future urban expansion on terrestrial vertebrate diversity'. In: *Nature Communications* 13.1 (Dec. 2022), p. 1628. DOI: 10.1038/s41467-022-29324-2 (cit. on pp. 1, 2).

[11] Bradley J. Cardinale et al. 'Biodiversity loss and its impact on humanity'. In: *Nature* 486.7401 (June 2012), pp. 59–67. DOI: 10.1038/nature11148 (cit. on p. 1).

[12] Moises Exposito-Alonso et al. 'Genetic diversity loss in the Anthropocene'. In: *Science* 377.6613 (Sept. 2022), pp. 1431–1435. DOI: 10.1126/SCIENCE.ABN5642 (cit. on p. 1).

[13] Kristen Ruegg and Sheela Turbek. 'Estimating global genetic diversity loss'. In: *Science* 377.6613 (Sept. 2022), pp. 1384–1385. DOI: 10.1126/science.add0007 (cit. on p. 1).

[14] Anthony D. Barnosky et al. 'Has the Earth's sixth mass extinction already arrived?' In: *Nature* 471.7336 (Mar. 2011), pp. 51–57. DOI: 10.1038/nature09678 (cit. on p. 1).

[15] Zeke Hausfather and Frances C. Moore. 'Net-zero commitments could limit warming to below 2°C'. In: *Nature* 604.7905 (Apr. 2022), pp. 247–248. DOI: 10.1038/d41586-022-00874-1 (cit. on p. 1).

[16] Katherine Calvin et al. 'Bioenergy for climate change mitigation: Scale and sustainability'. In: *GCB Bioenergy* 13.9 (Sept. 2021), pp. 1346–1371. DOI: 10.1111/GCBB.12863 (cit. on p. 1).

[17] Arthur J. Ragauskas et al. 'The path forward for biofuels and biomaterials'. In: *Science* 311.5760 (Jan. 2006), pp. 484–489. DOI: 10.1126/SCIENCE.1114736 (cit. on p. 2).

[18] Josep G. Canadell and E. Detlef Schulze. 'Global potential of biospheric carbon management for climate mitigation'. In: *Nature Communications* 5.1 (Nov. 2014), pp. 1–12. DOI: 10.1038/ncomms6282 (cit. on p. 2).

[19] Richard Orange. *Is there enough wood in the world to feed sustainability? | Global Ideas | DW | 01.05.2020*. May 2020. URL: https://p.dw.com/p/3bKUF (cit. on p. 2).

[20] *Is There Enough Biomass to Fuel the World? Part III — Mr. Sustainability*. URL: https://www.mr-sustainability.com/stories/2020/is-there-enough-biomass-to-fuel-the-world-3 (cit. on p. 2).

[21] Roeland Bosch, Mattheüs Van De Pol and Jim Philp. 'Policy: Define biomass sustainability'. In: *Nature* 523.7562 (July 2015), pp. 526–527. DOI: 10.1038/523526a (cit. on p. 2).

[22] Matti Parikka. 'Global biomass fuel resources'. In: *Biomass and Bioenergy* 27.6 (Dec. 2004), pp. 613–620. DOI: 10.1016/J.BIOMBIOE.2003.07.005 (cit. on p. 2).

[23] William R. L. Anderegg et al. 'A climate risk analysis of Earth's forests in the 21st century'. In: *Science* 377.6610 (Sept. 2022), pp. 1099–1103. DOI: 10.1126/SCIENCE.ABP9723 (cit. on p. 2).

[24] Lars Gamfeldt et al. 'Higher levels of multiple ecosystem services are found in forests with more tree species'. In: *Nature Communications* 4.1 (Jan. 2013), pp. 1–8. DOI: 10.1038/ncomms2328 (cit. on pp. 2, 3).

[25] David R. Williams et al. 'Proactive conservation to prevent habitat losses to agricultural expansion'. In: *Nature Sustainability* 4.4 (Dec. 2020), pp. 314–322. DOI: 10.1038/s41893-020-00656-5 (cit. on p. 2).

[26] Per Sandström et al. 'On the decline of ground lichen forests in the Swedish boreal landscape: Implications for reindeer husbandry and sustainable forest management'. In: *Ambio* 45.4 (May 2016), pp. 415–429. DOI: 10.1007/S13280-015-0759-0 (cit. on p. 2).

[27] Greta Thunberg et al. *Burning forests for energy isn't 'renewable' – now the EU must admit it | Greta Thunberg and others | The Guardian*. Sept. 2022. URL: https://www.theguardian.com/world/commentisfree/2022/sep/05/burning-forests-energy-renewable-eu-wood-climate (cit. on p. 2).

[28] E. Dinerstein et al. 'A Global Deal for Nature: Guiding principles, milestones, and targets'. In: *Science Advances* 5.4 (2019). DOI: 10.1126/SCIADV.AAW2869 (cit. on p. 2).

[29] European Commission. *Protecting biodiversity worldwide – towards an international agreement at COP 15*. URL: https://environment.ec.europa.eu/international/protecting-biodiversity-worldwide-towards-international-agreement-cop-15_en (cit. on p. 2).

[30] Florence Pendrill et al. 'Disentangling the numbers behind agriculture-driven tropical deforestation'. In: *Science* 377.6611 (Sept. 2022), eabm9267. DOI: 10.1126/SCIENCE.ABM9267 (cit. on p. 2).

[31] Sarah Hurtes and Weiyi Cai. *Europe Is Sacrificing Its Ancient Forests for Energy - The New York Times*. New York, Sept. 2022. URL: https://www.nytimes.com/interactive/2022/09/07/world/europe/eu-logging-wood-pellets.html (cit. on pp. 2, 3).

[32] Kristina Back. *FSC-certifierat bolag avverkar fjällnära skog med höga naturvärden | Natursidan*. Nov. 2021. URL: https://www.natursidan.se/aktuellt/fsc-certifierat-bolag-avverkar-fjallnara-skog-med-hoga-naturvarden/ (cit. on p. 3).

[33] Joe Crowley and Tim Robinson. *Drax: UK power station owner cuts down primary forests in Canada - BBC News*. Oct. 2022. URL: https://www.bbc.com/news/science-environment-63089348 (cit. on p. 3).

[34] Hazel Sheffield. *'Carbon-neutrality is a fairy tale': how the race for renewables is burning Europe's forests | Climate crisis | The Guardian*. Jan. 2021. URL: https://www.theguardian.com/world/2021/jan/14/carbon-neutrality-is-a-fairy-tale-how-the-race-for-renewables-is-burning-europes-forests (cit. on p. 3).

[35] Iris M. Hertog, Sara Brogaard and Torsten Krause. *The Swedish forestry model: intensifying production for sustainability? - InnoForESt*. Aug. 2019. URL: https://innoforest.eu/blog/the-swedish-forestry-model-intensifying-production-for-sustainability/ (cit. on p. 3).

[36] Palle Liljebäck. 'Dialog och handling är vägen framåt'. In: *Naturvetaren* (Sept. 2022), pp. 19–24 (cit. on p. 3).

[37] Felix Creutzig et al. 'Bioenergy and climate change mitigation: an assessment'. In: *GCB Bioenergy* 7.5 (Sept. 2015), pp. 916–944. DOI: 10.1111/GCBB.12205 (cit. on pp. 3, 4).

[38] Steffen Schlömer et al. 'Annex III Technology-specific Cost and Performance Parameters'. In: *Climate Change 2014: Mitigation of Climate Change. Contribution of Working Group III to the Fifth Assessment Report of the Intergovernmental Panel on Climate Change*. Ed. by O. Edenhofer et al. Cambridge, United Kingdom and New York, NY, USA: Cambridge University Press, 2014 (cit. on pp. 3, 4).

[39] Weiguo Liu et al. 'Analysis of the Global Warming Potential of Biogenic CO2 Emission in Life Cycle Assessments'. In: *Scientific Reports* 7.1 (Jan. 2017), pp. 1–8. DOI: 10.1038/srep39857 (cit. on p. 3).

[40] Anil Baral and Chris Malins. *Comprehensive carbon accounting for identification of sustainable biomass feedstocks*. Tech. rep. San Francisco: International Council on Clean Transportation, 2014 (cit. on p. 4).

[41] Abhijeet Mishra et al. 'Land use change and carbon emissions of a transformation to timber cities'. In: *Nature Communications* 13.1 (Aug. 2022), pp. 1–12. DOI: 10.1038/s41467-022-32244-w (cit. on p. 4).

[42] Coralie Jehanno et al. 'Critical advances and future opportunities in upcycling commodity polymers'. In: *Nature* 603.7903 (Mar. 2022), pp. 803–814. DOI: 10.1038/s41586-021-04350-0 (cit. on pp. 4, 5).

[43] IEA. *Direct CO2 emissions from primary chemical production in the Net Zero Scenario, 2015-2030 – Charts – Data & Statistics - IEA*. 2021. URL: https://www.iea.org/data-and-statistics/charts/direct-co2-emissions-from-primary-chemical-production-in-the-net-zero-scenario-2015-2030 (cit. on p. 4).

[44] IEA. *Putting CO2 to Use - Analysis - IEA*. Tech. rep. Paris: IEA, 2019 (cit. on p. 5).

[45] Qiang Liu et al. 'Using carbon dioxide as a building block in organic synthesis'. In: *Nature Communications* 6.1 (Jan. 2015), pp. 1–15. DOI: 10.1038/ncomms6933 (cit. on p. 5).

[46] Paolo Gabrielli, Matteo Gazzani and Marco Mazzotti. 'The Role of Carbon Capture and Utilization, Carbon Capture and Storage, and Biomass to Enable a Net-Zero-CO2 Emissions Chemical Industry'. In: *Industrial and Engineering Chemistry Research* 59.15 (Apr. 2020), pp. 7033–7045. DOI: 10.1021/ACS.IECR.9B06579 (cit. on p. 5).

[47] La Shanda T.J. Korley et al. 'Toward polymer upcycling—adding value and tackling circularity'. In: *Science* 373.6550 (July 2021), pp. 66–69. DOI: 10.1126/science.abg4503 (cit. on p. 5).

[48] Matthew MacLeod et al. 'The global threat from plastic pollution'. In: *Science* 373.6550 (July 2021), pp. 61–65. DOI: 10.1126/science.abg5433 (cit. on p. 5).

[49] Jeannette M. Garcia and Megan L. Robertson. 'The future of plastics recycling'. In: *Science* 358.6365 (Nov. 2017), pp. 870–872. DOI: 10.1126/science.aaq0324 (cit. on p. 5).

[50] Ina Vollmer et al. 'Beyond mechanical recycling: giving new life to plastic waste'. In: *Angew. Chem. Int. Ed.* 59.36 (Sept. 2020), pp. 15402–15423. DOI: 10.1002/anie.201915651 (cit. on p. 5).

[51] Geoffrey W. Coates and Yutan D.Y.L. Getzler. 'Chemical recycling to monomer for an ideal, circular polymer economy'. In: *Nat. Rev. Mater.* 5.7 (July 2020), pp. 501–516. DOI: 10.1038/s41578-020-0190-4 (cit. on p. 5).

[52] Jian Bo Zhu et al. 'A synthetic polymer system with repeatable chemical recyclability'. In: *Science* 360.6387 (Apr. 2018), pp. 398–403. DOI: 10.1126/science.aar5498 (cit. on p. 5).

[53] Kim Ragaert, Laurens Delva and Kevin Van Geem. 'Mechanical and chemical recycling of solid plastic waste'. In: *Waste Manage.* 69 (Nov. 2017), pp. 24–58. DOI: 10.1016/j.wasman.2017.07.044 (cit. on p. 5).

[54] Bruce Adams. *Germany to Get Europe's Largest Advanced Recycling Plant | plasticstoday.com*. Sept. 2022. URL: https://www.plasticstoday.com/advanced-recycling/germany-get-europes-largest-advanced-recycling-plant (cit. on p. 5).

[55] Yangsiyu Lu et al. 'Plant conversions and abatement technologies cannot prevent stranding of power plant assets in 2°C scenarios'. In: *Nature Communications* 13.1 (Feb. 2022), pp. 1–11. DOI: 10.1038/s41467-022-28458-7 (cit. on p. 5).

[56] Yi Cheng, Fei Wei and Yong Jin. 'Multiphase reactor engineering for clean and low-carbon energy applications'. In: (2017) (cit. on p. 5).

[57] Jianrong Jiang et al. 'Comparative technoeconomic analysis and life cycle assessment of aromatics production from methanol and naphtha'. In: *Journal of Cleaner Production* 277 (Dec. 2020), p. 123525. DOI: 10.1016/J.JCLEPRO.2020.123525 (cit. on pp. 5, 10).

[58] Anthony Anukam and Jonas Berghel. 'Biomass Pretreatment and Characterization: A Review'. In: *Biotechnological Applications of Biomass*. Ed. by Thalita Peixoto Basso, Thiago Olitta Basso and Luiz Carlos Basso. Rijeka: IntechOpen, 2020. Chap. 2. DOI: 10.5772/intechopen.93607 (cit. on p. 6).

[59] Edward S. Lipinsky. 'Pretreatment of Biomass for Thermochemical Biomass Conversion'. In: *Fundamentals of Thermochemical Biomass Conversion*. Ed. by R. P. Overend, T. A. Milne and L. K. Mudge. Dordrecht: Springer Netherlands, 1985, pp. 77–87. DOI: 10.1007/978-94-009-4932-4_4 (cit. on p. 6).

[60] IHS Markit. *Distribution of primary petrochemical consumption worldwide in 2021, by type | Statista*. Nov. 2021. URL: https://www.statista.com/statistics/1319374/petrochemical-consumption-share-by-type-globally/ (cit. on p. 7).

[61] S. Matar and L.F. Hatch. *Chemistry of petrochemical processes*. Chemical, Petrochemical & Process. Gulf Professional Pub., 2001 (cit. on p. 7).

[62] Aromatics Producers Association (APA) - CEFIC. 2001. URL: https://www.petrochemistry.eu/wp-content/uploads/2018/01/APAEN.pdf (visited on 04/04/2020) (cit. on p. 7).

[63] The Business Research Company. 2018. URL: https://www.thebusinessresearchcompany.com/report/aromatics-global-market-briefing-2018 (visited on 04/04/2020) (cit. on p. 7).

[64] Alexander M. Niziolek et al. 'Biomass-Based Production of Benzene, Toluene, and Xylenes via Methanol: Process Synthesis and Deterministic Global Optimization'. In: *Energy and Fuels* 30.6 (June 2016), pp. 4970–4998. DOI: 10.1021/acs.energyfuels.6b00619 (cit. on p. 7).

[65] *Chemical Prices Database and Industry Market Insights - ECHEMI*. URL: https://www.echemi.com/weekly-price.html (cit. on p. 7).

[66] AgileIntel Research (ChemIntel360). *Benzene global market volume 2015-2029 | Statista*. Apr. 2022. URL: https://www.statista.com/statistics/1245172/benzene-market-volume-worldwide/ (cit. on p. 7).

[67] AgileIntel Research (ChemIntel360). *Toluene global market volume 2015-2029 | Statista*. Feb. 2022. URL: https://www.statista.com/statistics/1245224/toluene-market-volume-worldwide/ (cit. on p. 7).

[68] Statista. *Global xylene demand & capacity 2015-2022 | Statista*. June 2020. URL: https://www.statista.com/statistics/1246700/xylene-demand-capacity-forecast-worldwide/ (cit. on p. 7).

[69] W. A. Sweeney and P. F. Bryan. 'BTX Processing'. In: *Kirk-Othmer Encyclopedia of Chemical Technology*. American Cancer Society, 2000. DOI: 10.1002/0471238961.02202419230505.a01 (cit. on p. 7).

[70] Michèle Besson, Pierre Gallezot and Catherine Pinel. 'Conversion of Biomass into Chemicals over Metal Catalysts'. In: *Chemical Reviews* 114.3 (2014). PMID: 24083630, pp. 1827–1870. DOI: 10.1021/cr4002269 (cit. on p. 8).

[71] Manuel Moliner, Yuriy Román-Leshkov and Mark E. Davis. 'Tin-containing zeolites are highly active catalysts for the isomerization of glucose in water'. In: *Proceedings of the National Academy of Sciences* 107.14 (Apr. 2010), pp. 6164–6168. DOI: 10.1073/PNAS.1002358107 (cit. on p. 8).

[72] Yuriy Román-Leshkov, Juben N Chheda and James A Dumesic. 'Phase Modifiers Promote Efficient Production of Hydroxymethylfurfural from Fructose'. In: *Science* 312.5782 (June 2006), p. 1933. DOI: 10.1126/science.1126337 (cit. on p. 8).

[73] Guang-Hui Wang et al. 'Platinum–cobalt bimetallic nanoparticles in hollow carbon nanospheres for hydrogenolysis of 5-hydroxymethylfurfural'. In: *Nature Materials* 13.3 (2014), pp. 293–300. DOI: 10.1038/nmat3872 (cit. on pp. 8, 9).

[74] Todd A Werpy, John E Holladay and James F White. 'Top Value Added Chemicals From Biomass: I. Results of Screening for Potential Candidates from Sugars and Synthesis Gas'. In: *U.S. Department of energy* 1 (Nov. 2004), p. 76. DOI: 10.2172/926125 (cit. on p. 8).

[75] Joseph J. Bozell and Gene R. Petersen. 'Technology development for the production of biobased products from biorefinery carbohydrates - The US Department of Energy's "top 10" revisited'. In: *Green Chemistry* 12.4 (2010), pp. 539–554. DOI: 10.1039/b922014c (cit. on p. 8).

[76] Saikat Dutta and Navya Subray Bhat. 'Catalytic synthesis of renewable p-xylene from biomass-derived 2,5-dimethylfuran: a mini review'. In: *Biomass Conversion and Biorefinery* (2020). DOI: 10.1007/s13399-020-01042-z (cit. on pp. 8, 12, 33, 50).

[77] Leena Nurmi et al. *From biomass to value-added furan-based platform chemicals: FURCHEM and CatBio roadmap*. Tech. rep. Espoo: VTT Technical Research Centre of Finland, Mar. 2018, pp. 1–80 (cit. on p. 8).

[78] BIS Research. *Polyethylene furanoate global market value by application 2025 | Statista*. Dec. 2018. URL: https://www.statista.com/statistics/950678/polyethylene-furanoate-global-market-value-by-application/ (cit. on p. 8).

[79] Chun-Chih Chang et al. 'Ultra-selective cycloaddition of dimethylfuran for renewable p-xylene with H-BEA'. In: *Green Chem.* 16.2 (Jan. 2014), pp. 585–588. DOI: 10.1039/C3GC40740C (cit. on pp. 8, 12, 46, 50).

[80] Fan Yang et al. 'Integral techno-economic comparison and greenhouse gas balances of different production routes of aromatics from biomass with CO2 capture'. In: *Journal of Cleaner Production* 372 (Oct. 2022), p. 133727. DOI: 10.1016/J.JCLEPRO.2022.133727 (cit. on pp. 9, 10).

[81] Inc Anellotech. *Chemicals | Anellotech, Inc | Cost Competitive Bio-Sourced Chemicals and Fuels*. URL: https://www.anellotech.com/ (cit. on p. 9).

[82] Jane L. Price and Jeremy B. Joseph. 'Demand management – a basis for waste policy: a critical review of the applicability of the waste hierarchy in terms of achieving sustainable waste management'. In: *Sustainable Development* 8.2 (2000), pp. 96–105. DOI: 10.1002/(SICI)1099-1719(200005)8:2 (cit. on p. 10).

[83] Mangesh Gharfalkar et al. 'Analysis of waste hierarchy in the European waste directive 2008/98/EC'. In: *Waste Management* 39 (May 2015), pp. 305–313. DOI: 10.1016/J.WASMAN.2015.02.007 (cit. on p. 10).

[84] I. Chorkendorff and J. W. Niemantsverdriet. 'Introduction to Catalysis'. In: *Concepts of Modern Catalysis and Kinetics*. 3rd ed. Vol. 3. Weinheim: Wiley-VCH, 2017. Chap. 1, p. 452 (cit. on pp. 10, 11).

[85] V. Smil. 'Detonator of the population explosion'. In: *Nature* 400.6743 (July 1999), p. 415. DOI: 10.1038/22672 (cit. on p. 10).

[86] 'Global climate strike'. In: *Nature Catalysis* 2.10 (Oct. 2019), p. 831. DOI: 10.1038/s41929-019-0374-8 (cit. on p. 11).

[87] Christopher Sauer. 'Green aromatics for a bio-based economy - Valorization of biomass derived model compounds over zeolites studied by online analysis'. Licentiate Thesis. Gothenburg: Chalmers University of Technology, 2021 https://research.chalmers.se/en/publication/522878 (cit. on pp. 11, 17, 18, 20, 34).

[88] George W. W. Huber and Avelino Corma. 'Synergies between bio- and oil refineries for the production of fuels from biomass'. In: *Angewandte Chemie - International Edition* 46.38 (Sept. 2007), pp. 7184–7201. DOI: 10.1002/anie.200604504 (cit. on p. 11).

[89] Torren R. R. Carlson, Tushar P. P. Vispute and George W. W. Huber. 'Green gasoline by catalytic fast pyrolysis of solid biomass derived compounds.' In: *ChemSusChem* 1.5 (May 2008), pp. 397–400. DOI: 10.1002/cssc.200800018 (cit. on p. 11).

[90] Yu Ting Cheng and George W. Huber. 'Chemistry of furan conversion into aromatics and olefins over HZSM-5: A model biomass conversion reaction'. In: *ACS Catalysis* 1.6 (June 2011), pp. 611–628. DOI: 10.1021/cs200103j (cit. on pp. 11, 19, 26, 27, 40, 42).

[91] Nima Nikbin et al. 'A DFT study of the acid-catalyzed conversion of 2,5-dimethylfuran and ethylene to p-xylene'. In: *Journal of Catalysis* 297 (Jan. 2013), pp. 35–43. DOI: 10.1016/j.jcat.2012.09.017 (cit. on pp. 11, 50).

[92] Xinqiang Feng et al. 'Ultra-selective p-xylene production through cycloaddition and dehydration of 2,5-dimethylfuran and ethylene over tin phosphate'. In: *Applied Catalysis B: Environmental* 259 (Dec. 2019), p. 118108. DOI: 10.1016/j.apcatb.2019.118108 (cit. on pp. 12, 46).

[93] Sebastian Kozuch and Jan M.L. Martin. '"Turning over" definitions in catalytic cycles'. In: *ACS Catalysis* 2.12 (Dec. 2012), pp. 2787–2794. DOI: 10.1021/CS3005264 (cit. on p. 15).

[94] Yu Ting Cheng and George W. Huber. 'Production of targeted aromatics by using Diels-Alder classes of reactions with furans and olefins over ZSM-5'. In: *Green Chemistry* 14.11 (Oct. 2012), pp. 3114–3125. DOI: 10.1039/c2gc35767d (cit. on pp. 16, 19, 33).

[95] Qiang Lu et al. 'Catalytic Fast Pyrolysis of Biomass Impregnated with Potassium Phosphate in a Hydrogen Atmosphere for the Production of Phenol and Activated Carbon'. In: *Frontiers in Chemistry* 6 (Feb. 2018), p. 32. DOI: 10.3389/fchem.2018.00032 (cit. on p. 16).

[96] Juliana S Espindola et al. 'Conversion of furan over gallium and zinc promoted ZSM-5: The effect of metal and acid sites'. In: *Fuel Processing Technology* 201.August 2019 (2020), p. 106319. DOI: 10.1016/j.fuproc.2019.106319 (cit. on p. 16).

[97] Evgeny A. Uslamin et al. 'Catalytic conversion of furanic compounds over Ga-modified ZSM-5 zeolites as a route to biomass-derived aromatics'. In: *Green Chemistry* 20.16 (2018), pp. 3818–3827. DOI: 10.1039/C8GC01528G (cit. on pp. 16, 19, 26, 38, 41, 44, 50, 51).

[98] Evgeny A. Uslamin et al. 'Gallium-promoted HZSM-5 zeolites as efficient catalysts for the aromatization of biomass-derived furans'. In: *Chemical Engineering Science* 198 (Apr. 2019), pp. 305–316. DOI: 10.1016/j.ces.2018.09.023 (cit. on pp. 16, 46).

[99] Evgeny A. Uslamin et al. 'Co-Aromatization of Furan and Methanol over ZSM-5—A Pathway to Bio-Aromatics'. In: *ACS Catalysis* 9.9 (Sept. 2019), pp. 8547–8554. DOI: 10.1021/acscatal.9b02259 (cit. on p. 16).

[100] Christopher Sauer et al. 'On-Line Composition Analysis of Complex Hydrocarbon Streams by Time-Resolved Fourier Transform Infrared Spectroscopy and Ion–Molecule Reaction Mass Spectrometry'. In: *Analytical Chemistry* 93.39 (Oct. 2021), pp. 13187–13195. DOI: 10.1021/ACS.ANALCHEM.1C01929 (cit. on pp. 16, 19, 22–25).

[101] D. Bassi, P. Tosi and R. Schlögl. 'Ion-molecule-reaction mass spectrometer for on-line gas analysis'. In: *Journal of Vacuum Science & Technology A: Vacuum, Surfaces, and Films* 16.1 (Jan. 1998), pp. 114–122. DOI: 10.1116/1.580957 (cit. on p. 17).

[102] Cyrill Hornuss et al. 'Real-time monitoring of propofol in expired air in humans undergoing total intravenous anesthesia'. In: *Anesthesiology* 106.4 (Apr. 2007), pp. 665–674. DOI: 10.1097/01.anes.0000264746.01393.e0 (cit. on p. 17).

[103] Arja. Hakuli et al. 'FT-IR in the Quantitative Analysis of Gaseous Hydrocarbon Mixtures'. In: *Analytical Chemistry* 67.11 (1995), pp. 1881–1886. DOI: 10.1021/ac00107a019 (cit. on p. 18).

[104] Deru Qin and Gardy Cadet. 'Quantitative Analysis of Process Streams by On-Line FT-IR Spectrometry'. In: *Analytical Chemistry* 69.10 (May 1997), pp. 1942–1945. DOI: 10.1021/ac9610826 (cit. on pp. 18, 24).

[105] John P Coates. 'Infrared Spectroscopy for Process Analytical Applications'. In: *Process Analytical Technology*. John Wiley & Sons, Ltd, 2010. Chap. 6, pp. 157–194. DOI: 10.1002/9780470689592.ch6 (cit. on p. 18).

[106] Peter J. Larkin. 'General Outline for IR and Raman Spectral Interpretation'. In: *Infrared and Raman Spectroscopy*. Elsevier, Jan. 2018, pp. 135–151. DOI: 10.1016/b978-0-12-804162-8.00007-0 (cit. on p. 18).

[107] Krzysztof B. Beć, Justyna Grabska and Christian W. Huck. 'Biomolecular and bioanalytical applications of infrared spectroscopy – A review'. In: *Analytica Chimica Acta* 1133 (Oct. 2020), pp. 150–177. DOI: 10.1016/J.ACA.2020.04.015 (cit. on pp. 18, 24).

[108] Hongkui. Xiao, Steven P Levine and James B D'Arcy. 'Iterative least-squares fit procedures for the identification of organic vapor mixtures by Fourier-transform infrared spectrophotometry'. In: *Analytical Chemistry* 61.24 (1989), pp. 2708–2714. DOI: 10.1021/ac00199a006 (cit. on p. 24).

[109] Hisham Khaled et al. 'Fast Quantitative Modelling Method for Infrared Spectrum Gas Logging Based on Adaptive Step Sliding Partial Least Squares'. In: *Energies* 15.4 (Feb. 2022), p. 1325. DOI: 10.3390/EN15041325 (cit. on p. 27).

[110] Guosheng Zhang et al. 'Optimized adaptive Savitzky-Golay filtering algorithm based on deep learning network for absorption spectroscopy'. In: *Spectrochimica Acta Part A: Molecular and Biomolecular Spectroscopy* 263 (Dec. 2021), p. 120187. DOI: 10.1016/J.SAA.2021.120187 (cit. on p. 27).

[111] Yu V. Kistenev et al. 'Super-resolution reconstruction of noisy gas-mixture absorption spectra using deep learning'. In: *Journal of Quantitative Spectroscopy and Radiative Transfer* 289 (Oct. 2022), p. 108278. DOI: 10.1016/J.JQSRT.2022.108278 (cit. on p. 27).

[112] Rola Houhou and Thomas Bocklitz. 'Trends in artificial intelligence, machine learning, and chemometrics applied to chemical data'. In: *Analytical Science Advances* 2.3-4 (Apr. 2021), pp. 128–141. DOI: 10.1002/ANSA.202000162 (cit. on p. 27).

[113] Ruocheng Han, Rangsiman Ketkaew and Sandra Luber. 'A Concise Review on Recent Developments of Machine Learning for the Prediction of Vibrational Spectra'. In: *Journal of Physical Chemistry A* 126.6 (Feb. 2022), pp. 801–812. DOI: 10.1021/ACS.JPCA.1C10417 (cit. on p. 27).

[114] Carlos A. Meza Ramirez et al. 'Applications of machine learning in spectroscopy'. In: *Applied Spectroscopy Reviews* 56.8-10 (2020), pp. 733–763. DOI: 10.1080/05704928.2020.1859525 (cit. on p. 27).

[115] Nan Yu Topsøe, Karsten Pedersen and Eric G. Derouane. 'Infrared and temperature-programmed desorption study of the acidic properties of ZSM-5-type zeolites'. In: *Journal of Catalysis* 70.1 (July 1981), pp. 41–52. DOI: 10.1016/0021-9517(81)90315-8 (cit. on p. 28).

[116] G. D. McLellan et al. 'Effects of coke formation on the acidity of ZSM-5'. In: *Journal of Catalysis* 99.2 (June 1986), pp. 486–491. DOI: 10.1016/0021-95178690373-8 (cit. on p. 29).

[117] Shanshan Shao et al. 'Catalytic conversion of biomass-derivates by in situ DRIFTS: Evolution of coke'. In: *Journal of Analytical and Applied Pyrolysis* 127.December 2016 (Sept. 2017), pp. 258–268. DOI: 10.1016/j.jaap.2017.07.026 (cit. on p. 31).

[118] Shanshan Shao et al. 'Evolution of coke in the catalytic conversion of biomass-derivates by combined in-situ DRIFTS and ex-situ approach: Effect of functional structure'. In: *Fuel Processing Technology* 178 (Sept. 2018), pp. 88–97. DOI: 10.1016/j.fuproc.2018.05.021 (cit. on p. 31).

[119] Xiaochao Xian et al. 'Characterization of the location of coke deposited on spent HZSM-5 zeolite by special temperature-programmed oxidation and isothermal oxidation methods'. In: *Applied Catalysis A: General* 547 (Oct. 2017), pp. 37–51. DOI: 10.1016/J.APCATA.2017.08.023 (cit. on p. 31).

[120] C. A. Querini and S. C. Fung. 'Coke characterization by temperature programmed techniques'. In: *Catalysis Today* 37.3 (Aug. 1997), pp. 277–283. DOI: 10.1016/S0920-5861(97)00020-5 (cit. on p. 32).

[121] D. M. Bibby, G. D. McLellan and R. F. Howe. 'Effects of Coke Formation and Removal on the Acidity Of ZSM-5'. In: *Studies in Surface Science and Catalysis* 34.C (Jan. 1987), pp. 651–658. DOI: 10.1016/S0167-2991(09)60399-2 (cit. on p. 32).

[122] Jiří Čejka, Russell E Morris and Petr Nachtigall, eds. *Zeolites in Catalysis. Properties and Applications*. Catalysis Series. The Royal Society of Chemistry, 2017, P001–527 (cit. on pp. 33, 39).

[123] Ana Palčić and Valentin Valtchev. 'Analysis and control of acid sites in zeolites'. In: *Applied Catalysis A: General* 606 (Sept. 2020), p. 117795. DOI: 10.1016/J.APCATA.2020.117795 (cit. on pp. 33–36).

[124] N. V. Choudary and B. L. Newalkar. 'Use of zeolites in petroleum refining and petrochemical processes: Recent advances'. In: *Journal of Porous Materials* 18.6 (Dec. 2011), pp. 685–692. DOI: 10.1007/s10934-010-9427-8 (cit. on p. 33).

[125] Ch. Baerlocher and L.B. McCusker. *Database of Zeolite Structures*. URL: http://www.iza-structure.org/databases/ (cit. on pp. 33, 34).

[126] Jiři Čejka, Avelino Corma and Stacey Zones. *Zeolites and Catalysis: Synthesis, Reactions and Applications*. Vol. 1-2. Wiley-VCH, June 2010 (cit. on pp. 34, 47, 49).

[127] Jungho Jae et al. 'Investigation into the shape selectivity of zeolite catalysts for biomass conversion'. In: *Journal of Catalysis* 279.2 (Apr. 2011), pp. 257–268. DOI: 10.1016/J.JCAT.2011.01.019 (cit. on p. 34).

[128] Hideshi Hattori and Yoshio Ono. 'Catalysts and catalysis for acid-base reactions'. In: *Metal Oxides in Heterogeneous Catalysis*. Elsevier, Jan. 2018, pp. 133–209. DOI: 10.1016/B978-0-12-811631-9.00004-1 (cit. on p. 34).

[129] D. H. Dompas et al. 'The influence of framework-gallium in zeolites: Electronegativity and infrared spectroscopic study'. In: *Journal of Catalysis* 129.1 (May 1991), pp. 19–24. DOI: 10.1016/0021-9517(91)90004-N (cit. on p. 34).

[130] Simone Creci. 'Tuned acidity in zeotypes: A descriptor to unravel the direct conversion of methane to methanol'. PhD thesis. Gothenburg: Chalmers University of Technology, 2020 (cit. on pp. 34–36, 45).

[131] Xueting Wang et al. 'Methanol Desorption from Cu-ZSM-5 Studied by in Situ Infrared Spectroscopy and First-Principles Calculations'. In: *Journal of Physical Chemistry C* 121.49 (Dec. 2017), pp. 27389–27398. DOI: 10.1021/acs.jpcc.7b07067 (cit. on pp. 35, 36, 41).

[132] Simone Creci et al. 'Acidity as Descriptor for Methanol Desorption in B-, Ga- and Ti-MFI Zeotypes'. In: *Catalysts* 11.1 (Jan. 2021), p. 97. DOI: 10.3390/CATAL11010097 (cit. on pp. 35, 36).

[133] Simone Creci et al. 'Tuned Acidity for Catalytic Reactions: Synthesis and Characterization of Fe- and Al-MFI Zeotypes'. In: *Topics in Catalysis* 62.7-11 (Aug. 2019), pp. 689–698. DOI: 10.1007/s11244-019-01155-4 (cit. on pp. 35, 36).

[134] Rosemarie Szostak, Vinayan Nair and Tudor L Thomas. 'Incorporation and stability of iron in molecular-sieve structures. Ferrisilicate analogues of zeolite ZSM-5'. In: *Journal of the Chemical Society, Faraday Transactions 1: Physical Chemistry in Condensed Phases* 83.2 (Jan. 1987), pp. 487–494. DOI: 10.1039/F19878300487 (cit. on p. 35).

[135] Zeid A. Alothman. 'A Review: Fundamental Aspects of Silicate Mesoporous Materials'. In: *Materials* 5.12 (Dec. 2012), pp. 2874–2902. DOI: 10.3390/MA5122874 (cit. on p. 35).

[136] Matthias Thommes et al. 'Physisorption of gases, with special reference to the evaluation of surface area and pore size distribution (IUPAC Technical Report)'. In: *Pure and Applied Chemistry* 87.9-10 (Oct. 2015), pp. 1051–1069. DOI: 10.1515/PAC-2014-1117 (cit. on p. 36).

[137] J. Rouquerol, P. Llewellyn and F. Rouquerol. 'Is the bet equation applicable to microporous adsorbents?' In: *Studies in Surface Science and Catalysis* 160 (Jan. 2007), pp. 49–56. DOI: 10.1016/S0167-2991(07)80008-5 (cit. on p. 36).

[138] Pol Mestre Tosas. 'Investigation of zeolite acid sites for 2,5-dimethylfuran conversion'. MA thesis. Gothenburg: Chalmers University of Technology, 2022 (cit. on pp. 36, 41, 46).

[139] Christopher Sauer et al. 'Valorisation of 2,5-dimethylfuran over zeolite catalysts studied by on-line FTIR-MS gas phase analysis'. In: *Catalysis Science & Technology* 12.3 (Feb. 2022), pp. 750–761. DOI: 10.1039/D1CY01312B (cit. on pp. 36, 37, 40, 41, 50).

[140] I Kiricsi et al. 'Progress toward Understanding Zeolite .beta. Acidity: An IR and 27Al NMR Spectroscopic Study'. In: *The Journal of Physical Chemistry* 98.17 (Apr. 1994), pp. 4627–4634. DOI: 10.1021/j100068a024 (cit. on p. 37).

[141] Dominique M Roberge, Heike Hausmann and Wolfgang F Hölderich. 'Dealumination of zeolite beta by acid leaching: a new insight with two-dimensional multi-quantum and cross polarization 27Al MAS NMR'. In: *Phys. Chem. Chem. Phys.* 4.13 (2002), pp. 3128–3135. DOI: 10.1039/B110679C (cit. on p. 37).

[142] Anton A. Gabrienko et al. 'Strong acidity of silanol groups of zeolite beta: Evidence from the studies by IR spectroscopy of adsorbed CO and 1H MAS NMR'. In: *Microporous and Mesoporous Materials* 131.1-3 (June 2010), pp. 210–216. DOI: 10.1016/j.micromeso.2009.12.025 (cit. on p. 37).

[143] A. S. Rodionov et al. 'An in situ study of dimethyl ether conversion over HZSM-5/Al 2O3 zeolite catalysts by high-temperature diffuse reflectance infrared fourier transform spectroscopy'. In: *Petroleum Chemistry* 53.5 (Sept. 2013), pp. 316–321. DOI: 10.1134/S0965544113050083 (cit. on p. 37).

[144] Michael Renz et al. 'Selective and Shape-Selective Baeyer–Villiger Oxidations of Aromatic Aldehydes and Cyclic Ketones with Sn-Beta Zeolites and H2O2'. In: *Chemistry - A European Journal* 8.20 (Oct. 2002), pp. 4708–4717. DOI: 10.1002/1521-3765(20021018)8:20<4708::AID-CHEM4708>3.0.CO;2-U (cit. on p. 37).

[145] Ludmila Kubelková, Jiří Čejka and Jana Nováková. 'Surface reactivity of ZSM-5 zeolites in interaction with ketones at ambient temperature (a FT-i.r. study)'. In: *Zeolites* 11.1 (Jan. 1991), pp. 48–53. DOI: 10.1016/0144-2449(91)80355-4 (cit. on p. 37).

[146] Silvia Bordiga et al. 'Probing zeolites by vibrational spectroscopies'. In: *Chemical Society Reviews* 44.20 (Oct. 2015), pp. 7262–7341. DOI: 10.1039/c5cs00396b (cit. on p. 37).

[147] Philipp Müller et al. 'Mechanistic Study on the Lewis Acid Catalyzed Synthesis of 1,3-Butadiene over Ta-BEA Using Modulated Operando DRIFTS-MS'. In: *ACS Catalysis* 6.10 (Oct. 2016), pp. 6823–6832. DOI: 10.1021/acscatal.6b01642 (cit. on p. 37).

[148] R. Piffer, H. Förster and W. Niemann. 'IR and XAS investigations on the interaction of butadiene with zeolite CuY'. In: *Catalysis Today* 8.4 (Mar. 1991), pp. 491–500. DOI: 10.1016/0920-5861(91)87026-J (cit. on p. 38).

[149] Yu-Ting Cheng et al. 'Production of Renewable Aromatic Compounds by Catalytic Fast Pyrolysis of Lignocellulosic Biomass with Bifunctional Ga/ZSM-5 Catalysts'. In: *Angewandte Chemie* 124.6 (Feb. 2012), pp. 1416–1419. DOI: 10.1002/ange.201107390 (cit. on pp. 38, 44, 45).

[150] Jana Engeldinger et al. 'Elucidating the role of Cu species in the oxidative carbonylation of methanol to dimethyl carbonate on CuY: An in situ spectroscopic and catalytic study'. In: *Applied Catalysis A: General* 382.2 (July 2010), pp. 303–311. DOI: 10.1016/j.apcata.2010.05.009 (cit. on p. 41).

[151] Mark A. Newton et al. 'Active sites and mechanisms in the direct conversion of methane to methanol using Cu in zeolitic hosts: A critical examination'. In: *Chemical Society Reviews* 49.5 (Mar. 2020), pp. 1449–1486. DOI: 10.1039/c7cs00709d (cit. on p. 41).

[152] C. M. Lok, J. Van Doorn and G. Aranda Almansa. 'Promoted ZSM-5 catalysts for the production of bio-aromatics, a review'. In: *Renewable and Sustainable Energy Reviews* 113 (Oct. 2019), p. 109248. DOI: 10.1016/J.RSER.2019.109248 (cit. on pp. 44, 55).

[153] Jian Li et al. 'Optimizing the Aromatic Product Distribution from Catalytic Fast Pyrolysis of Biomass Using Hydrothermally Synthesized Ga-MFI Zeolites'. In: *Catalysts* 9.10 (Oct. 2019), p. 854. DOI: 10.3390/catal9100854 (cit. on p. 44).

[154] Tobias Weissenberger et al. 'Hierarchical ZSM-5 Catalysts: The Effect of Different Intracrystalline Pore Dimensions on Catalyst Deactivation Behaviour in the MTO Reaction'. In: *ChemCatChem* 12.9 (May 2020), pp. 2461–2468. DOI: 10.1002/CCTC.201902362 (cit. on p. 45).

[155] R. M. Dessau. 'Base- and acid-catalysed cyclization of diketones over ZSM-5'. In: *Zeolites* 10.3 (Mar. 1990), pp. 205–206. DOI: 10.1016/0144-2449(90)90047-U (cit. on p. 49).

[156] Xinqiang Feng et al. 'Is hydrolysis a bad news for p-xylene production from 2,5-dimethylfuran and ethylene? Mechanism investigation into the role of acid strength during 2,5-hexanedione conversion'. In: *Journal of Catalysis* 401 (Sept. 2021), pp. 214–223. DOI: 10.1016/J.JCAT.2021.07.026 (cit. on p. 50).

[157] Rongrong Zhao et al. 'Renewable p-xylene synthesis via biomass-derived 2,5-dimethylfuran and ethanol by phosphorous modified H-Beta zeolite'. In: *Microporous and Mesoporous Materials* 334 (Mar. 2022), p. 111787. DOI: 10.1016/J.MICROMESO.2022.111787 (cit. on p. 50).

[158] Jiabin Yin et al. 'Highly Selective Production of p-Xylene from 2,5-Dimethylfuran over Hierarchical NbOx-Based Catalyst'. In: *ACS Sustainable Chemistry and Engineering* 6.2 (Feb. 2018), pp. 1891–1899. DOI: 10.1021/acssuschemeng.7b03297 (cit. on p. 50).

[159] Roman Bielski and Grzegorz Grynkiewicz. 'Furan platform chemicals beyond fuels and plastics'. In: *Green Chemistry* 23.19 (Oct. 2021), pp. 7458–7487. DOI: 10.1039/D1GC02402G (cit. on p. 55).

[160] Philippe Kernen and Pierre Vogel. 'Total asymmetric synthesis of polypropionate fragments and doubly branched heptono-1,4-lactones'. In: *Tetrahedron Letters* 34.15 (Apr. 1993), pp. 2473–2476. DOI: 10.1016/S0040-4039(00)60444-6 (cit. on p. 55).

[161] Yoshikazu Shizuri et al. 'Total synthesis of (±)-citreoviral'. In: *Journal of the Chemical Society, Chemical Communications* 5 (Jan. 1985), pp. 292–293. DOI: 10.1039/C39850000292 (cit. on p. 55).

[162] Pranjali D. Muley et al. 'Microwave-assisted heterogeneous catalysis'. In: *Catalysis: Volume 33*. Vol. 33. The Royal Society of Chemistry, 2021, pp. 1–37. DOI: 10.1039/9781839163128-00001 (cit. on p. 55).